



3 4456 0515321 3

ORNL-5234

cy.1



ORR Irradiation Experiment OF-1: Accelerated Testing of HTGR Fuel

T. N. Tiegs
E. L. Long, Jr.
M. J. Kania
K. R. Thoms
E. J. Allen

OAK RIDGE NATIONAL LABORATORY
CENTRAL RESEARCH LIBRARY
DOCUMENT COLLECTION
LIBRARY LOAN COPY
DO NOT TRANSFER TO ANOTHER PERSON
If you wish someone else to see this
document, send its name with document
and the library will arrange a loan.
HEN-1263
13 4-57

OAK RIDGE NATIONAL LABORATORY
OPERATED BY UNION CARBIDE CORPORATION FOR THE ENERGY RESEARCH AND DEVELOPMENT ADMINISTRATION

Printed in the United States of America. Available from
National Technical Information Service
U.S. Department of Commerce
5285 Port Royal Road, Springfield, Virginia 22161
Price: Printed Copy \$5.00; Microfiche \$3.00

This report was prepared as an account of work sponsored by the United States Government. Neither the United States nor the Energy Research and Development Administration/United States Nuclear Regulatory Commission, nor any of their employees, nor any of their contractors, subcontractors, or their employees, makes any warranty, express or implied, or assumes any legal liability or responsibility for the accuracy, completeness or usefulness of any information, apparatus, product or process disclosed, or represents that its use would not infringe privately owned rights.

ORNL-5234
Distribution Category UC-77

Contract No. W-7405-eng-26

METALS AND CERAMICS DIVISION
HTGR BASE TECHNOLOGY PROGRAM
Fueled Graphite Development (189a 01330)

ORR IRRADIATION EXPERIMENT OF-1: ACCELERATED TESTING OF HTGR FUEL

T. N. Tiegs, E. L. Long, Jr., M. J. Kania, K. R. Thoms, and E. J. Allen

Date Issued: August 1977

OAK RIDGE NATIONAL LABORATORY
Oak Ridge, Tennessee 37830
operated by
UNION CARBIDE CORPORATION
for the
ENERGY RESEARCH AND DEVELOPMENT ADMINISTRATION



3 4456 0515321 3

Contents

ABSTRACT	1
INTRODUCTION	1
CAPSULE DESIGN	2
PARTICLE FABRICATION	6
ROD FABRICATION	6
CAPSULE OPERATION	18
DOSIMETRY ANALYSIS	20
FUEL SPECIMEN TEMPERATURES	22
DISASSEMBLY, VISUAL EXAMINATION, AND DIMENSIONAL INSPECTION	31
METALLOGRAPHY	45
Performance Evaluation of Fuel Types	45
Comparison of Matrices	51
COMPARISON OF FISSILE PARTICLES FROM THE 2.5-cm-(1-INCH-) AND 12.7-cm-(5-INCH-) DIAMETER COATERS	51
PERFORMANCE OF FERTILE PARTICLES	61
CONCLUSIONS	61
ACKNOWLEDGMENTS	63
APPENDIX A	64
APPENDIX B	64

ORR IRRADIATION EXPERIMENT OF-1: ACCELERATED TESTING OF HTGR FUEL

T. N. Tiegs, E. L. Long, Jr., M. J. Kania,
K. R. Thoms* and E. J. Allen*

ABSTRACT

The OF-1 capsule, the first in a series of High-Temperature Gas-Cooled Reactor fuel irradiations in the Oak Ridge Research Reactor, was irradiated for more than 9300 hr at full reactor power (30 MW). Peak fluences of 1.08×10^{22} neutrons/cm² (>0.18 MeV) were achieved. The capsule was a joint venture between General Atomic Company and Oak Ridge National Laboratory. General Atomic Company's magazine P13Q occupied the upper two-thirds of the test space and the ORNL magazine OF-1 the lower one-third. The ORNL portion tested various HTGR recycle particles and fuel bonding matrices at accelerated flux levels under reference HTGR irradiation conditions of temperature, temperature gradient, and fast fluence exposure (>0.18 MeV).

Results are as follows:

1. good irradiation performance for fuel rods carbonized in packed Al₂O₃ and in-block,
2. little effect of different carbonization techniques on the irradiation performance of the fuel particles,
3. no difference in performance between particles made in the 2.5-cm-diam (1-in.) coater and the 13-cm-diam (5-in.) coater,
4. nearly identical performance of kernels containing ²³³U with that of kernels containing ²³⁵U, and
5. no real difference between matrices using different filler particle types.

INTRODUCTION

The OF-1 irradiation experiment was the first in a series of High-Temperature Gas-Cooled Reactor (HTGR) fuel capsules irradiated in the Oak Ridge Research Reactor (ORR). The capsule was a joint venture between General Atomic Company (GAC) and the Oak Ridge National Laboratory (ORNL). The capsule was divided into two sections: one containing a GAC experiment designated as P13Q and the ORNL OF-1 magazine.^{1,2} This report will discuss the fabrication, operation, and examination of the ORNL portion of the experiment.

The fuel to be used in a commercial HTGR consists of coated particles that are bonded into rods with a carbonaceous matrix and inserted into large hexagonal graphite fuel elements. These elements, containing passages for the coolant gas, are stacked into a close packed array to make up the reactor core. The particle design consists of a fuel kernel containing uranium as the fissile material and/or thorium as the fertile material with either a Biso or Triso coating. A Biso-coated particle has two types of coating layers: a low-density pyrolytic carbon buffer and a high-density isotropic pyrolytic carbon to retain the fission

*Engineering Technology Division.

1. R. A. Bradley et al., "Fuel Stick Fabrication," *Gas-Cooled Reactor and Thorium Utilization Programs Annu. Prog. Rep. Sept. 30, 1971*, ORNL-4760, pp. 52--55.

2. C. L. Smith, *Preirradiation Report. Fuel Materials for Irradiation P13Q*, General Atomic Company, GA-A-13265 (June 1975).

products. A Triso-coated particle is basically a Biso coating with the addition of a silicon carbide layer and another high-density pyrolytic carbon layer.

The ORNL portion of the capsule tested various candidate HTGR recycle particles and recycle fuel bonding matrices at accelerated flux levels under reference HTGR temperature, temperature gradient, fast fluence exposure and heavy metal burnup conditions. The capsule was designed to meet these conditions for an irradiation time of about 330 full power days or about one calendar year of operation.

The OF-1 magazine was designed to determine:

1. the irradiation performance of recycle fuel rods prepared by in-block and packed bed carbonization techniques;
2. the comparative performance of coated particles prepared to the same specifications in 2.5-cm-diam (1 in.) fluidized bed (laboratory-scale) and in 13-cm-diam (5 in.) prototype coaters;
3. the comparative performance of $(4.2 \text{ Th,U})\text{O}_2$ Biso-coated particles containing ^{235}U with similar particles containing ^{233}U ;
4. the performance of fuel rods made with different filler materials; and
5. the in-reactor thermal conductance of a slug-injected fuel rod.¹

CAPSULE DESIGN

The capsule was a double-wall, stainless steel, right circular cylinder (Fig. 1). The GAC portion of the experiment occupied approximately the upper two-thirds of the test space [~ 40 cm (16 in.)] and the ORNL portion the lower one-third [~ 23 cm (9 in.)]. The portions were separated by a nickel bulkhead.

The ORNL magazine, made of near isotropic type H-451 graphite,³ had a diameter of 6.1504 cm (2.4214 in.) and a length of 20.3 cm (8.0 in.). Although the top of the magazine was round, the bottom was hexagonal for centering the magazine in the capsule (Fig. 2). Each of five 1.27-cm-diam (0.50 in.) holes contained four fuel rods with diameters of 1.250 cm (0.492 in.) and lengths of 4.602 cm (1.812 in.), except for hole 3, which contained three 4.602-cm-long (1.812 in.) and two 2.301-cm-long (0.906 in.) rods.

The ORNL magazine contained a total of 16 thermocouples of which 14 were Chromel-P vs Alumel (C/A) and 2 were tungsten-rhenium (W/Re) (Fig. 2). The C/A thermocouples were all stainless-steel sheathed and alumina insulated. Four of the C/A thermocouples were 0.16 cm (0.06 in.) OD and 10 were 0.102 cm (0.040 in.) OD. Each of the four thermocouple holes on the outside of holes 1, 2, 3, and 4 contained two 0.102-cm-OD (0.040 in.) C/A thermocouples to measure the axial and circumferential variation of the temperature near the periphery of the magazine. The three additional C/A thermocouples around hole 3 and the central thermocouple in that hole provided a measure of the thermal conductance of the fuel rod at a location 5 cm (2 in.) above the bottom of the magazine. The two tungsten – rhenium thermocouples in hole 5 monitored the maximum fuel rod temperatures at two axial locations.

In addition to the thermocouples, dosimeter packages were placed in ten holes in the OF-1 graphite magazine (Fig. 3). Each of the packages contained iron, niobium, titanium, and cobalt flux monitor wires and had BeO sleeves to provide physical separation between the flux monitors and the graphite. Vanadium encapsulated the pure cobalt monitors and served as the base metal for new iron and cobalt alloy wires.

3. Manufactured by Great Lakes Carbon Company.

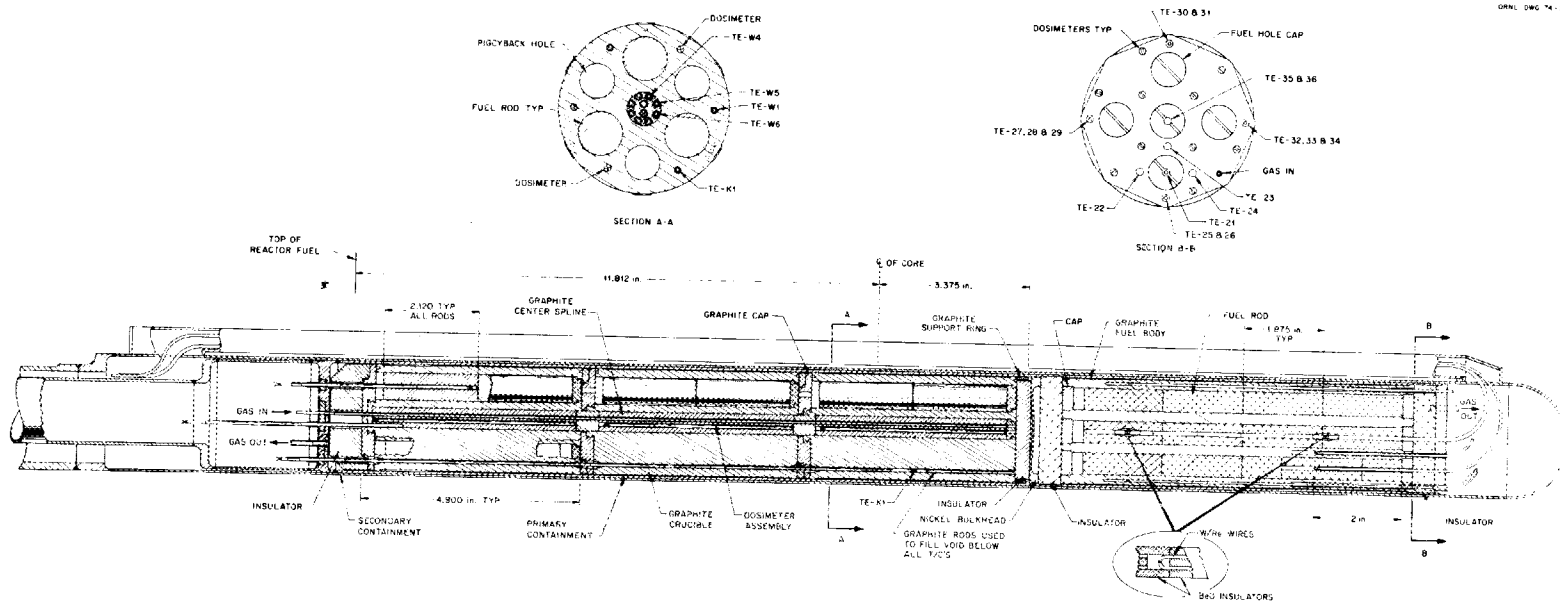


Fig. 1. In-core section of Capsule OF-1. Section A-A is GAC magazine. Section B-B is ORNL magazine showing hexagonal bottom.

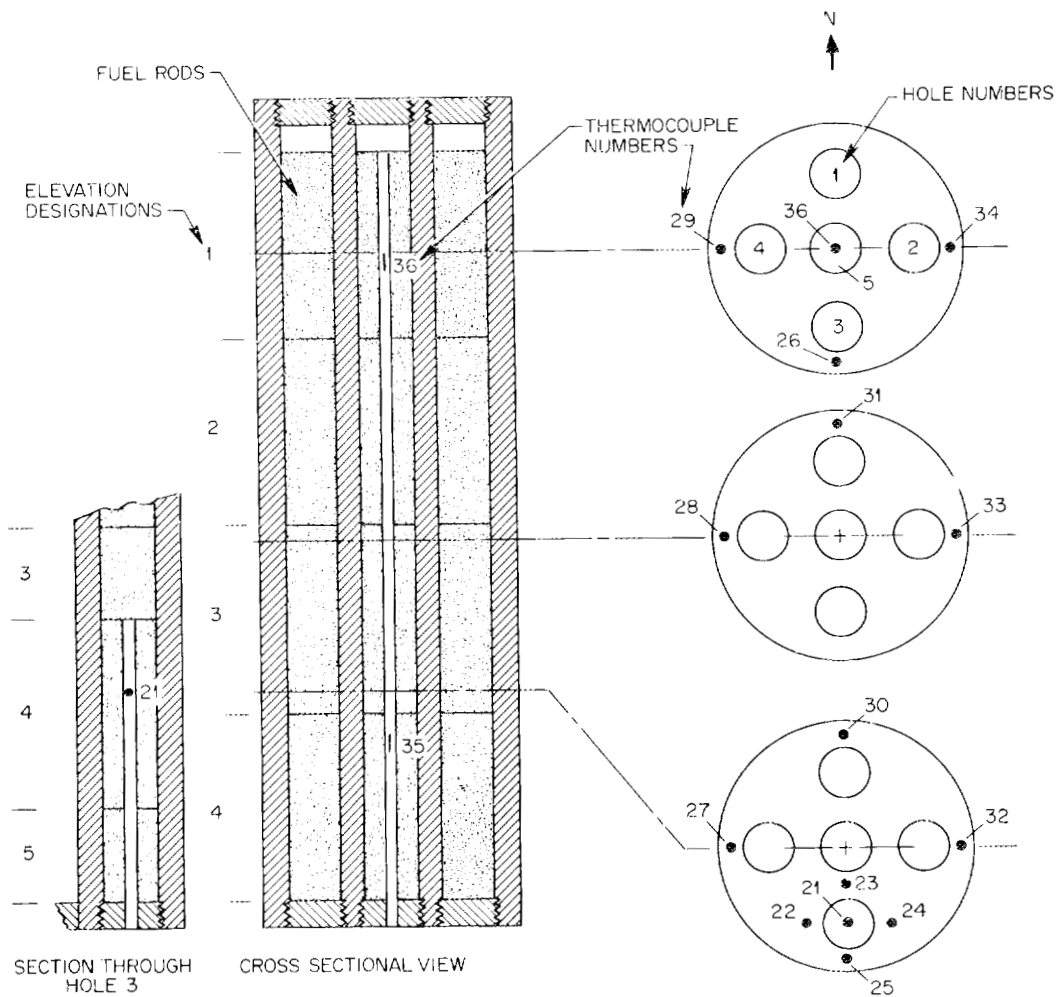
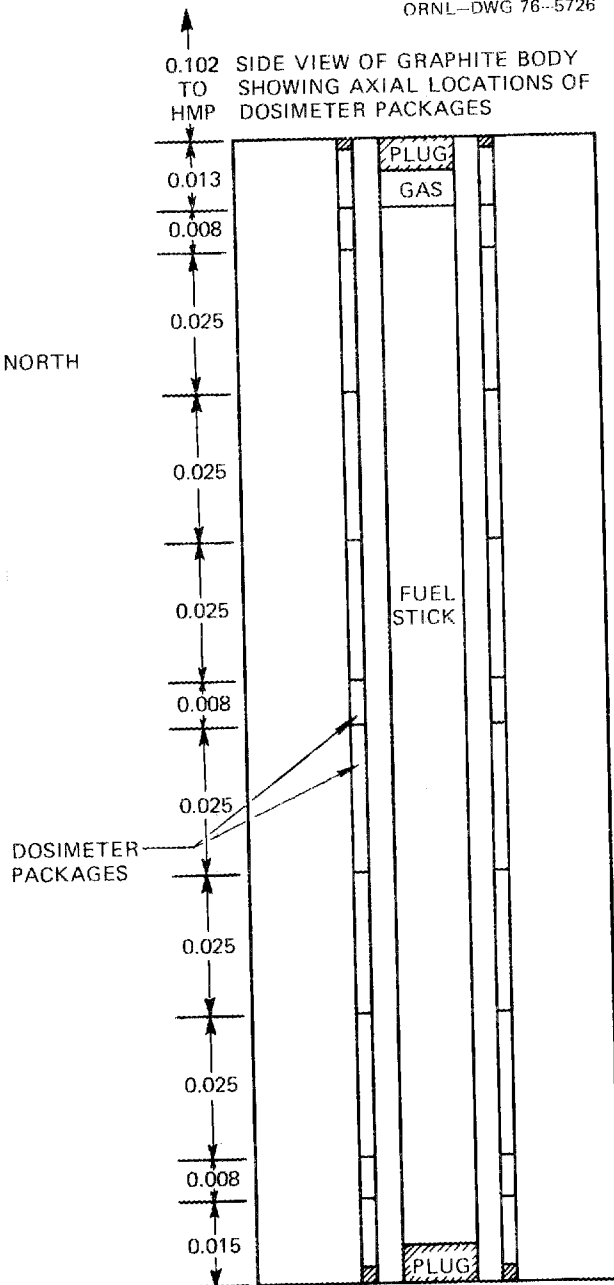
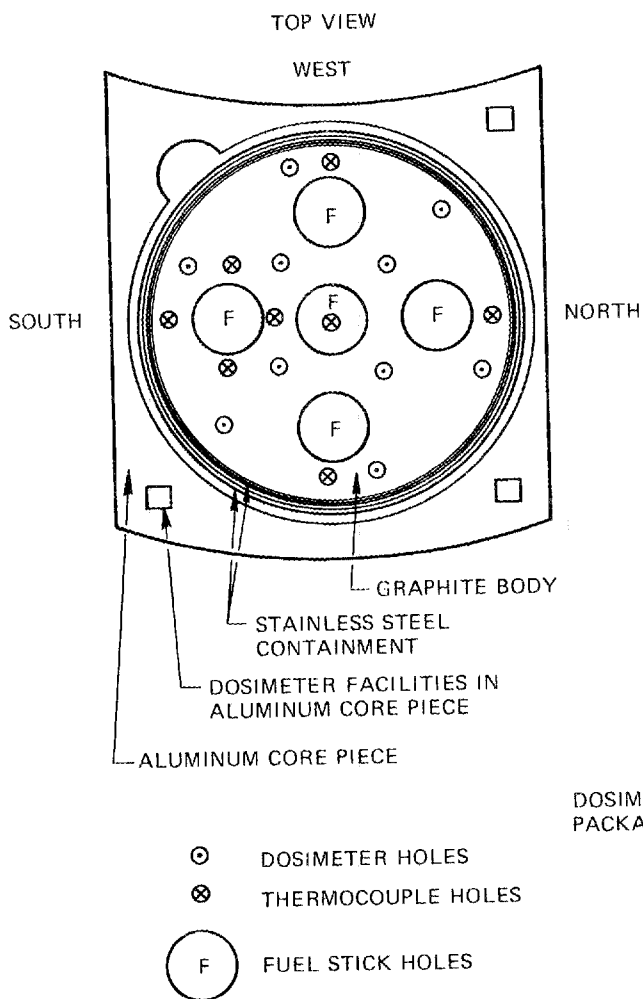


Fig. 2. Fuel rod and thermocouple locations in ORNL cell of Capsule OF-1.



EACH DOSIMETER PACKAGE CONSISTS OF TWO OR MORE Fe, Ni, Co, OR Ti DOSIMETERS IN A BeO SLEEVE

ALL DISTANCES IN METERS

Fig. 3. Location of dosimetry packages in the OF-1 magazine.

The ORNL portion was designed to meet the following irradiation conditions:

1. a maximum center line temperature of 1573 K in the central hole and 1473 K in the peripheral holes;
2. maintenance of the fuel rod center line temperature in the peripheral holes at a location 5 cm (2 in.) above the bottom of the magazine (the fully instrumented location) at 1323 K;
3. a maximum thermal gradient at the edge of the fuel rods of about 873 K/cm; and
4. a peak fast neutron flux of about 3×10^{14} neutrons/cm² sec. (> 0.18 MeV) to produce the full HTGR exposure of 8×10^{21} n/cm² fast fluence.

Each test space had its own sweep gas system to allow independent fission gas monitoring and temperature control. The sweep gas was operated at the same pressure in each cell so that there was no pressure differential across the nickel bulkhead. The thermocouples and gas lines from the bottom cell (ORNL) were run inside a 1.3-cm-OD (0.5 in.) tube external to the secondary containment to a point above the top end cap where they entered the capsule lead pipe. There was an initial 0.0089 cm (0.0035 in.) helium gas gap between the primary containment tube and the stainless steel secondary containment tube.

PARTICLE FABRICATION

All fueled particles for the ORNL portion of the OF-1 experiment were either Biso-coated (4.2 Th,U)O₂ or ThO₂ which were the reference recycle particles when the capsule was designed. The present reference recycle fissile particle is Triso-coated with a weak-acid-resin-derived uranium oxide-carbide kernel.^{4,5} The reference recycle fertile particle remains Biso-coated ThO₂.

There were eight types of fuel rods in the ORNL portion OF-1. The fertile particles for all rods and the fissile particles for five fuel types were coated in the 13-cm-diam (5 in.) coater. The fissile particles for two rod types were coated in a 2.5-cm-diam (1 in.) laboratory coater; and those which contained ²³³U were coated in 2.5-cm-diam (1 in.) coater in the ORNL plutonium laboratory. Acetylene diluted with helium was used for depositing the inner buffer coating on all particles, and propene was used for depositing the outer isotropic coating. In each case, conical gas distributors were used. The important characteristics of the particles are summarized in Table 1.

ROD FABRICATION

The particles were formed into rods by the slug-injection method, where hot pitch and filler are injected into a bed of particles held in a mold. Table 2 gives some of the parameters used in the fabrication of the eight types of fuel rods for the ORNL magazine. The solid fuel rods were formed on the prototype automatic¹ fuel rod machine, while the annular rods (which contained the thermocouples) were formed on a manual press. Each rod contained approximately the same uranium and thorium loading along with about 20 vol % GLC-1089 shim particles⁶ and enough pyrolytic carbon-coated inert particles for a total loading volume of 62%.

4. F. J. Homan et al., *Development of a Fissile Particle for HTGR Fuel Recycle*, ORNL/TM-5602 (December 1976).

5. F. J. Homan et al., "Stoichiometry Effects on Performance of HTGR Fuels from the U-C-O System," to be published in *Nuclear Technology*.

6. Manufactured by Great Lakes Carbon Company.

Table 1. Summary of coated particle properties^a

Batch Number	Fertile		Fissile			
	J-238 ^b	J-262 ^b	13-cm-diam (5 in.) prototype coater		2.5-cm-diam (1 in.) laboratory coater	Pu-lab coater
	(unannealed)	(annealed)	J-257 ^c (unannealed)	J-263 ^c (annealed)	OR-1977	Pu-291
Kernel diameter, μm	496.5 \pm 0.6		353.8 \pm 1.0		357	350.8
Kernel density, g/cm^3	10.0		9.8 \pm 0.15		9.85	10.0
Buffer thickness, μm	84.0 \pm 2.7		101.2		93	104.7
Buffer density, ^d g/cm^3	1.188		1.39 \pm 0.05 ^e		1.18 ^f	1.35 ^f
Sealer thickness, μm	3.5 ^f		none		none	none
LTI ^h thickness, μm	86.1 \pm 2.2	82.4	91.8 \pm 2.7		106	85
LTI density, g/cm^3 - Observed ⁱ	1.948 \pm 0.004	2.007 \pm 0.004	1.966 \pm 0.004	2.012 \pm 0.004	1.96	1.982
Corrected ⁱ	1.868	1.921	1.899	1.927		
LTI deposition rate, $\mu\text{m}/\text{min}$.	8.3		7.6			
LTI open porosity, ^k vol. %	4.1	4.3	3.4	4.2		
Particle diameter μm	839.2 \pm 4.9	827.4 \pm 5.7	734.8 \pm 6.1	717.5 \pm 9.6		
Particle density ^l g/cm^3	3.355 \pm 0.007	3.415 \pm 0.007	2.640 \pm 0.007	2.690 \pm 0.007	2.44	2.665
Wt % Th/particle		54.08		29.74	27.5	23.81
Wt % U/particle				7.25 ^m	6.16 ⁿ	5.50 ^o
Exposed actinide, ^m ppm	4, 10	1.1, 1.6	2, 1	22, 39		
Particle crush strength, newton (lb)	25.6 \pm 0.9 (5.7 \pm 0.2)	28.9 \pm 0.9 (6.5 \pm 0.2)	25.8 \pm 1.3 (5.8 \pm 0.3)	27.6 \pm 1.8 (6.2 \pm 0.4)		
Crush strength standard deviation, newton (lb)	4.0 (0.9)	3.6 (0.8)	3.6 (0.8)	5.3 (1.2)		

^aIn each case the reported uncertainty is the 95% confidence interval for the mean.

^bJ-262 are annealed particles from batch J-238; only J-262 was irradiated.

^cJ-263 are annealed particles from batch J-257; only J-263 was irradiated.

^dCalculated from mercury pycnometry determined particle density before and after coating and wt. % carbon determined by burning, unless otherwise noted. In the case of fissile particles, the burnoff results were corrected to account for the increase in % ratio during burning.

^eSealer not used; calculated from mercury pycnometer particle density, LTI gradient density, kernel density, and kernel and coating dimensions. This is the buffer density after deposition of the LTI.

^fCalculated.

^gDetermined metallographically.

^hLow temperature isotropic coating.

ⁱMeasured by gradient column.

^jCorrected (1 - fraction of LTI volume that is open porosity) \times observed density.

^kMercury pycnometer at 15,000 psi.

^lMercury pycnometer at 250 psi.

^mBased on particle weight; two numbers are for duplicate measurements by aqueous leach.

ⁿ93.17% ²³³U.

^o97.97% ²³³U.

For fuel types 1 through 7, the matrix was injected through the particle bed at 453K and a pressure of 70,300 gm/cm^2 (1000 psi). Fuel type 8 was injected at 448K and 70,300 gm/cm^2 (1000 psi). The rods were carbonized either in packed Al_2O_3 or in the OF-1 graphite magazine (Table 2). Fuel types 1 through 7 were carbonized by heating at 60K/hr to 773K and holding for 1 hr, then continuing to 1173K at 300K/hr and holding for 1 hr. Fuel type 8 experienced the same carbonization conditions except that it was heated to 1073K instead of 1173K in the final step. All rods were annealed at 2073K for 1/2 hr. The differences between type 8 and the other rods were not process variables, but were because the type 8 contained ²³³U and had to be handled in separate facilities.

Table 2. Rod fabrication parameters

Rod type	Carbonization mode	Fissile isotope	Fissile particle coater, cm (in.)	Matrix materials		Central thermocouple present	Fissile particle batch used
				Filler ^a	Binder (Ashland A240, wt %)		
1	Packed Al ₂ O ₃	²³⁵ U	13 (5)	29 wt % Asbury 6353 ^b	71		J-263
2	In-block	²³⁵ U	13 (5)	29 wt % Asbury 6353	71		J-263
3	In-block	²³⁵ U	13 (5)	38.5 wt % GLC 1089	61.5		J-263
4	Packed Al ₂ O ₃	²³⁵ U	2.5 (1)	29 wt % Asbury 6353	71		OR-1977
5	Packed Al ₂ O ₃	²³⁵ U	13 (5)	29 wt % Asbury 6353	71	X	J-263
6	Packed Al ₂ O ₃	²³⁵ U	13 (5)	29 wt % Asbury 6353	71	X	J-263
7	Packed Al ₂ O ₂	²³⁵ U	2.5 (1) ^d	29 wt % Asbury 6353	71	X	OR-1977
8	Packed Al ₂ O ₃	²³³ U	2.5 (1) ^e	29 wt % Asbury 6353	71	X	Pu-291

^aFor GLC-1089 the range of particle sizes determined by Coulter Counter was 6 μm - 37 μm with 50 wt % < 16.5 μm .

^bManufactured by Asbury Graphite Mills.

^cManufactured by Ashland Oil Company.

^dOne-in-diam laboratory coater.

^eOne-in-diam laboratory coater in plutonium laboratory.

Table 3 gives the important characteristics of the rods. The matrix density was linearly related to the pitch-coke yield. The pitch-coke yield fell into 4 categories:

1. rods carbonized in graphite element (Types 2 and 3), > 40%;
2. solid rods carbonized in packed Al₂O₃ (Types 1 and 4), 13.7 to 14.6%;
3. annular rods carbonized in packed Al₂O₃ (Types 5 through 7), 19.4 to 21.2%; and
4. annular rods carbonized in packed Al₂O₃ (Type 8), 11.7%.

The differences in pitch-coke yield of rods carbonized in packed Al₂O₃ in different furnaces were apparently due to small differences in heating rates.

The appearance of the fuel rods carbonized in packed Al₂O₃ (fuel types 1, 4, 5, 6, 7, 8) is shown in Figs. 4, 5, and 6. The rods carbonized in the graphite element (types 2 and 3) could not be observed after carbonization. Rods fabricated identically to those rods were carbonized in graphite process tubes to simulate in-block carbonization (Figs. 7 and 8). The rod appearances will be compared to those in the postirradiation examination.

Metallographic examination of samples subjected to the same conditions as the test rods showed that those rods carbonized in packed Al₂O₃ powder had matrices with open, porous microstructures in which the individual filler particles were clearly visible (fuel types 1, 4, 5, 6, 7, and 8). On the other hand, the rods carbonized in graphite process tubes had denser microstructures (fuel types 2 and 3). Apparently the pitch coke had filled in between the filler particles, so individual filler particles were not discernible in most cases. The matrices from each fuel type (except 6, since 5 is representative of type 6) are compared (Figs. 9 through 15). The observations from the preirradiation metallographic examination are summarized in Table 4.

A comparison of fuel types 2 and 3 (Figs. 10 and 11 respectively) shows that different filler particles produce matrices that appear the same. Both matrices were carbonized in graphite process tubes and used Ashland A240 binder, but fuel type 2 used Asbury 6353 filler particles and fuel type 3 used GLC 1089 filler particles. In addition, six particles were observed in which the outer pyrocarbon coating was torn

Table 3. Fuel rod characteristics

Rod position ^a	Rod number	Rod type	Average diameter, cm (in.)	Length cm, (in.)	Matrix density (g/cm ³)	Pitch coke yield ^b (%)	Heavy metal loading (g)	
							U	Th
1-1	M105A077	1	1.250 (0.492)	4.3734 (1.7218)	0.468	12.82	0.1156	1.5719
1-2	M105A075	1	1.250 (0.492)	4.3835 (1.7258)	0.472	13.03	0.1156	1.5719
1-3	M105A072	1	1.250 (0.492)	4.3772 (1.7233)	0.475	13.79	0.1156	1.5719
1-4	M105A068	1	1.250 (0.492)	4.4198 (1.7381)	0.497	15.69	0.1156	1.5719
2-1	M105A094	2	N.D. ^c	N.D. ^c	0.732 ^d	44.9 ^d	0.1156	1.5719
2-2	M105A093	2	N.D. ^c	N.D. ^c	0.732 ^d	44.9 ^d	0.1156	1.5719
2-3	M105A092	2	N.D. ^c	N.D. ^c	0.732 ^d	44.9 ^d	0.1156	1.5719
2-4	M105A091	2	N.D. ^c	N.D. ^c	0.732 ^d	44.9 ^d	0.1156	1.5719
3-1	M105A114	4	1.250 (0.492)	4.6977 (1.8495)	0.486	14.25	0.1061	1.6149
3-2	M105A113	4	1.250 (0.492)	4.6581 (1.8339)	0.490	13.66	0.1061	1.6149
3-3	M105A121	6	1.247 (0.491)	2.3378 (0.9204)	0.543	18.93	0.0578	0.7859
3-4	M105A117	5	1.250 (0.492)	4.8204 (1.8978)	0.537	19.46	0.1156	1.5719
3-5	M105A122	6	1.247 (0.491)	2.3381 (0.9205)	0.516	18.09	0.0578	0.7859
4-1	M115A079	3	N.D. ^c	N.D. ^c	N.D. ^e	N.D. ^e	0.1156	1.5719
4-2	M115A078	3	N.D. ^c	N.D. ^c	N.D. ^e	N.D. ^e	0.1156	1.5719
4-3	M115A077	3	N.D. ^c	N.D. ^c	N.D. ^e	N.D. ^e	0.1156	1.5719
4-4	M115A076	3	N.D. ^c	N.D. ^c	N.D. ^e	N.D. ^e	0.1156	1.5719
5-1	M105A135	8	1.252 (0.493)	4.633 (1.824)	N.D. ^c	N.D. ^c	0.0930	1.5718
5-2	M105A125	7	1.247 (0.491)	4.6642 (1.8363)	0.574	21.03	0.1061	1.6149
5-3	M105A137	8	1.255 (0.494)	4.628 (1.822)	0.463	11.4	0.0930	1.5718
5-4	M105A127	7	1.250 (0.492)	4.5926 (1.8081)	0.573	21.29	0.1061	1.6149

^aFuel rod position is as follows: the first number designates the hole numbers and the second number designates the elevation as shown in Fig. 2.

^bPitch-coke yield is the weight fraction of pitch plus additives remaining in the rod after carbonization.

^cNot determined.

^dAverage value calculated from control samples simulating the conditions of the rods carbonized in the graphite magazine.

^eNot determined because portions of rods adhered to graphite process tube making it impossible to obtain accurate weights of the rods after carbonization.

(apparently due to matrix-particle interaction)⁷ in fuel type 3, but none was found in fuel type 2. An example of matrix-particle interaction is shown in Fig. 16.

Radiographs of the rods showed that there was an even distribution of the fissile and fertile particles with respect to the shim and inert particles. To determine the failure fraction of coated particles, archive fuel rods were electrolytically disintegrated and the loose particles were subjected to a nitric acid leach solution; then the electrolytic and leach solutions were analyzed for thorium and uranium. The broken particle analyses (Table 5) indicate that the rod containing GLC-1089 and carbonized in-block (fuel type 3) contained about two broken fissile particles and two broken fertile particles. One annular rod containing Asbury 6353 and carbonized in packed Al₂O₃ (fuel type 7) also appeared to have about two broken fissile particles.

7. T. N. Tiegs et al., *Irradiation Performance of HTGR Fuel Rods in HFIR Experiment HT-26 and -27*, ORNL/TM-5404 (March 1976).

Slug Injected Specimens for OF-1

Carbonized in Al_2O_3 Powder

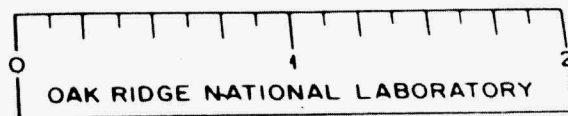
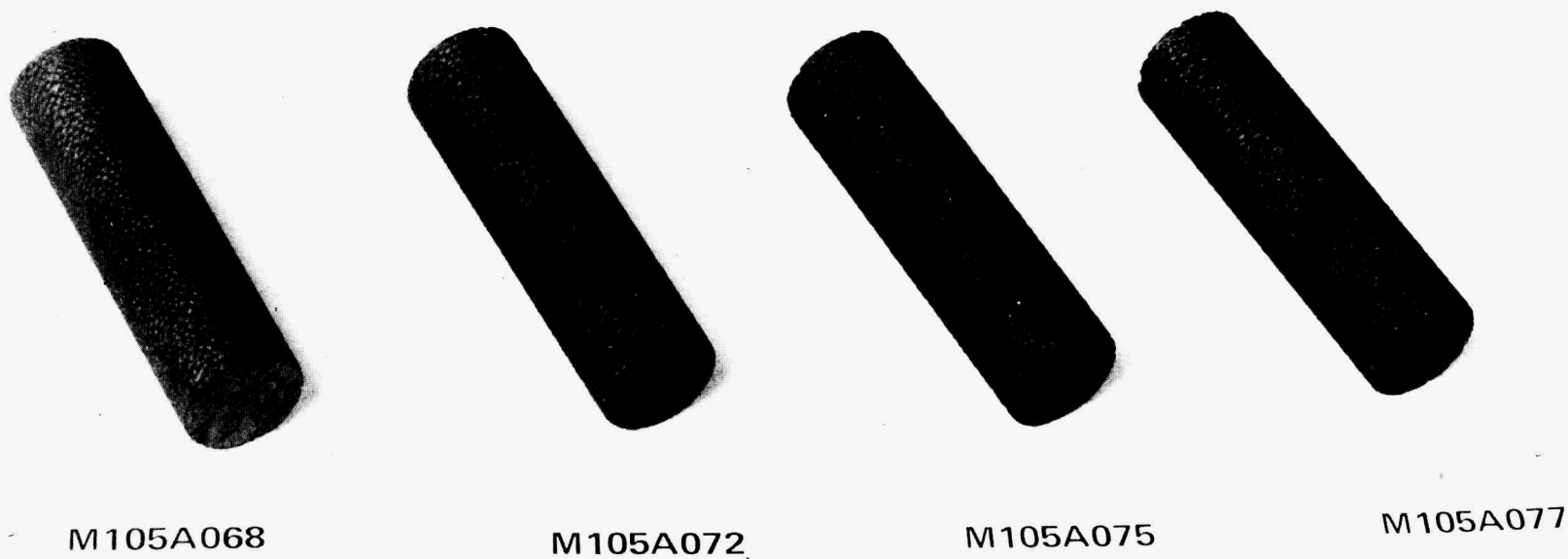


Fig. 4. Fuel rods 1-1, 1-2, 1-3 and 1-4 (right to left) before irradiation. Carbonized in packed Al_2O_3 .

Slug Injected Specimens for OF-1

Carbonized in Al_2O_3 Powder

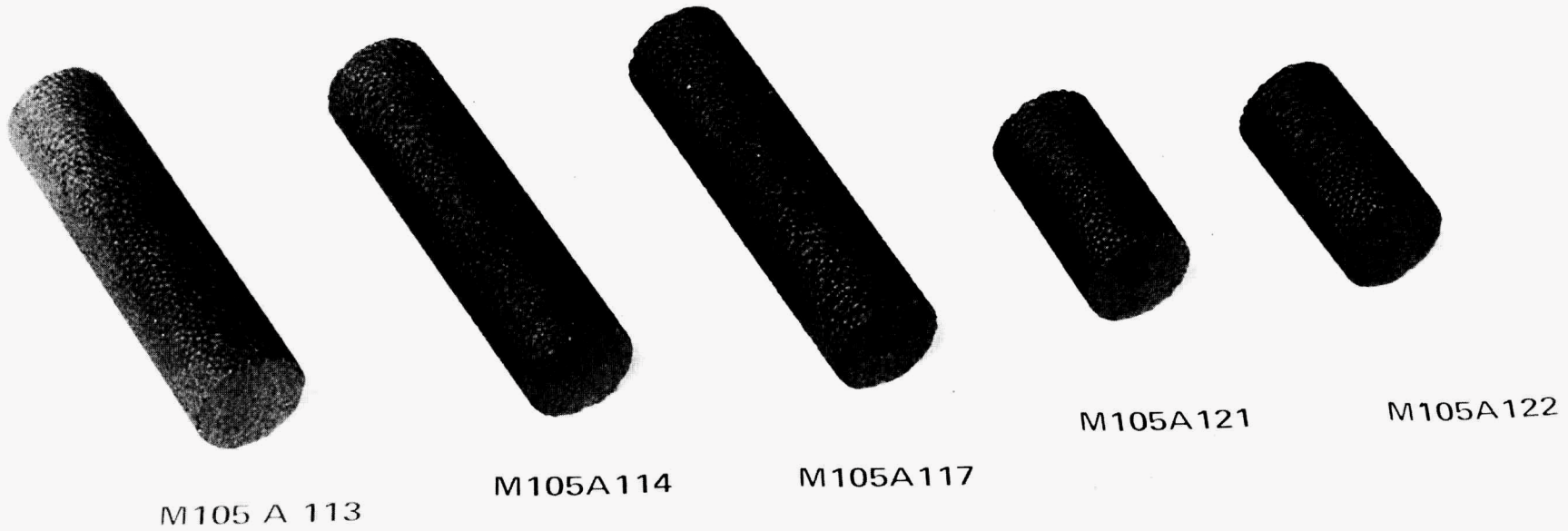
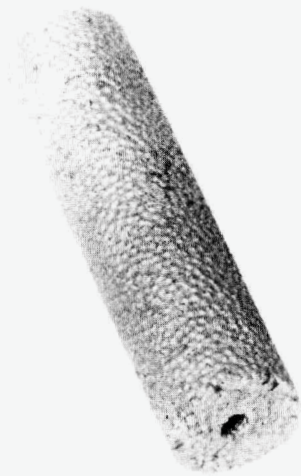


Fig. 5. Fuel rods (left to right) 3-5, 3-3, 3-4, 3-1 and 3-2 before irradiation. Carbonized in packed Al_2O_3 .

Slug Injected Specimens for OF-1

ORNL Photo 1576 73

Carbonized in Al_2O_3 Powder



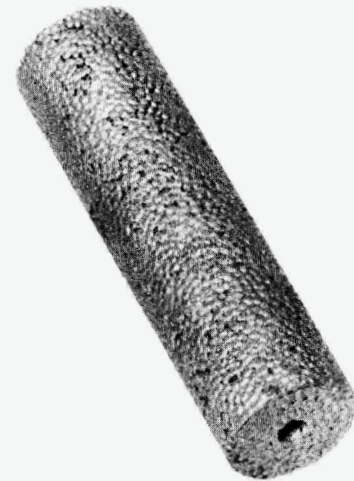
M105A125



M105A127



M105A135



M105A136

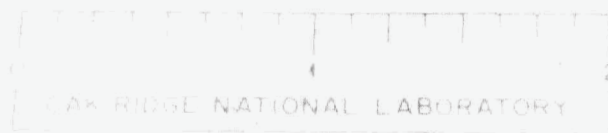


Fig. 6. Fuel rods (left to right) 5-2, 5-4, 5-1 and 5-3 before irradiation. Carbonized in packed Al_2O_3 .

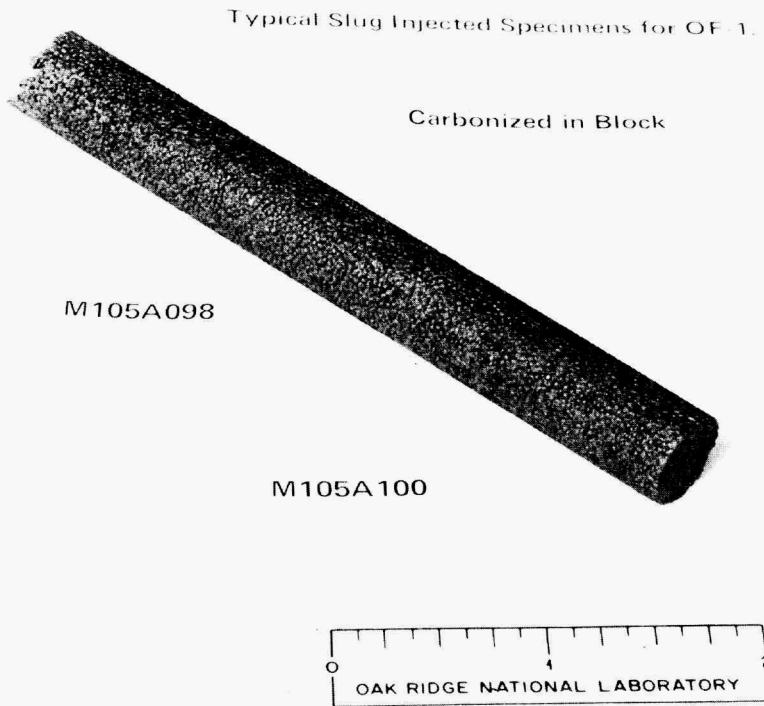


Fig. 7. Fuel rods fabricated identically to fuel rods 2-1, 2-2, 2-3 and 2-4 before irradiation. Carbonized in graphite process tubes. Note that two adjoining rods are bonded together.

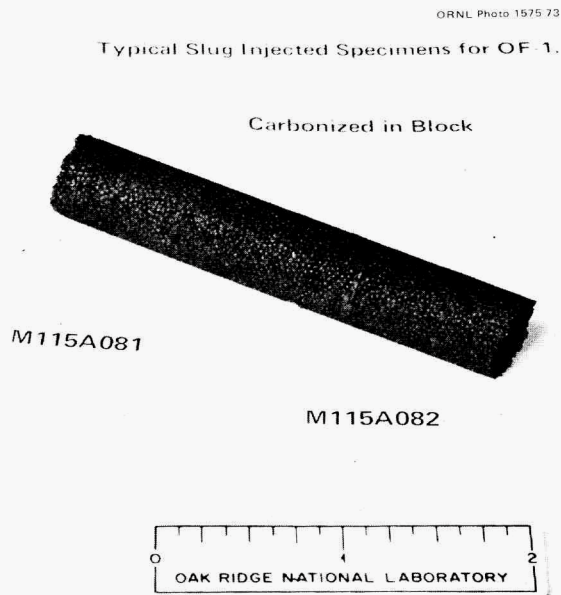


Fig. 8. Fuel rods fabricated identically to fuel rods 4-1, 4-2, 4-3 and 4-4 before irradiation. Carbonized in graphite process tubes. Note that two adjoining rods are bonded together.

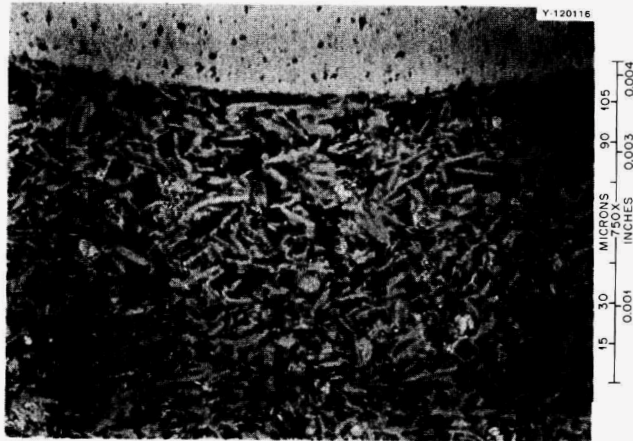


Fig. 9. Microstructure of matrix from fuel type 1. Asbury 6353 filler particles, Ashland A240 binder, carbonized in packed Al_2O_3 .



Fig. 10. Microstructure of matrix from fuel type 2. Asbury 6353 filler particles, Ashland A240 binder, carbonized in graphite process tubes (simulating in-block carbonization).

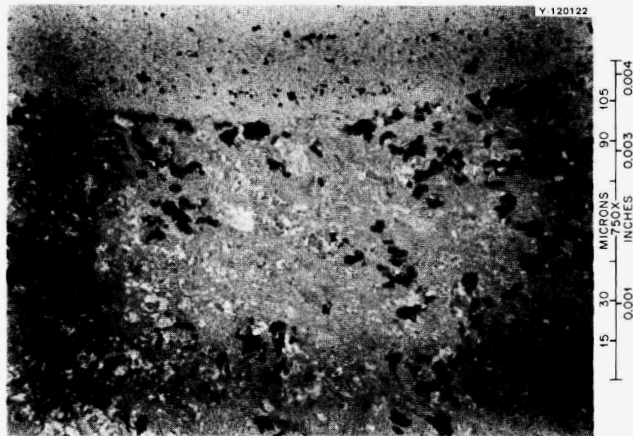


Fig. 11. Microstructure of matrix from fuel type 3. GLC 1098 filler particles, Ashland A240 binder, carbonized in graphite process tubes (simulating in-block carbonization).

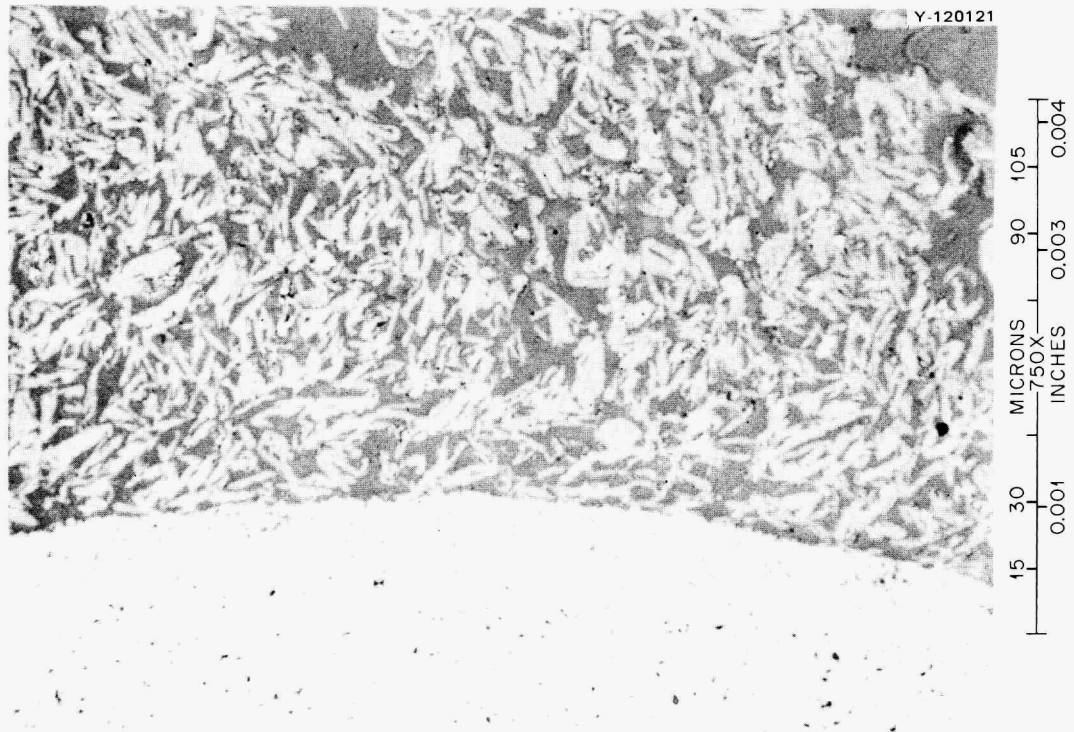


Fig. 12. Microstructure of matrix from fuel type 4. Asbury 6353 filler particles, Ashland A240 binder, carbonized in packed Al_2O_3 .

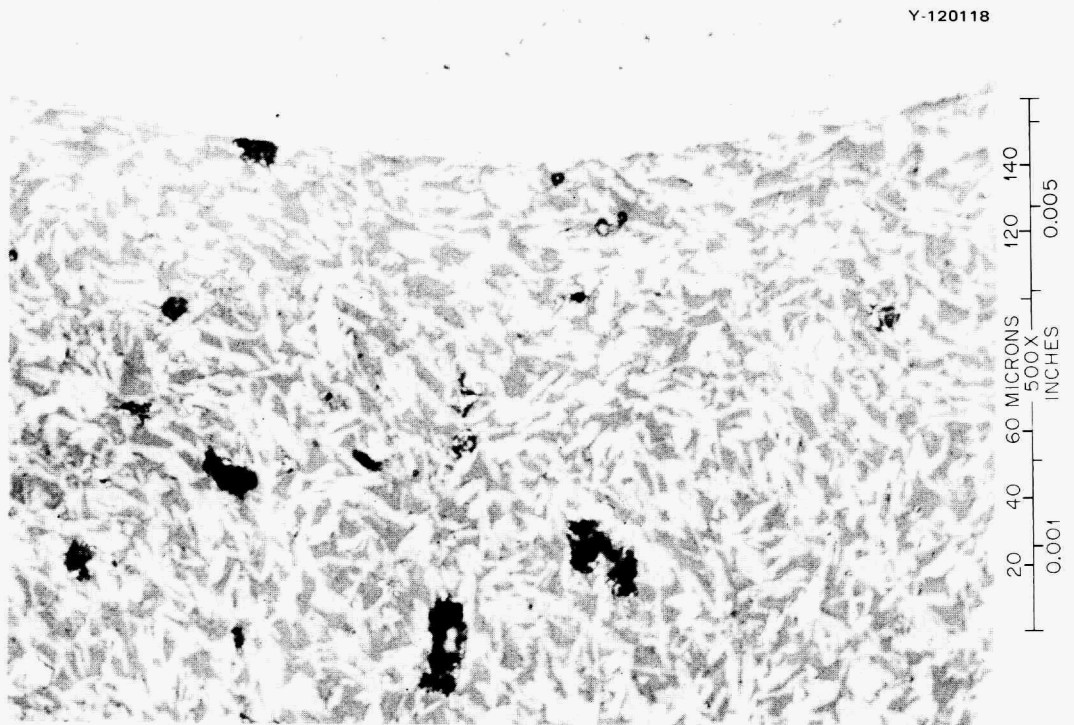


Fig. 13. Microstructure of matrix from fuel type 5. Asbury 6353 filler particles, Ashland A240 binder, carbonized in packed Al_2O_3 .

Y-120119



Fig. 14. Microstructure of matrix from fuel type 7. Asbury 6353 filler particles, Ashland A240 binder, carbonized in packed Al_2O_3 .

Y-120265

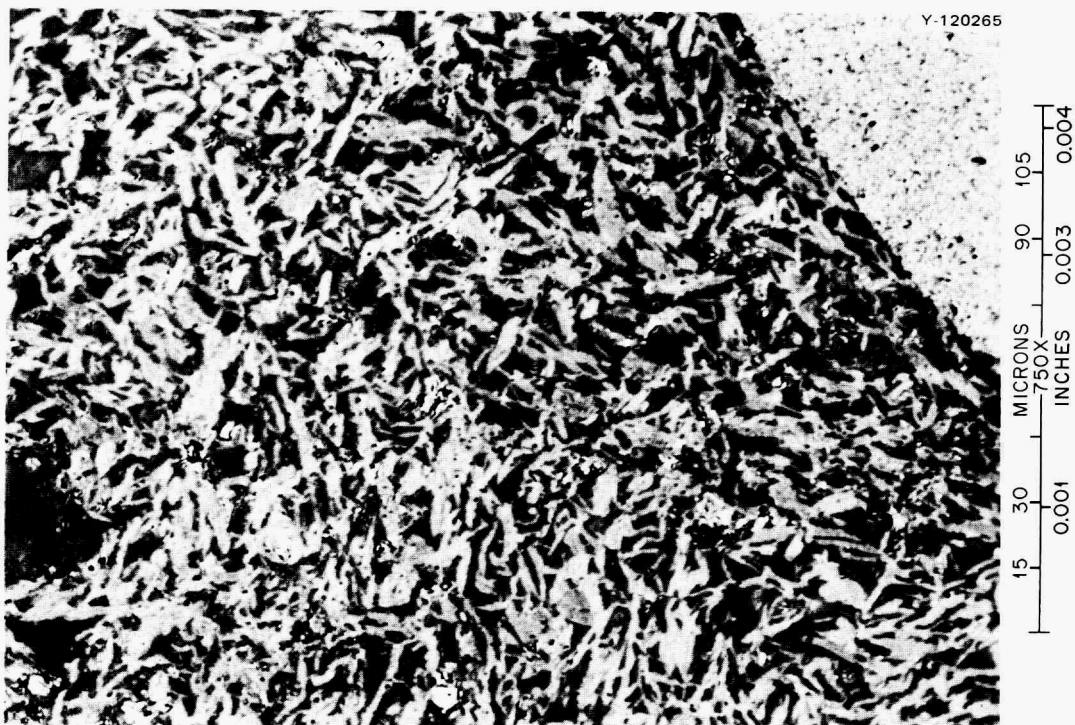


Fig. 15. Microstructure of matrix from fuel type 8. Asbury 6353 filler particles, Ashland A240 binder, carbonized in packed Al_2O_3 .

Table 4. Results of preirradiation metallographic examination of OF-1 fuel rods

Type	Particle integrity	Matrix microstructure
1	Unbroken	Open; individual filler particles clearly visible
2	Unbroken	Filled in; looks denser than type 5, appears to be bonded to the particles in many areas
3	Six were torn	Partially filled in; individual filler particles not discernible
4	Unbroken	Open; individual filler particles clearly visible
5	Unbroken	Open; individual filler particles clearly visible
6	Unbroken	Open; individual filler particles clearly visible
7	Unbroken	Open; individual filler particles clearly visible
8	Unbroken ^a	Open; individual filler particles clearly visible

^aSeveral broken particles from sample preparation (sawing and grinding).

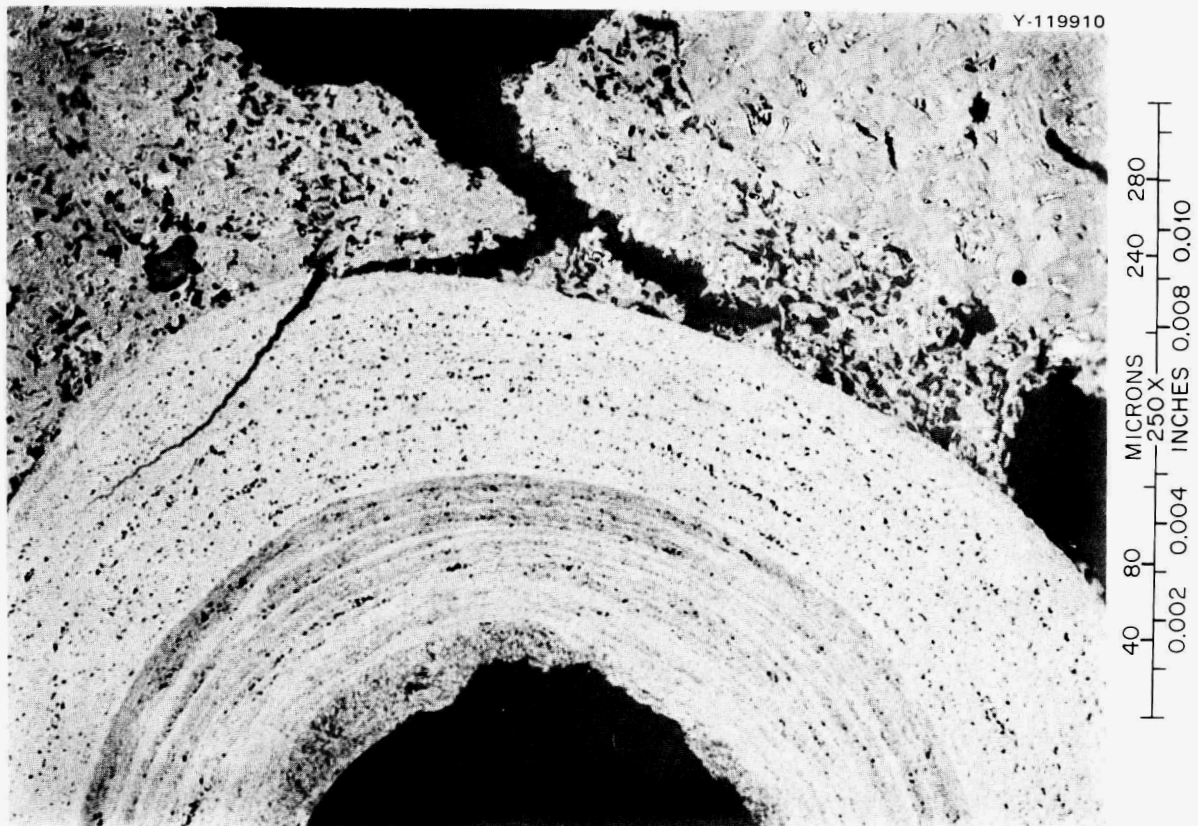


Fig. 16. Coating failure due to matrix-particle interaction in OF-1 fuel type 3.

Table 5. Results of broken particle analysis on fuel rods for OF-1

Rod type	Matrix filler ^a	Carbonization method	Heavy metal leached (μg)		Fraction leached ($\times 10^{-4}$)	
			U ^b	Th ^c	U	Th
1	29.0% Asbury 6353	Packed Al ₂ O ₃	13	<13	1.1	<0.1
2	29.0% Asbury 6353	In Block	1	8	<0.1	<0.1
3	38.5% GLC 1089	In Block	68	1613	5.8	10.3
4	29.0% Asbury 6353	Packed Al ₂ O ₃	3	<8	0.24	<0.1
5	29.0% Asbury 6353	Packed Al ₂ O ₃	4	11	0.34	<0.1
7	29.0% Asbury 6353	Packed Al ₂ O ₃	79	311	7.4	1.9
8	29.0% Asbury 6353	Packed Al ₂ O ₃	4	7	0.5	<0.1

^aAshland A240 pitch used as binder in all rods.

^bOne fissile particle contains approximately 38 μg uranium and 161 μg thorium.

^cOne fertile particle contains approximately 558 μg thorium.

CAPSULE OPERATION

Capsule OF-1 was installed in the E-3 position of the ORR on August 22, 1973; irradiation was stopped on February 23, 1975. During this time the capsule operated for 9340 hr with the reactor at full power (30 MW). This period covers ORR operating cycles 114 through 123. The capsule was out of the reactor for one entire cycle (cycle No. 119) due to an operational problem (Appendix A).

The two-cell design of the capsule allowed independent sampling of the GAC cell and the ORNL cell sweep gas systems. These samples were then analyzed to determine release-to-birth rate ratios (R/B) for selected fission-gas isotopes. Original plans called for sampling each cell once per week; however, after about 4000 hr of irradiation the nickel bulkhead that separated the two cells had failed, making it impossible to obtain accurate R/B data for each cell. The decision was made to cut off all sweep gas into the ORNL cell and operate the GAC cell at design conditions. This allowed for continued accurate sampling of the GAC cell, but eliminated any hope of obtaining R/B data in the ORNL cell. The R/B data for the first 3900 hr of operation of the ORNL cell is given (Table 6). Although sampling continued on this cell for a short period of time after the bulkhead failure, it is felt that only the data presented in Table 6 is accurate and representative of the behavior of the fuel in the ORNL cell. A performance requirement for HTGR fuel⁸ is that the R/B for ^{85m}Kr be $\leq 3 \times 10^{-5}$. Except for the second to the last reading the ORNL cell was below this level.

The average linear heat generation rate has been calculated for each fuel rod. The rate for fuel rod 3-4 (M105A117) is given (Fig. 17) because this rod was the most thoroughly instrumented. The heat generation rate history was calculated by the CACA computer code.⁹ Although no attempt was made to show each shutdown of the ORR, the total time at power and the total shutdown time are accurate. These times are lumped into larger time intervals for more convenient input to the CACA code.

The thermocouples in the ORNL cell of this capsule were unreliable (Table 7). Although all of the 0.16 cm (0.06 in.) C/A thermocouples operated throughout the test, seven of the ten 0.102 cm (0.040 in.) thermocouples had failed by the end of irradiation. The two W/Re thermocouples that measured the fuel center line temperature in hole 5 suffered severe decalibration on the order of 200–300 K.

8. D. P. Harmon and C. B. Scott, *Development on Irradiation Performance of HTGR Fuel*, General Atomic Company, GA-A13173 (October 1975).

9. E. J. Allen, *CACA-2: Revised Version of CACA- A Heavy Isotope and Fission-Product Concentration Calculational Code for Experimental Irradiation Capsules*, ORNL/TM-5266 (February 1976).

Table 6. Fission product release data for ORNL cell in capsule OF-1

Date	Operating time (hr)	Flow ^a rates He/Ne (cm ³ /min)	Temperature, K			Fission product release-to-birth ratio, R/B ($\times 10^{-5}$)				
			TE-21	TE-35	TE-36	^{85m} Kr	⁸⁷ Kr	⁸⁸ Kr	¹³³ Xe	¹³⁵ Xe
8-30-73	19.1	25.0/0	1136	1199	1383	1.01	0.365	0.442	0.192	b
8-31-73	44.5	11.0/9.1	1273	1318	1508	b	1.12	1.35	0.845	0.056
9-4-73	144	11.0/8.7	1242	1273	1453	1.97	0.775	0.900	1.45	0.318
9-11-73	291	7.5/8.2	1262	1293	1468	1.98	0.949	1.31	1.15	0.729
9-14-73	364	5.0/8.2	1259	1292	1460	1.44	0.862	0.907	1.60	0.140
9-18-73	458	5.0/11.8	1279	1306	1480	1.82	1.18	1.25	3.20	0.183
9-26-73	647	6.8/8.0	1280	1304	1473	1.94	1.64	1.43	1.76	0.273
10-5-73	862	5.0/8.0	1261	1279	1451	1.78	1.21	0.895	2.30	0.128
10-18-73	1081	7.5/10.6	1315	1340	1519	2.11	1.36	0.395	2.97	0.248
10-26-73	1264	6.0/8.3	1303	1323	1511	2.33	1.87	2.16	3.53	0.207
11-1-73	1409	5.0/11.8	1291	1316	1610	1.55	1.03	1.09	2.11	0.164
11-15-73	1662	5.0/14.6	1310	1327	1612	2.07	1.10	1.36	1.98	0.164
11-21-73	1794	6.0/14.5	1307	1321	1497	1.75	1.09	b	1.53	0.164
11-30-73	1997	1.5/7.7	1316	1322	1503	1.58	1.16	1.41	3.37	0.177
12-13-73	2199	5.0/9.7	1320	1317	1492	2.04	1.43	1.44	3.27	0.114
12-20-73	2367	2.0/8.7	1313	1302	1483	2.05	1.27	1.39	3.05	b
12-27-73	2529	4.0/8.7	1311	1300	1467	1.74	1.14	1.21	2.30	0.164
1-10-74	2858	4.2/7.8	1297	1273	1441	1.31	1.06	1.22	2.95	0.227
1-17-74	3026	1.5/10.5	1315	1286	1461	2.17	1.23	1.30	8.69	0.224
1-25-74	3210	1.5/13.1	1320	1283	1461	1.85	0.840	1.25	5.97	0.346
2-11-74	3497	2.0/11.2	1294	1258	1437	2.29	1.44	1.58	8.26	0.355
2-21-74	3720	1.5/8.5	1316	1271	out	4.40	1.88	2.07	22.8	1.53
3-1-74	3904 ^c	0/6.7	1258	1219	1386	2.50	1.17	1.28	9.68	1.28

^aDuring the time period covering samples 1-2b-1 to 1-2b-20 there was a leak in the helium emergency cooling solenoid valve which was estimated to be 5 cm³/min. Therefore the helium flow rates reported for these samples are estimated and not actually measured.

^bThe data for these samples was lost through malfunction of analysis equipment.

^cLast sample taken from ORNL cell; nickel bulkhead. Separating the ORNL magazine from the GAC magazine failed.

Table 7. Operating history of thermocouples in the ORNL cell of capsule OF-1

Thermocouple number	Type ^a	Sheath diam, cm (in.)	Operating temperature range,	Operating time (hr)	Fluence at end of test or time of failure (neutrons/cm ² $\times 10^{21}$)	
					Thermal (<1.86 eV)	Fast (>0.183 MeV)
21	C/A	0.16 (0.06)	973-1323		5.72	6.25
22	C/A	0.16 (0.06)	923-1123		5.72	6.25
23	C/A	0.16 (0.06)	973-1223		5.72	6.25
24	C/A	0.16 (0.06)	923-1123		5.72	6.25
25	C/A	0.102 (0.040)	873-1073	8950	5.48	5.99
26	C/A	0.102 (0.040)	1023-1223	9000	7.52	9.56
27	C/A	0.102 (0.040)	873-1073		6.05	7.23
28	C/A	0.102 (0.040)	1023-1123	3270	2.47	3.10
29	C/A	0.102 (0.040)	1073-1248	4990	4.60	5.78
30	C/A	0.102 (0.040)	823-1023		6.05	7.23
31	C/A	0.102 (0.040)	873-973	5850	4.42	5.54
32	C/A	0.102 (0.040)	823-1073	8440	5.17	5.65
33	C/A	0.102 (0.040)	998-1098	4040	2.73	3.40
34	C/A	0.102 (0.040)	1048-1248		7.80	9.92
35	W/Re	Bare Wire	1373-1523 ^c		5.58	6.05
36	W/Re	Bare Wire	1023-1373 ^c		8.14	10.4

^aThe C/A thermocouples are Chromel-P vs Alumel and W/Re (W-3% Re vs W-26% Re).

^bOperating time is given only for those thermocouples which gave indications of failure. All other thermocouples were still operating at the end of the 9340 hr test.

^cThese are the estimated ranges based on early operation. At the end of the test both thermocouples were indicating that they were operating in the 873 K to 1073 K range.

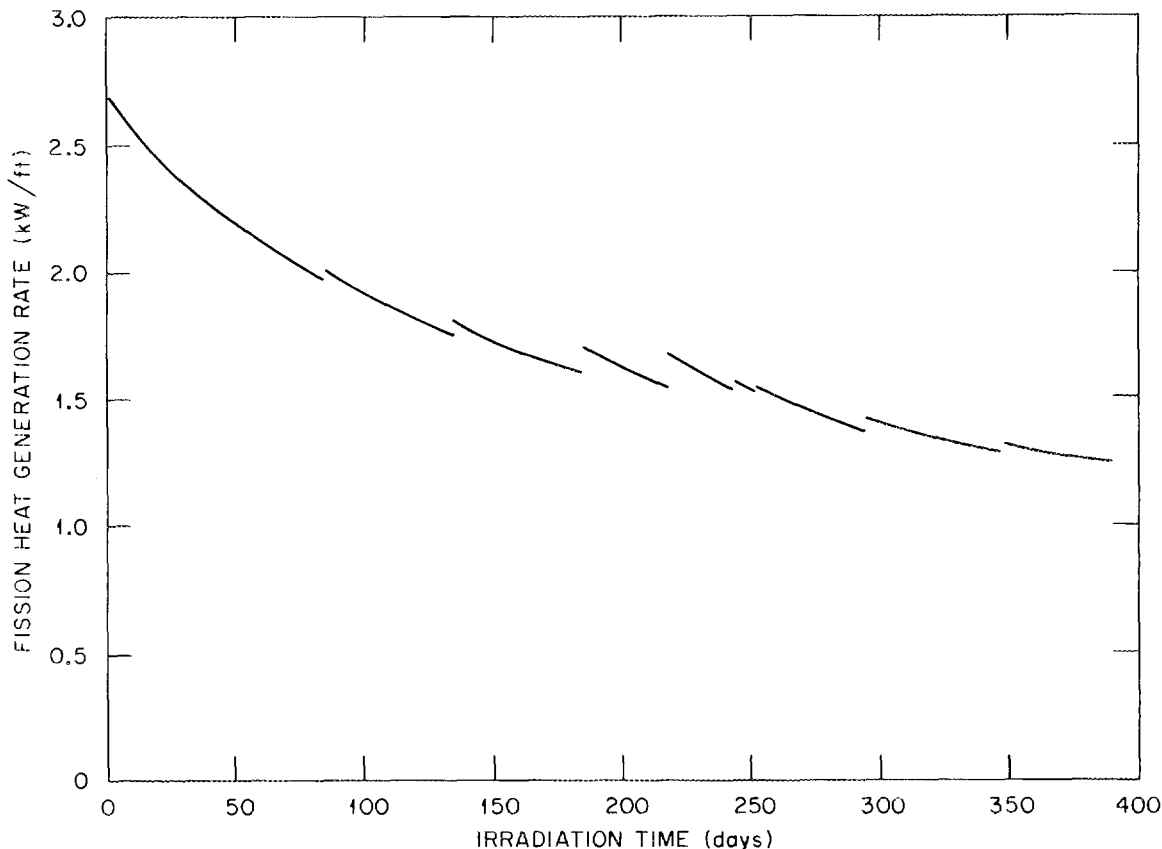


Fig. 17. History of linear heat generation rate for fuel rod 3-4 (M105A117).

DOSIMETRY ANALYSIS

An extensive dosimetry program was developed for the OF-1 experimental capsule to determine reaction rates in the fuel rods and neutron flux magnitudes and gradients.¹⁰ This program included dosimetry packages placed within the OF-1 graphite magazine and also single-cycle and multi-cycle dosimetry irradiations made in the aluminum core piece of the E-3 facility (Table 8). The additional dosimetry work measured magnitudes and gradients of neutron fluxes for different ORR core configurations. Induced activities in various dosimeter materials – including iron, cobalt, and titanium – were measured; and the following analysis for each dosimetry capsule was made.

A computer calculation¹¹ was made for a one-dimensional model of the OF-1 capsule to obtain neutron energy spectra for the fuel rods, graphite magazine, and aluminum core piece. With these spectra, the total fluxes, $\int_0^{\infty} \phi(E) dE$, and fast fluxes, $\int_{0.18 \text{ MeV}}^{\infty} \phi(E) dE$, required to induce the measured

10. E. J. Allen and H. T. Kerr, *A Summary of Neutronics Information for Irradiation Experiments in the Oak Ridge Research Reactor*, ORNL/TM-5271 (May 1976).

11. N. M. Greene et al., *AMPX: A Modular Code System for Generating Coupled Multigroup Neutron-Gamma Libraries from ENDF/B*, ORNL/TM-3706 (1974).

Table 8. Dosimetry irradiations in support of OF-1

Dosimetry capsule	Corner in E-3 facility	Cycles irradiated in ORR
S-1	NW	114-A
S-2	NE	114-A
L-1	SE	114-A
S-5	NW	117-A
S-6	NE	117-A
L-3	SE	117-A
S-3	NW	114-B to 116-D
S-4	NE	114-B to 116-D
L-2	SE	114-B to 116-D

Table 9. Calculated average burnup and fluences for the ORNL fuel rods irradiated in capsule OF-1

Fuel rod location ^a	Burnup (% FIMA)			Fluence (neutron/cm ² × 10 ²¹)	
	²³⁵ U	²³⁸ U	²³² Th	Thermal (<1.86 eV)	Fast (>0.18 MeV)
1-1	80.2	14.4	4.93	8.57	10.8
2	79.7	12.5	4.16	7.57	9.58
3	76.1	10.2	3.27	6.49	8.00
4	73.5	8.56	2.67	5.48	5.72
2-1	79.0	12.8	4.28	7.73	9.85
2	77.5	11.2	3.67	6.83	8.61
3	74.9	9.38	2.97	5.99	6.99
4	72.3	8.00	2.47	5.21	4.88
3-1	79.0	12.8	4.28	7.73	9.85
2	77.5	11.2	3.67	6.83	8.61
3	75.6	9.81	3.13	6.12	7.40
4	73.7	8.67	2.71	5.58	5.92
5	71.6	7.66	2.35	5.04	4.37
4-1	80.2	14.4	4.93	8.57	10.8
2	78.7	12.5	4.16	7.57	9.58
3	76.1	10.2	3.27	6.49	8.00
4	73.5	8.56	2.67	5.48	5.72
5-1	88.7 ^b	13.5	4.55	8.10	10.4
2	78.1	11.8	3.89	7.20	9.18
3	83.5 ^b	9.70	3.09	6.22	7.48
4	73.0	8.31	2.58	5.31	5.25

^aFuel rod location is defined as follows: the first number designates the hole number and the second number designates the elevation as shown in Fig. 1.

^bThese two fuel rods were fueled with ²³³U instead of ²³⁵U so the burnup numbers presented are for ²³³U.

activities in the dosimeters were calculated. The total fluxes and fast fluxes (> 0.18 MeV) were derived this way for each dosimetry capsule. The fluxes obtained from these dosimetry experiments have 10 to 20% gradients from the NW to the SE corner (Fig. 3) of the E-3 facility, but the neutron flux change is less than 5% for the different core configurations studied.

After removal of the OF-1 capsule from the ORR, the dosimeters were recovered and their induced activities measured. Some anomalies were observed in the activity data, particularly that of ^{54}Mn resulting from the $^{54}\text{Fe} (n,p) ^{54}\text{Mn}$ reaction. (The measured ^{54}Mn activities peaked at the lower end of the capsule. Recent information has shown this to be due to migration of the manganese.)¹² However, relative magnitudes of the other induced activities were in agreement.

With the neutron energy spectra obtained from the XSDRNPM model⁹ of the E-3 facility and the irradiation history, the total fluxes required to induce the measured activities were calculated. There was close agreement between these dosimetry results and the previous neutron flux measurements for the E-3 facility. Average fluxes for each of the fuel rods were estimated and the fluences calculated; from that information, burnup was calculated with the CACA computer code⁷ (Table 9).

FUEL SPECIMEN TEMPERATURES

As described previously the OF-1 capsule was designed so that real-time temperature data could be obtained during irradiation. Sixteen thermocouples were placed inside the capsule to monitor fuel center-line temperatures and H-451 graphite temperatures.

Real-time temperature data for the 13 graphite thermocouple positions (Fig. 2) are given (Figs. B1 through B8). Three thermocouples monitored center-line fuel temperatures. Two tungsten-rhenium thermocouples were placed in the fuel occupying central hole 5, and one Chromel-P vs Alumel thermocouple was placed in the fuel occupying peripheral hole 3 (thermocouples 35, 36, and 21 respectively in Fig. 2).

Real-time temperature data for thermocouple 21 (Fig. 18) is representative of the other peripheral fuel operating temperatures at this axial location (16.31 cm from the nickel bulkhead). Thermocouple temperatures were in the range of 1223K-1423K for ORR cycles 114 through 118. However, after cycle 119; control was lost and the temperature range dropped to 923K-1223K for cycles 120-123. The loss of temperature control was due to the failure of the nickel bulkhead separating the GAC Cell from the ORNL Cell, and the subsequent loss of the sweep-gas mixture necessary to maintain fuel temperatures. Real-time temperature data for the two tungsten-rhenium thermocouples (35 and 36) are not shown as they experienced severe decalibration due to the transmutation of rhenium to osmium.

A thermal analysis was made on the OF-1 capsule using the HEATING3 Heat Conduction Code¹³ and an appropriate two-dimensional $R-\theta$ grid model; this analysis was of ORR irradiation cycle 114 only. The $R-\theta$ grid model represented a $1/8$ circular cross section of the capsule. Because of HEATING3 geometry constraints an exact representation of the capsule could not be used (Fig. 19). Portions of fuel rods in fuel holes 3 and 5 were contained in the model. The peripheral fuel (fuel hole 3) was mocked up as a section of an annulus with its thickness the same as the fuel rod diameter. Total cross-sectional area was also the same as the fuel rod. Calculations were made at two axial planes, 5.51 cm (2.17 in.) and 16.31 cm (6.42 in.) respectively, which correspond to the axial positions of thermocouples 36 and 35 with respect to the nickel bulkhead.

12. Personal communication with H. Kerr.

13. W. D. Turner and M. Simon-Tov. *HEATING3- An IBM/360 Heat Conduction Program*, ORNL/TM-3208 (February 1971).

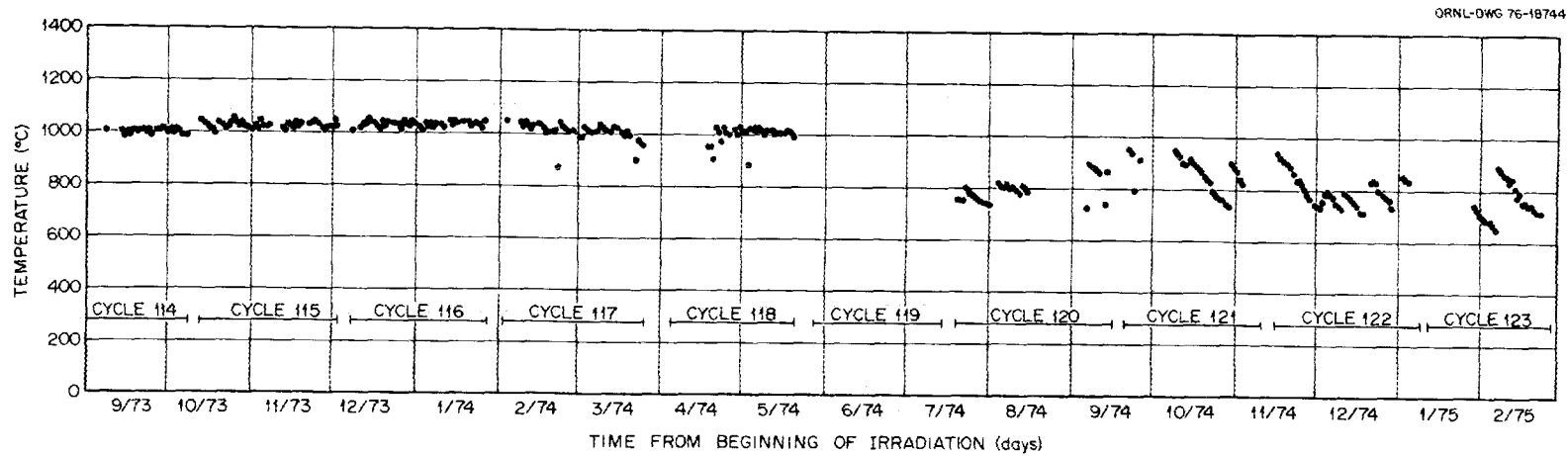


Fig. 18. Time temperature history of fuel centerline thermocouple no. 21 located in fuel hole 3 at a position about 16.31 cm (6.42 in.) from Nickel Bulkhead divider.

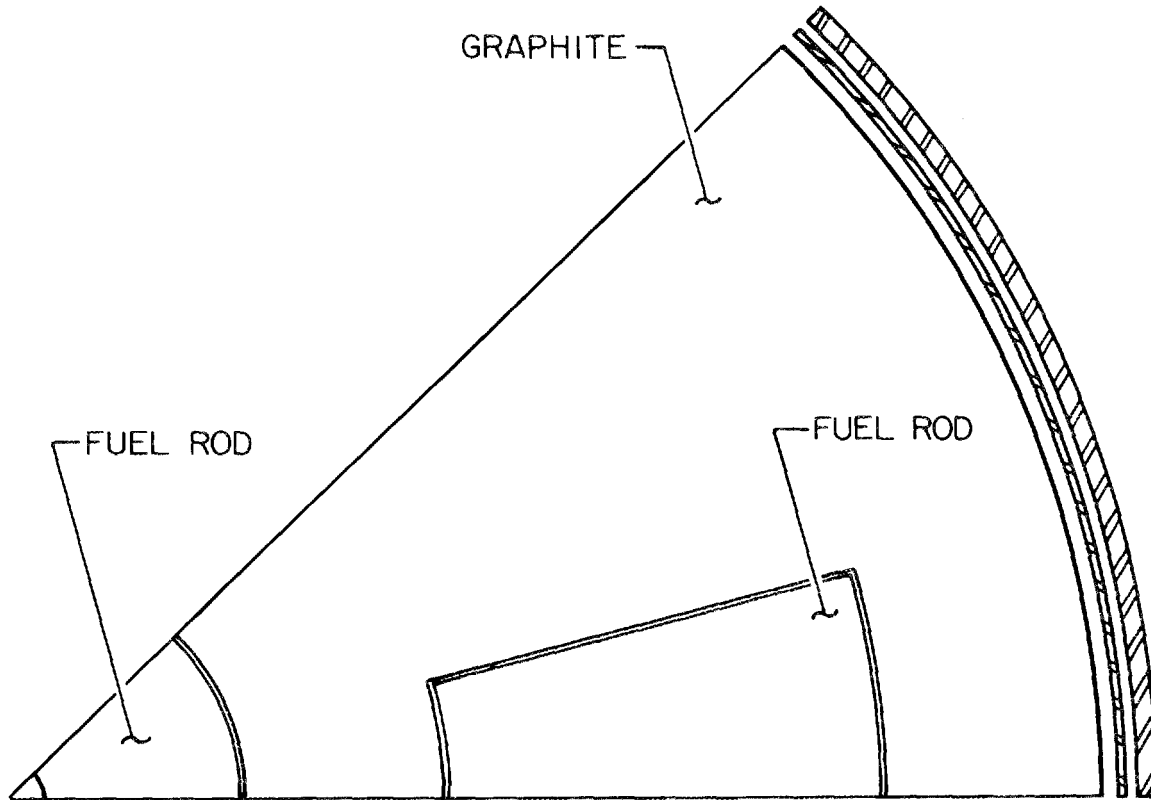


Fig. 19. Two dimensional (R- θ) grid mock-up of an $\frac{1}{6}$ section of a circular cross section of the OF-1 Irradiation Capsule.

Fission heating rates were determined from the initial fuel loadings, the total neutron flux and appropriate isotope cross sections for the E-3 position of the ORR core. These data were then used with the CACA-2 code⁷ to calculate average fission power densities for each fuel rod in holes 3 and 5 (Figs. 20 and 21). Gamma heating rates for each fuel rod were determined by Eq. (1). Both fission and γ heating¹⁴ were considered in this analysis.

$$\rho_i^\gamma = \rho_i \left\{ 7.94 - 6.22 \times 10^{-2} Z - 4.63 \times 10^{-2} Z^2 \right\}, \quad (1)$$

where

ρ_i^γ = gamma power density for the i th fuel rod,

ρ_i = density of the i th fuel rod,

Z = distance from nickel bulkhead at which calculation was made.

14. Personal communication K. R. Thoms to M. J. Kania, June 1974.

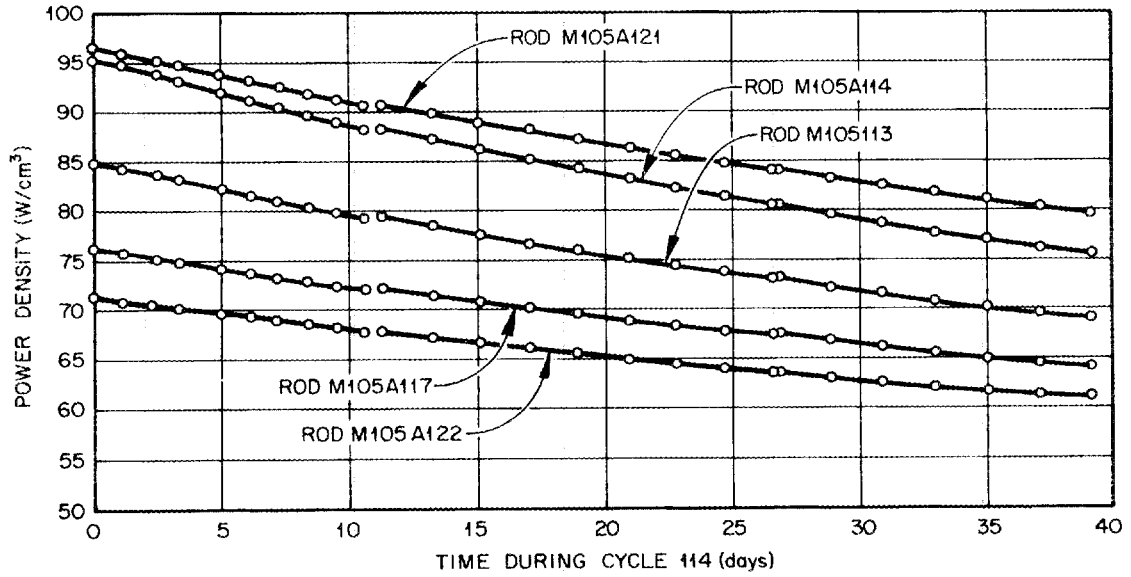


Fig. 20. Fission power density as a function of time during ORR cycle 114 for fuel rods located in peripheral fuel hole 3 of the OF-1 Irradiation Capsule.

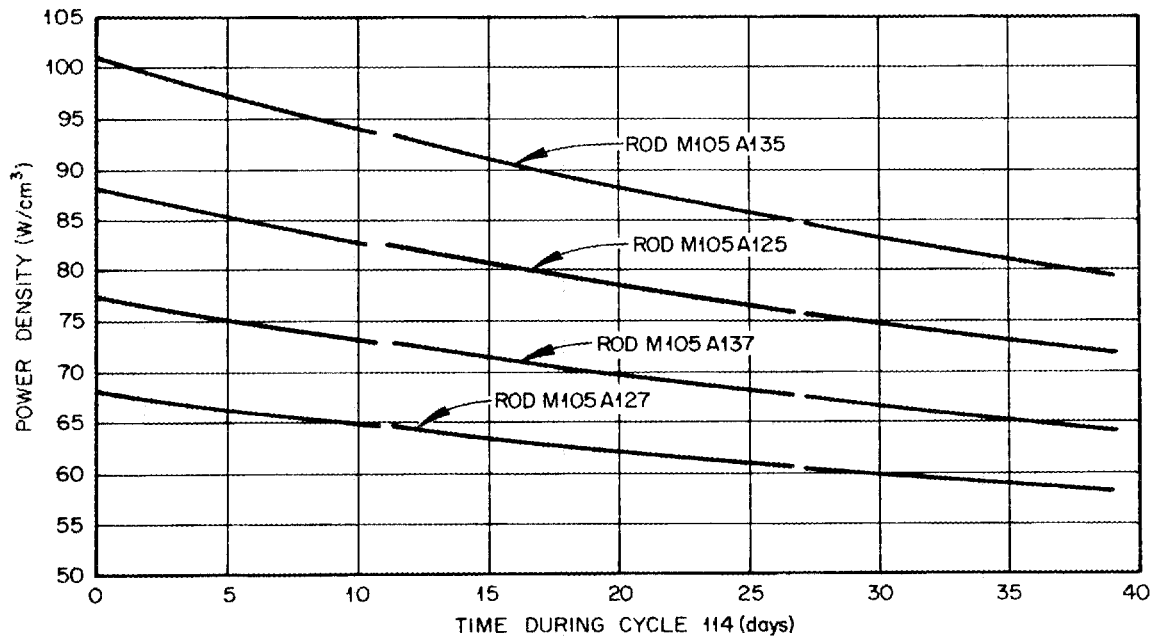


Fig. 21. Fission power density as a function of time during ORR cycle 114 for fuel rods located in central fuel hole 5 of the OF-1 Irradiation Capsule.

Beginning of life (BOL) thermal conductivities for the fuel rods and H-451 graphite magazine are shown in Fig. 22. The values for fuel rod thermal conductivity were obtained¹⁵ for rods containing 20 vol % shim particles. Also, thermal conductivity values were obtained¹⁶ for the graphite. Based on previous calculations for the OF-2 analysis¹⁷ the graphite values were reduced by 15%.

Temperature calculations were made at each axial position four times during cycle 114 at 274, 295, 485, and 862 hr of irradiation. The analysis after 274 hr provided the basis for the calculations at other times. Using the known sweep-gas composition of 100% He and BOL thermal conductivities, scaling factors were calculated for each axial position to account for axial heat flow at that position. A scaling factor of 1.0 was found at 5.51 cm (2.17 in.) and a scaling factor of 1.3 was found for the position at 16.31 cm (6.42 in.) from the nickel bulkhead. These values were used to correct the heat generation functions and were considered to be constant during this irradiation cycle. Temperature calculations after 274 hr were made for each axial position (Figs. 23 and 24).

15. W. R. Johnson, *Thermal Conductivity of Large HTGR Fuel Rods*, GA-A12910 (March 15, 1974), pp. 21–23.

16. R. J. Price, *Review of the Thermal Conductivity of Nuclear Graphite Under HTGR Conditions*, GA-A12615, (September 7, 1973), pp. 60–61.

17. K. R. Thoms and M. J. Kania, *Design, Fabrication and Initial Operation of HTGR-ORR Capsule OF-2*, ORNL/TM-5459 (in preparation).

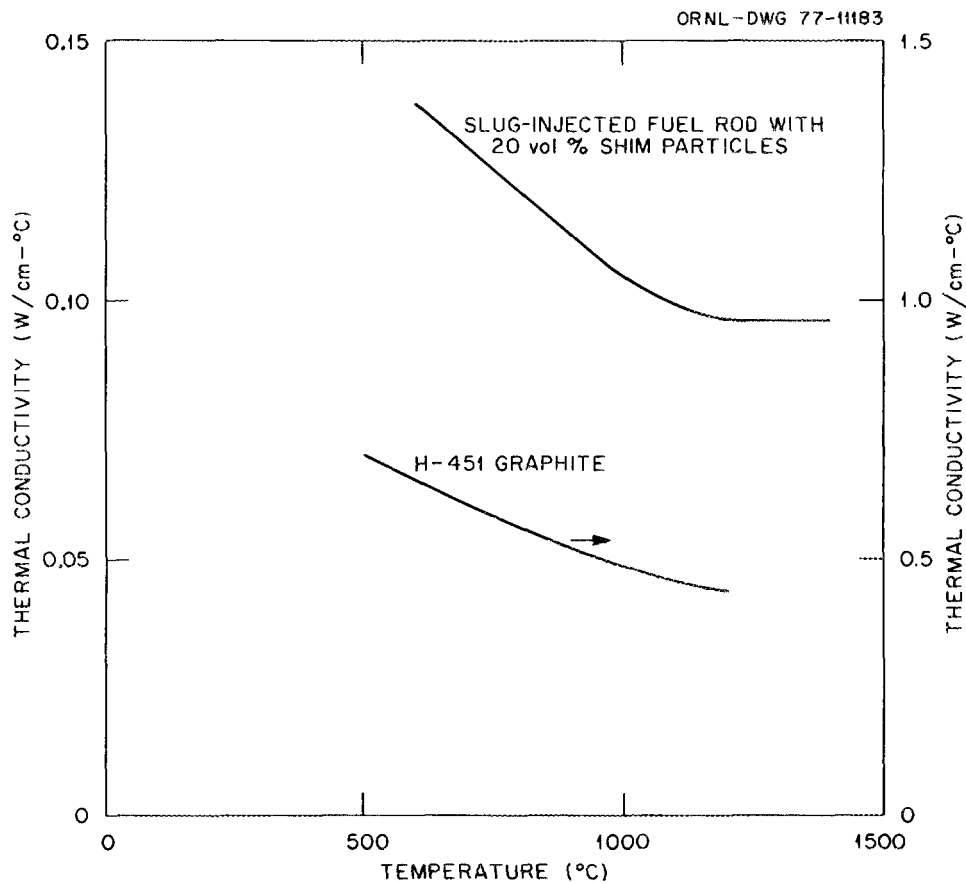


Fig. 22. Thermal conductivity as a function of temperature for beginning of life (BOL) conditions for the slug-injected fuel rods and the H-451 graphite magazine of the OF-1 Irradiation Capsule.

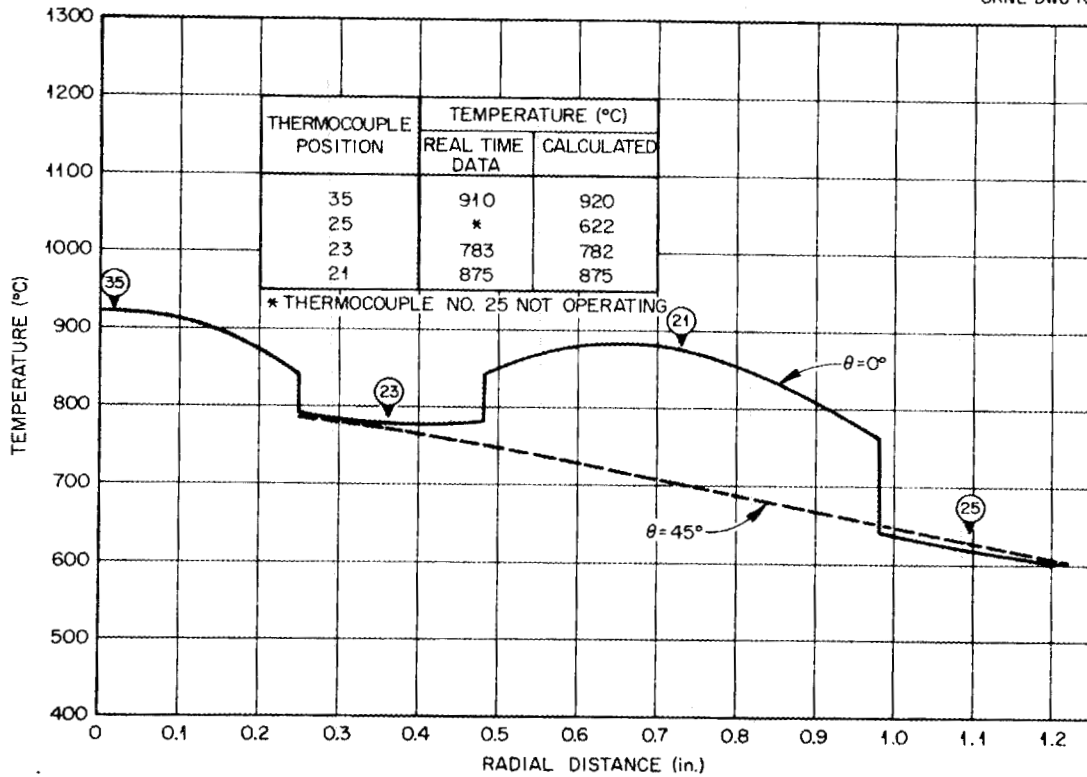


Fig. 23. Radial temperature distribution across OF-1 fuel magazine for $\theta = 0$ and 45° at a position 6.42 in. from nickel bulkhead. Calculations were made after 274 hr of irradiation with a 100% helium sweep-gas composition.

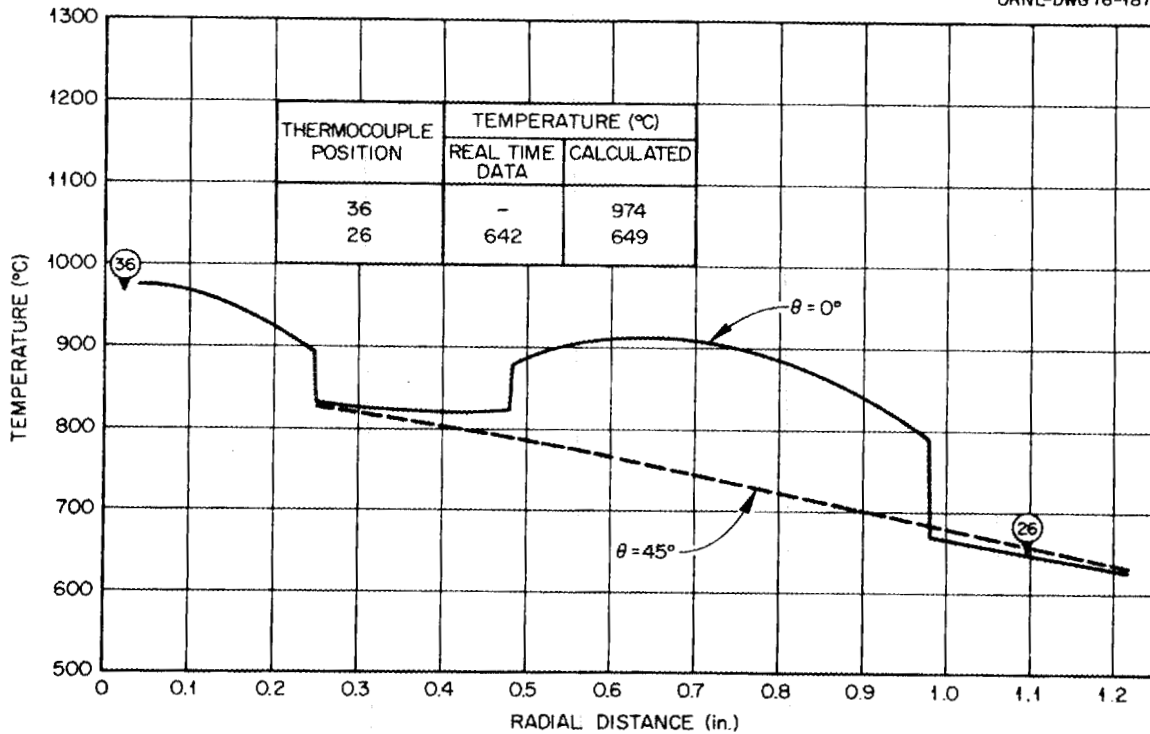


Fig. 24. Radial temperature distribution across OF-1 fuel magazine for $\theta = 0$ and 45° at a position 2.17 in. from nickel bulkhead. Calculations were made after 274 hr of irradiation with a 100% helium sweep-gas composition.

Temperature calculations after 295 hr were similar except for a mixed sweep-gas (Figs. 25 and 26). Iterating on the helium content in the sweep-gas indicated a composition of 71% He—29% Ne, providing the best agreement with the recorded thermocouple values. After 485 hr a similar iteration on sweep gas was done, but thermocouple temperatures could not be matched. The next step was to reduce the thermal conductivity of the fuel and rerun the calculations. A fuel thermal conductivity representing 87.7% of the BOL values and a sweep gas composition of 74% HE and 26% Ne provided the best agreement with observed temperatures (Figs. 27 and 28). For 862 hr, the last day of cycle 114, a reduction in fuel thermal conductivity to 75% of the initial values and a sweep gas composition of 71% He—29% Ne provided the best agreement between observed and calculated temperatures (Figs. 29 and 30).

For ORR cycles 114—118 an accurate estimate of the fuel operating temperatures can be made from the limited thermal analysis data and the real time temperature data. Operating temperatures at the axial position 16.31 cm (6.42 in.) from the nickel bulkhead were 1248 to 1348 K for the peripheral fuel and 1273 to 1373 K for the central fuel. At the axial position 5.51 cm (2.17 in.) from the nickel bulkhead operating temperatures were 1323 to 1423 K for the peripheral fuel and 1423 to 1523 K for the central fuel. From ORR cycle 120 to 123, when control was lost, fuel temperatures ranges were estimated from the Chromel-P vs Alumel thermocouple real-time data. At the lower axial position 16.31 (6.42 in.) the peripheral fuel operating temperature range was 923 to 1223 K and 973 to 1273 K for the central fuel. At the upper axial position 5.51 cm (2.17 in.) the operating temperature range was 1023 to 1323 K for the peripheral fuel and 1123 to 1423 K for the central fuel. The uncertainties in operating conditions for the OF-1 capsule during these last four ORR cycles preclude making an accurate operating temperature estimate.

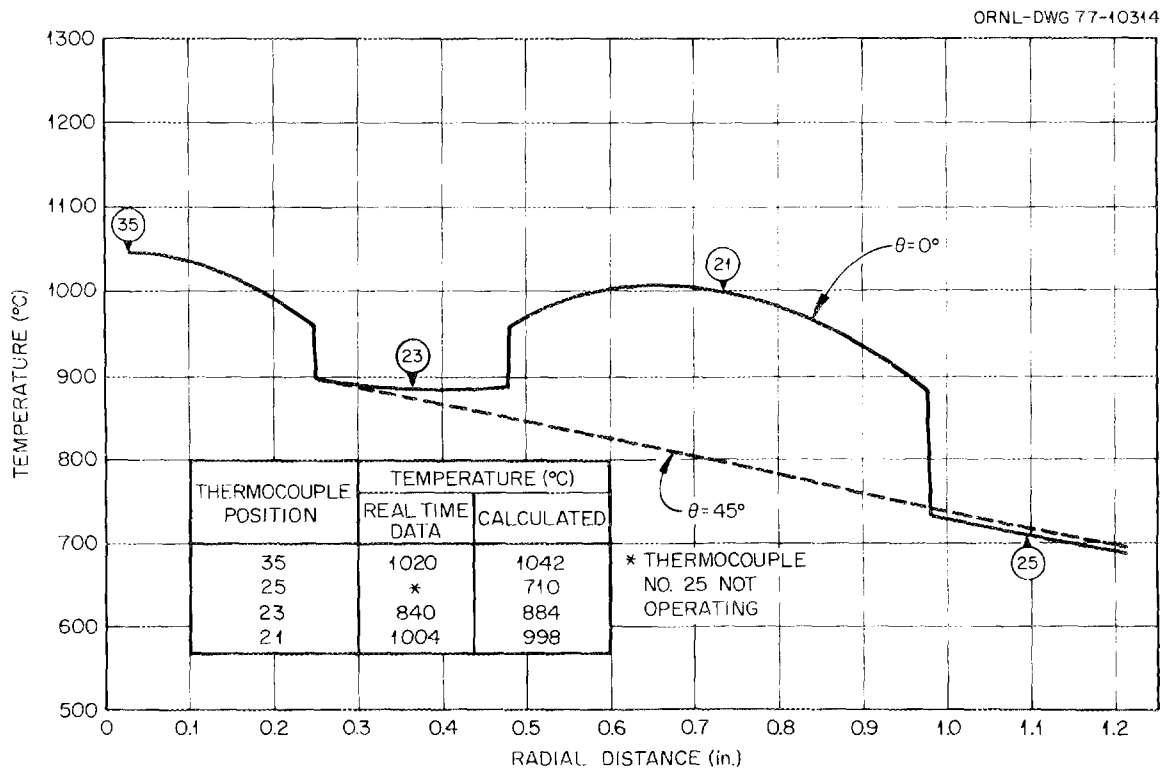


Fig. 25. Radial temperature distribution across OF-1 fuel magazine for $\theta = 0$ and 45° at a position 6.42 in. from nickel bulkhead. Calculations were made after 295 hr of irradiation with a 71% helium - 29% neon sweep-gas composition.

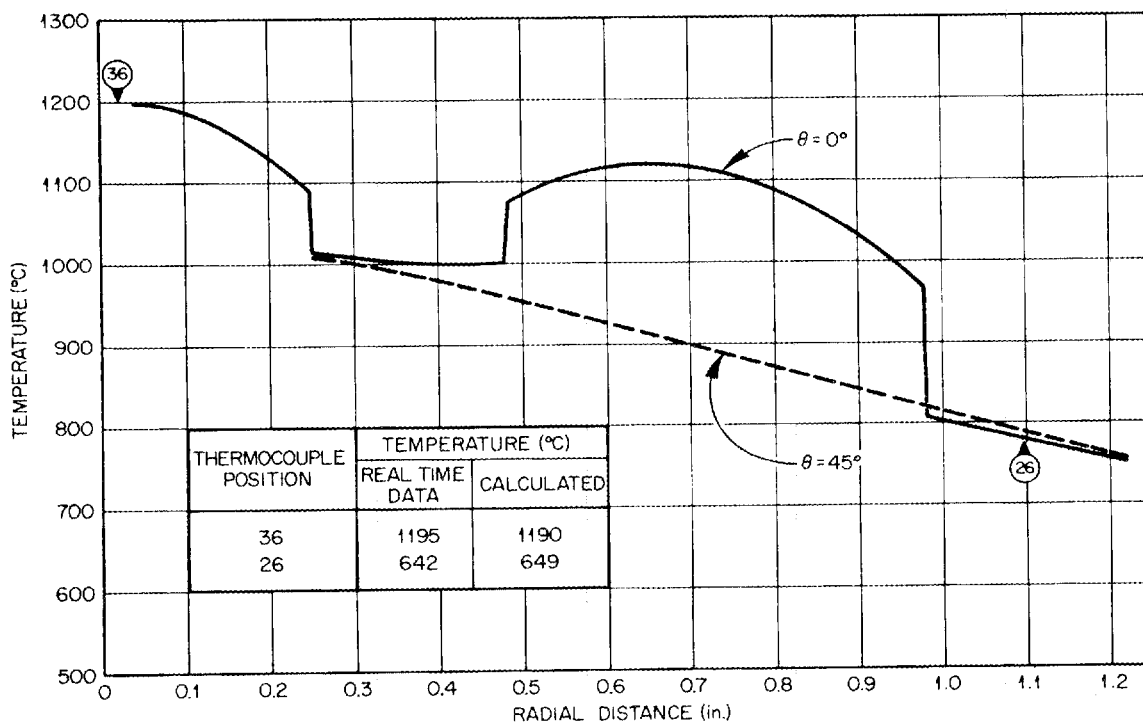


Fig. 26. Radial temperature distribution across OF-1 fuel magazine for $\theta = 0$ and 45° at a position 2.17 in. from nickel bulkhead. Calculations were made after 295 hr of irradiation with a 71% helium - 29% neon sweep-gas composition.

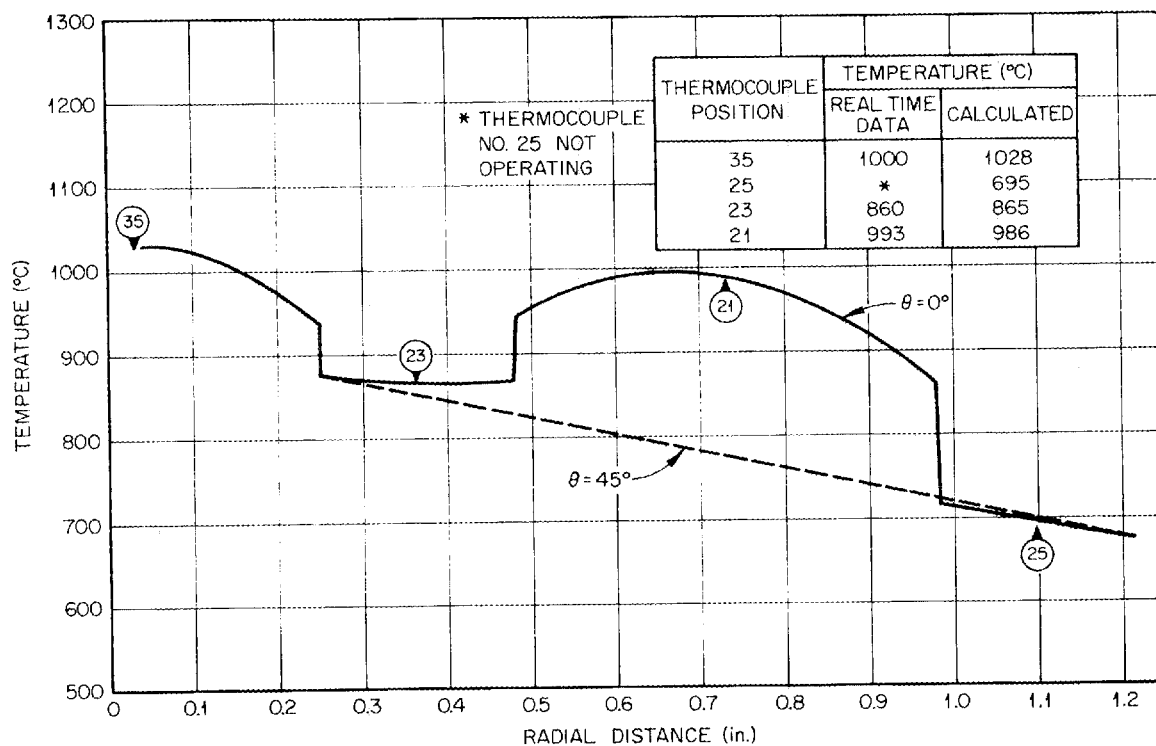


Fig. 27. Radial temperature distribution across OF-1 fuel magazine for $\theta = 0$ and 45° at a position 6.42 in. from nickel bulkhead. Calculations were made after 458 hr of irradiation with a 74% helium - 26% neon sweep-gas composition.

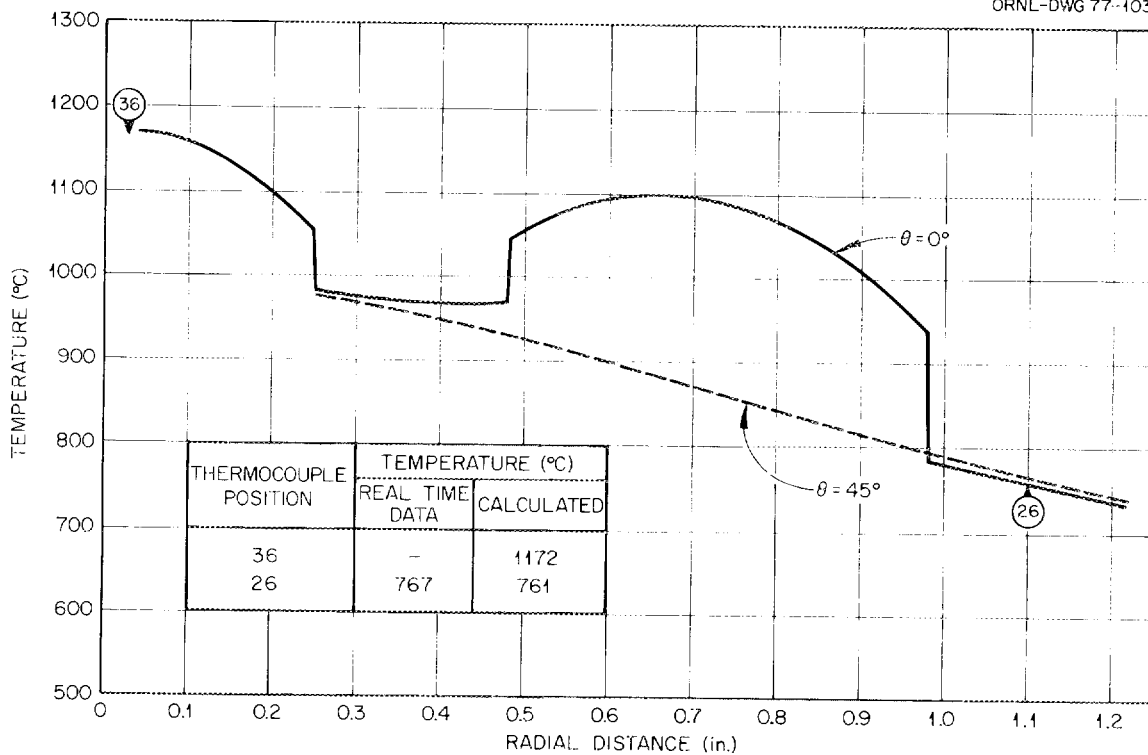


Fig. 28. Radial temperature distribution across OF-1 fuel magazine for $\theta = 0$ and 45° at a position 2.17 in. from nickel bulkhead. Calculations were made after 458 hr of irradiation with a 74% helium - 26% neon sweep-gas composition.

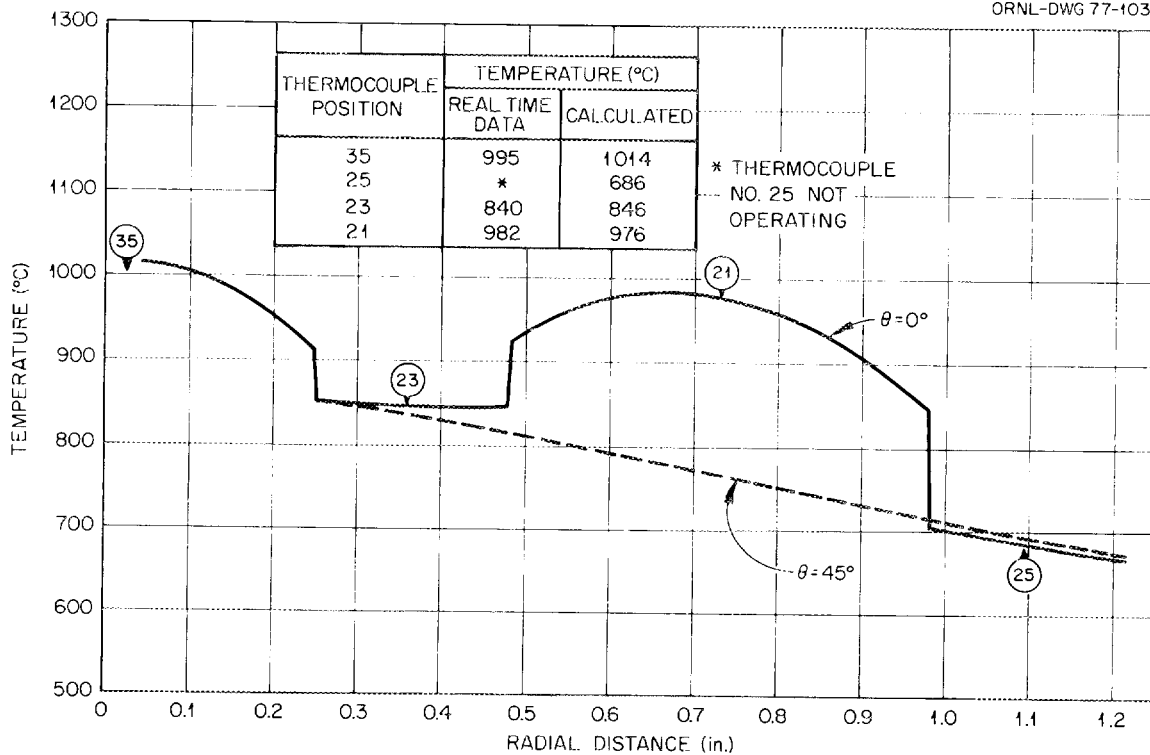


Fig. 29. Radial temperature distribution across OF-1 fuel magazine for $\theta = 0$ and 45° at a position 6.42 in. from nickel bulkhead. Calculations were made after 862 hr of irradiation with a 71% helium - 29% neon sweep-gas composition.

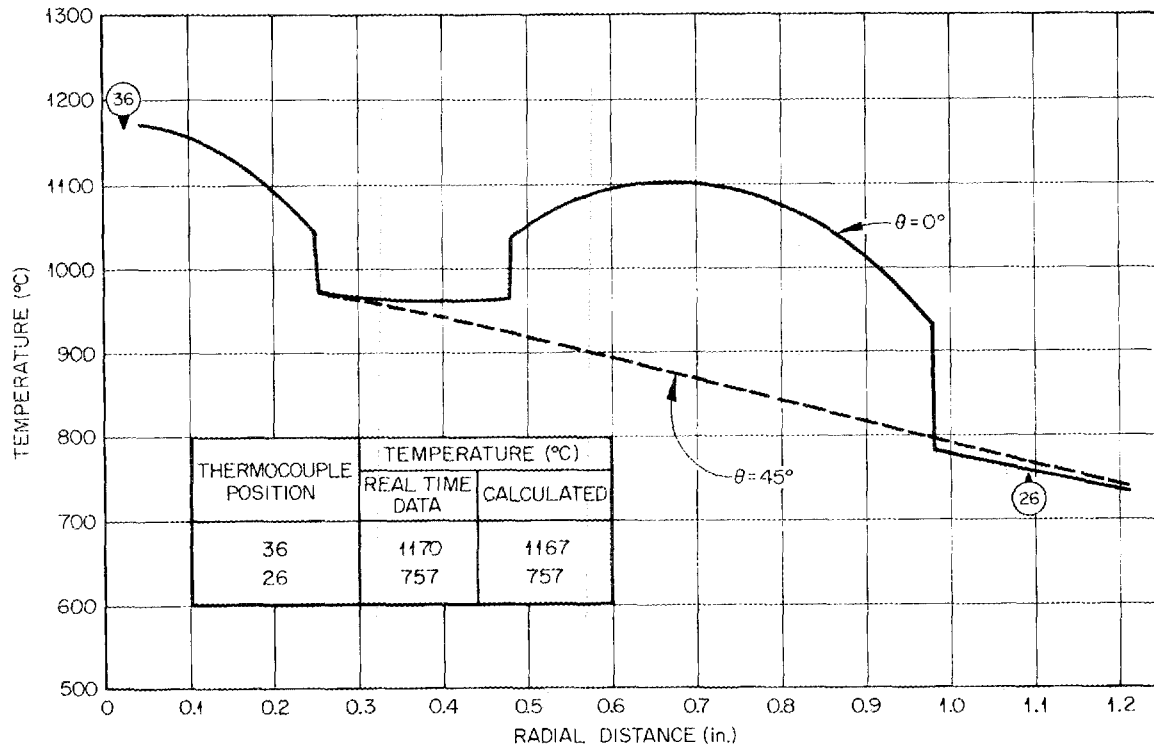


Fig. 30. Radial temperature distribution across OF-1 fuel magazine for $\theta = 0$ and 45° at a position 2.17 in. from nickel bulkhead. Calculations were made after 862 hr of irradiation with a 79% helium -- 29% neon sweep-gas composition.

DISASSEMBLY, VISUAL EXAMINATION, AND DIMENSIONAL INSPECTION

The two portions of the capsule were separated by circumferentially cutting through the two containments just below the nickel bulkhead. The GAC portion was placed in a special canister backfilled with dry, oil-free argon and shipped to San Diego for examination by GAC.

The general appearance of the OF-1 graphite magazine was excellent (Fig. 31). Differential gross gamma scans (0.55--0.75 MeV) were made along the length of the magazine at 0, 45, and 90° , respective to hole 1 (Figs. 32, 33, and 34). As expected, the average burnup decreases from the top of the magazine to the bottom. Some fuel rod interfaces are observed (Figs. 32 and 34) but they are not always clear. Hole 5 was isolated for Fig. 33 and rod interfaces can be picked out. A great deal of inhomogeneity was present in the fuel rods as indicated in Figs. 32--34.

The fuel rods carbonized in packed Al_2O_3 were easily removed by tapping the magazine on the cell floor. Removal of the fuel rods carbonized in-block required cutting the graphite magazine open (Fig. 35). With the exception of fuel type 8, all the rods were removed with essentially no apparent debonding. The rods carbonized in packed Al_2O_3 were in generally good condition, except that about half were broken into two pieces. About half of the in-block carbonized rods were also broken into pieces, but those pieces were often bonded to the adjoining rod. This result was not surprising, because the archive rods that were carbonized in graphite process tubes (simulating in-block carbonization) showed the same effect (Figs. 36--40). The visual and stereoscopic examination (Table 10) revealed a few broken particles on the surface of two rods; and in the case of rods 5-1 and 5-3 (fuel type 8), a large number of broken particles was noted (Fig. 41). This observation was not unexpected. The same batch of particles had been inserted in the HRB-6



Fig. 31. ORNL OF-1 graphite magazine and capsule endcap with thermocouples. 0.4x.

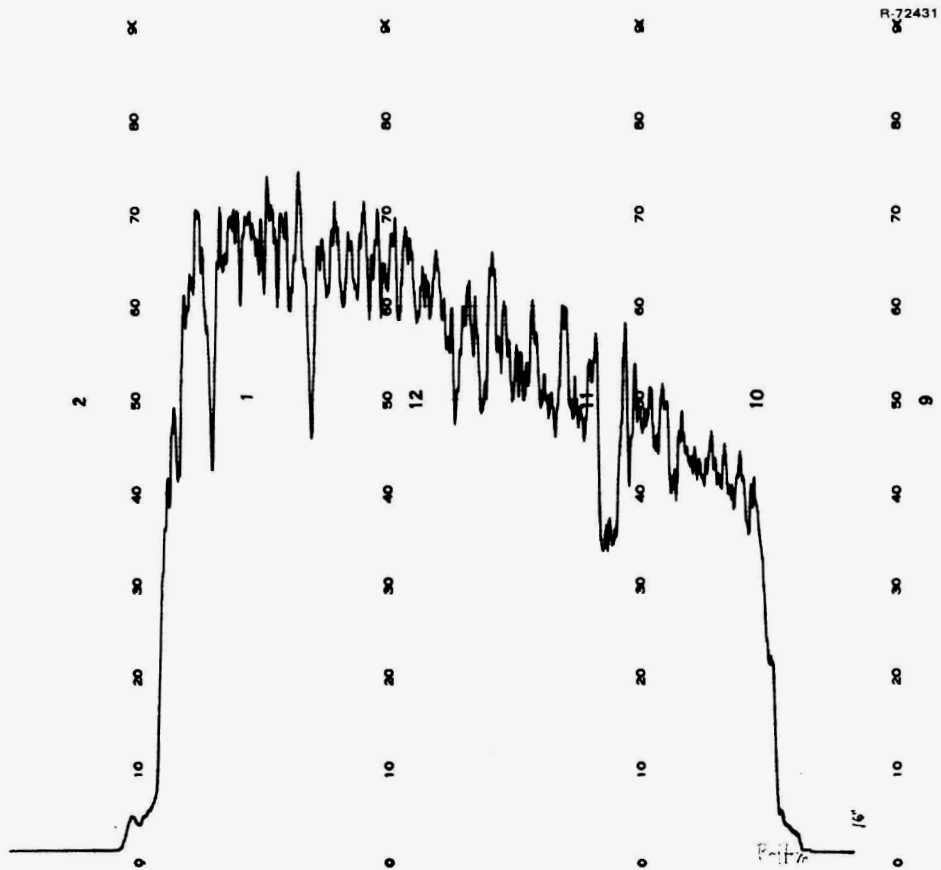


Fig. 32. Differential gross gamma scan (0.55–0.75 MeV) along the length of OF-1 magazine at 0° , respective to hole 1, from top to bottom. This configuration “looks” across holes 1, 3 and 5.

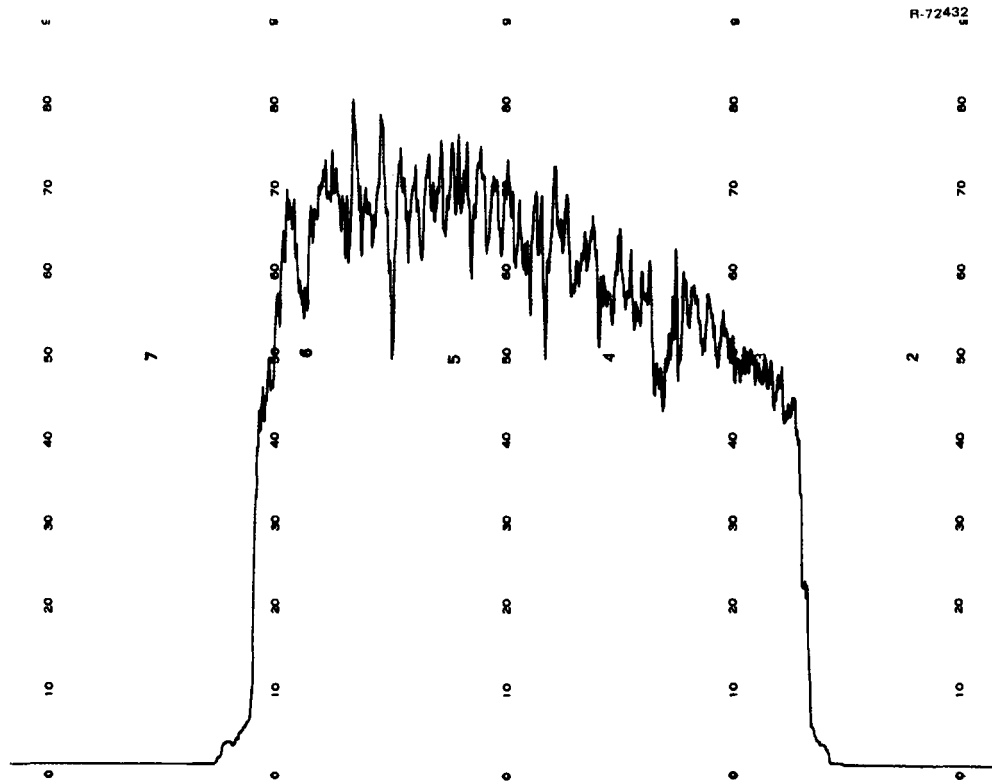


Fig. 33. Differential gross gamma scan (0.55–0.75 MeV) along length of OF-1 magazine at 45° , relative to hole 1, from top to bottom. This configuration is isolated on hole 5.

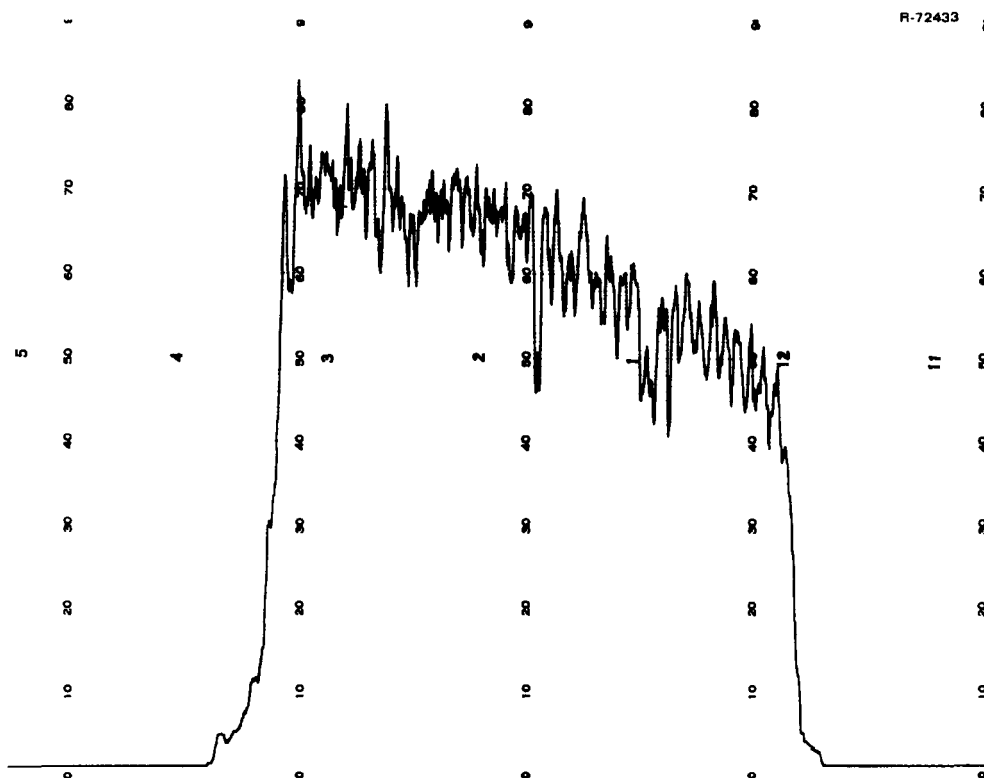


Fig. 34. Differential gross gamma scan (0.55–0.75 MeV) along length of OF-1 magazine at 90° , relative to hole 1, from top to bottom. This configuration "looks" across holes 2, 4 and 5.

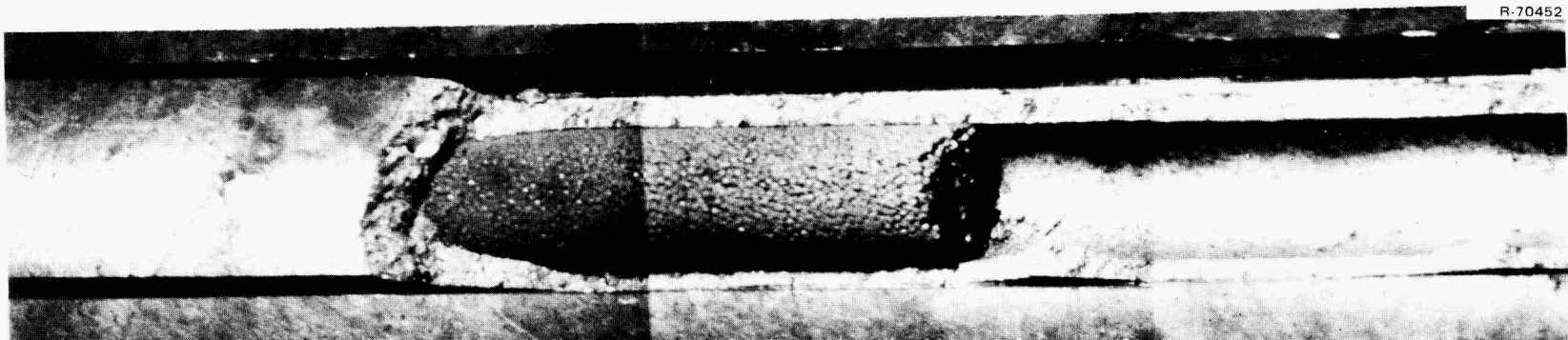


Fig. 35. Hole 2 where the OF-1 graphite magazine had to be cut open for fuel rod removal. (0.5×).

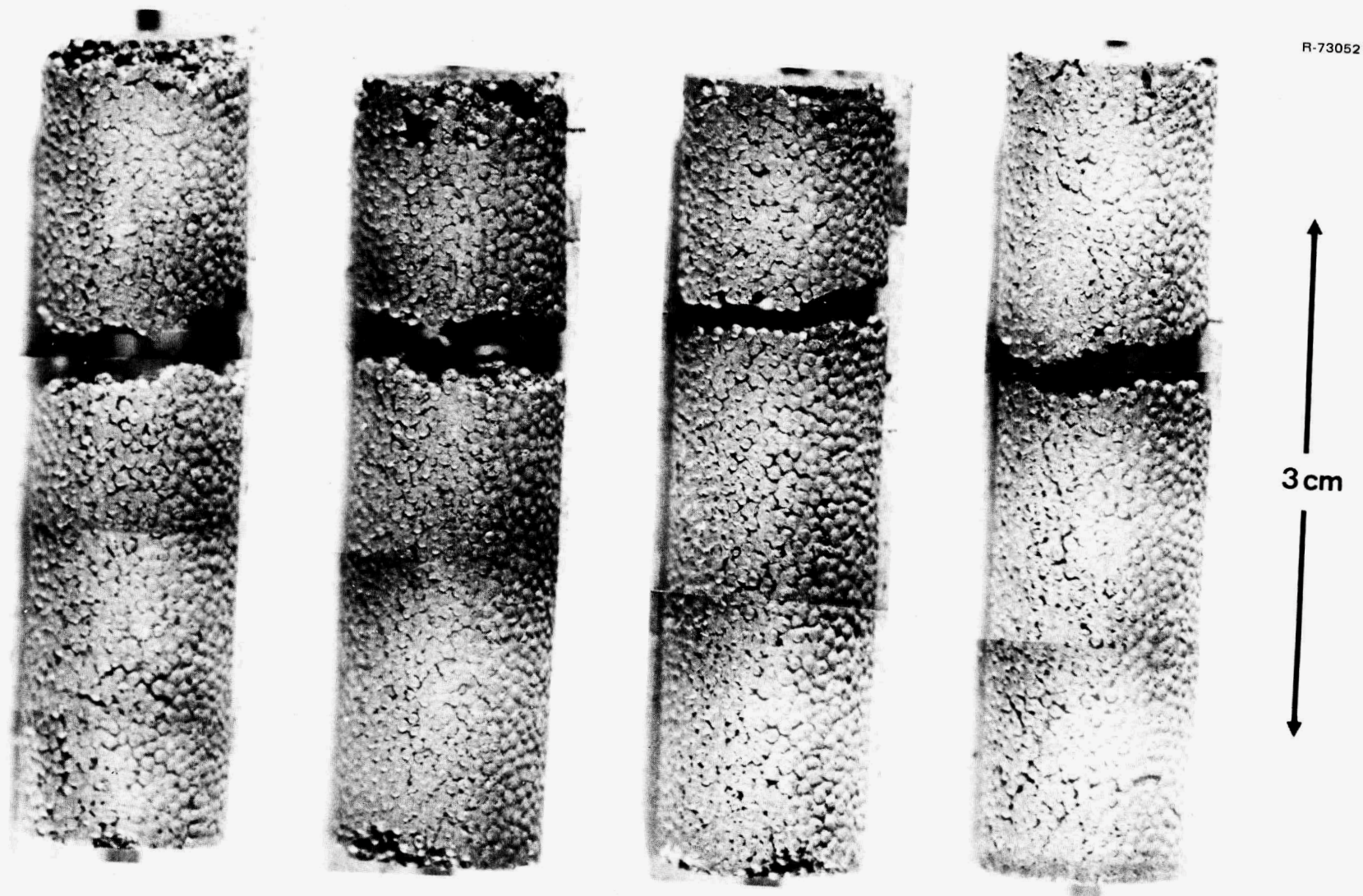


Fig. 36. Fuel rods 1-1, 1-2, 1-3 and 1-4 (left to right) after irradiation. Carbonized in packed Al_2O_3 .

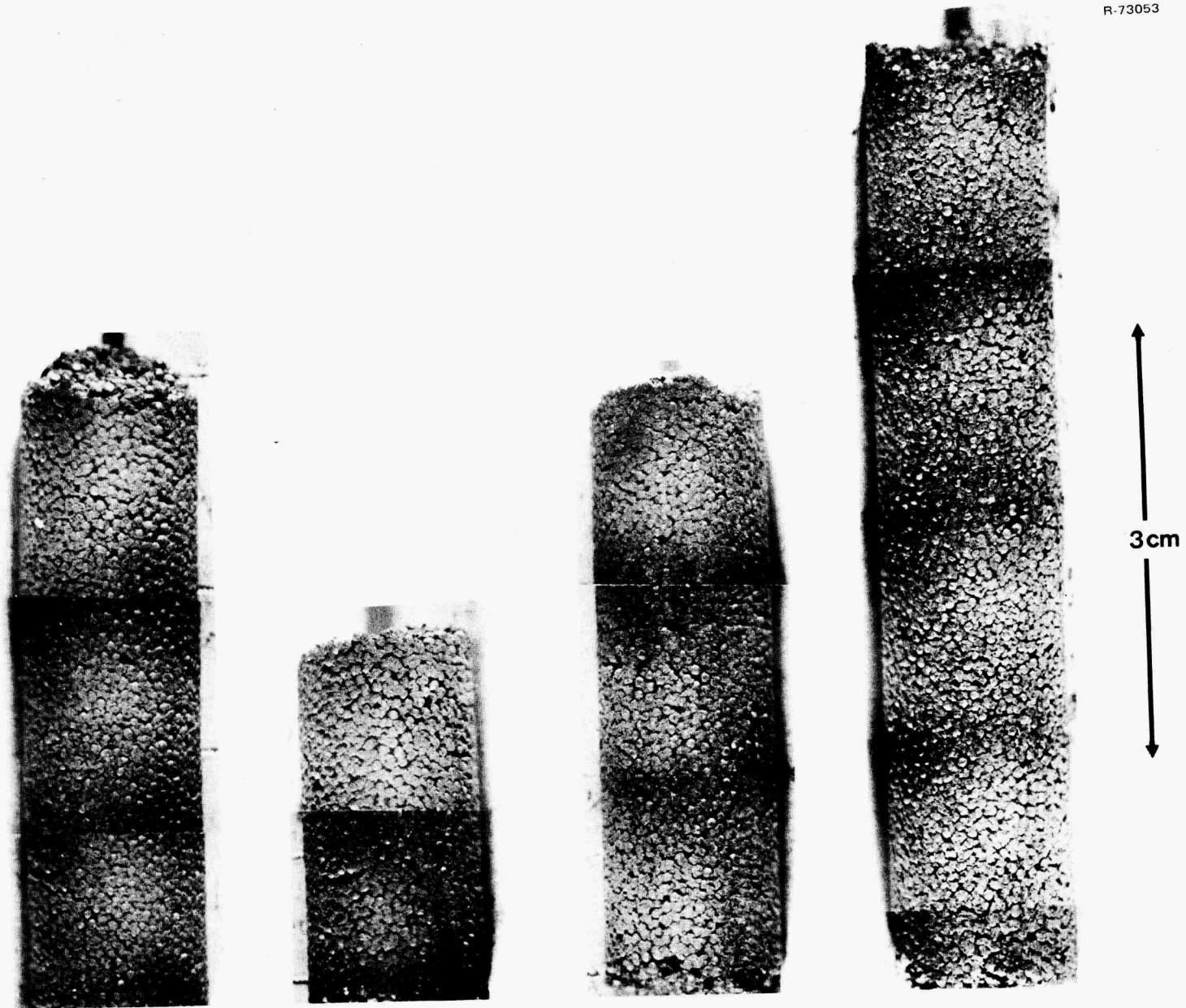
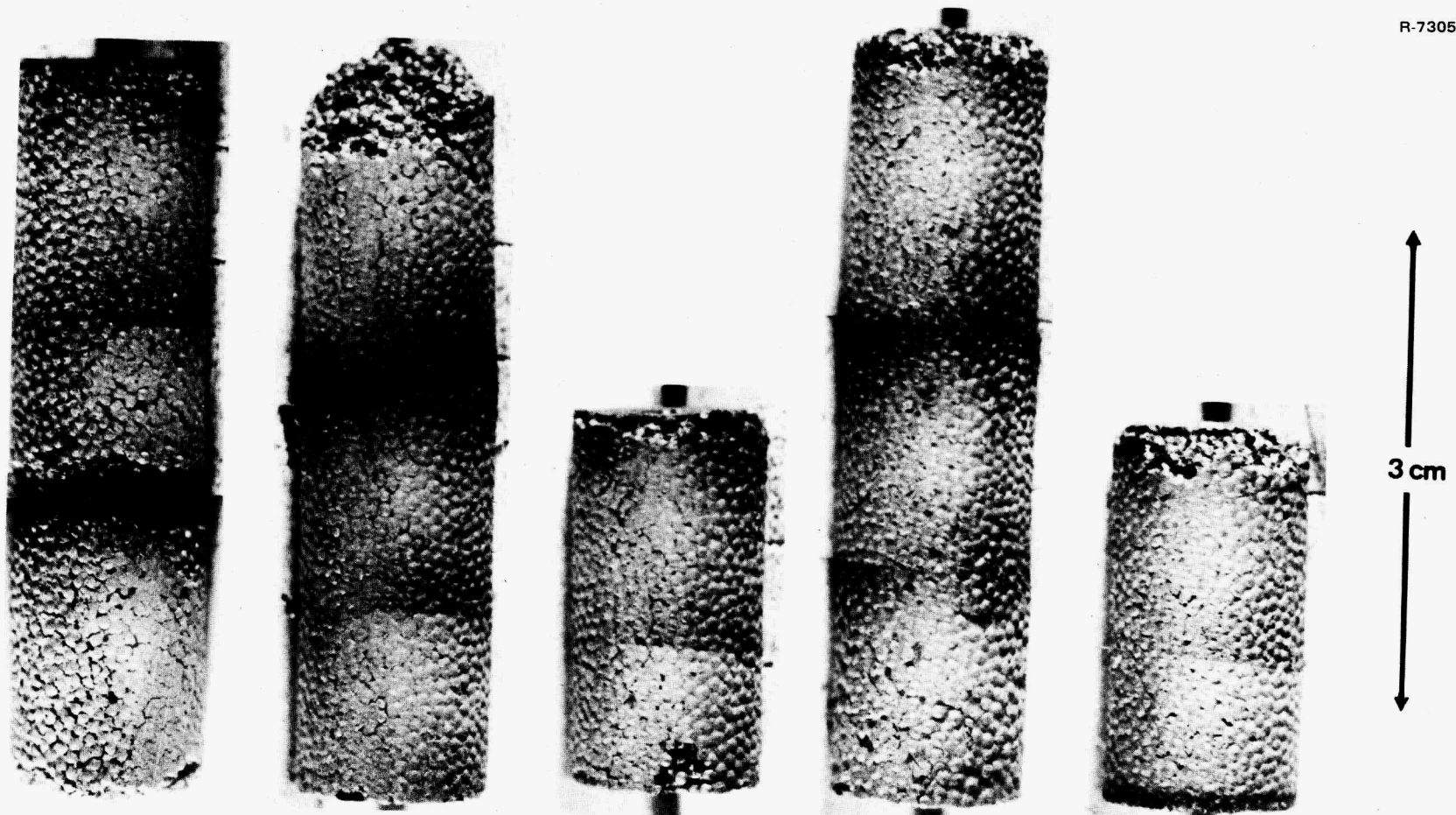


Fig. 37. Fuel rods from hole 2; (from left to right) fuel rod 2-1, top half of 2-2, the bottom of 2-2 bonded to the top of 2-3, and the bottom of 2-3 bonded to 2-4. These rods were carbonized in the graphite magazine.



R-73054

3 cm

Fig. 38. Fuel rods 3-1, 3-2, 3-3, 3-4 and 3-5 (left to right) after irradiation. Rods carbonized in packed Al₂O₃.

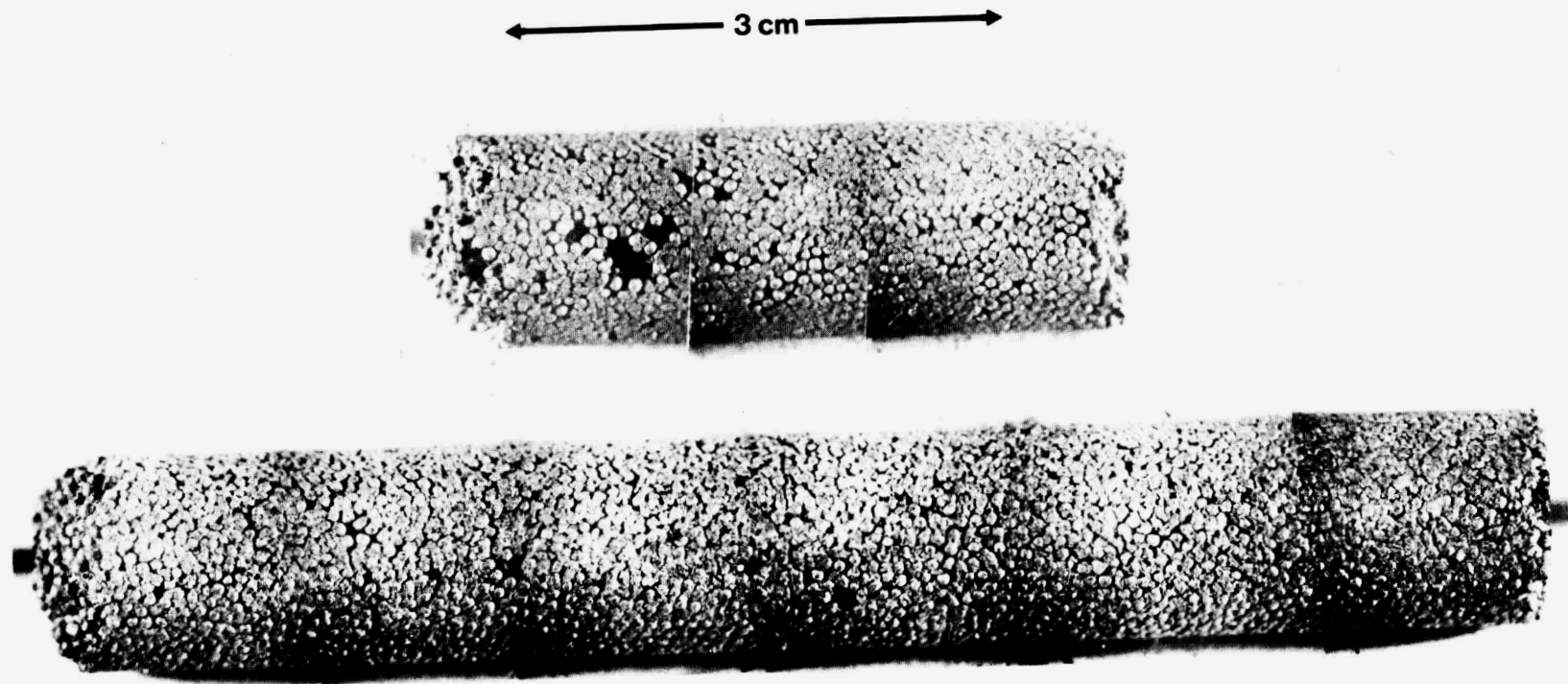


Fig. 39. Fuel rods 4-1 (top) and 4-3 bonded to 4-4 (bottom) after irradiation. Rods carbonized in graphite magazine.

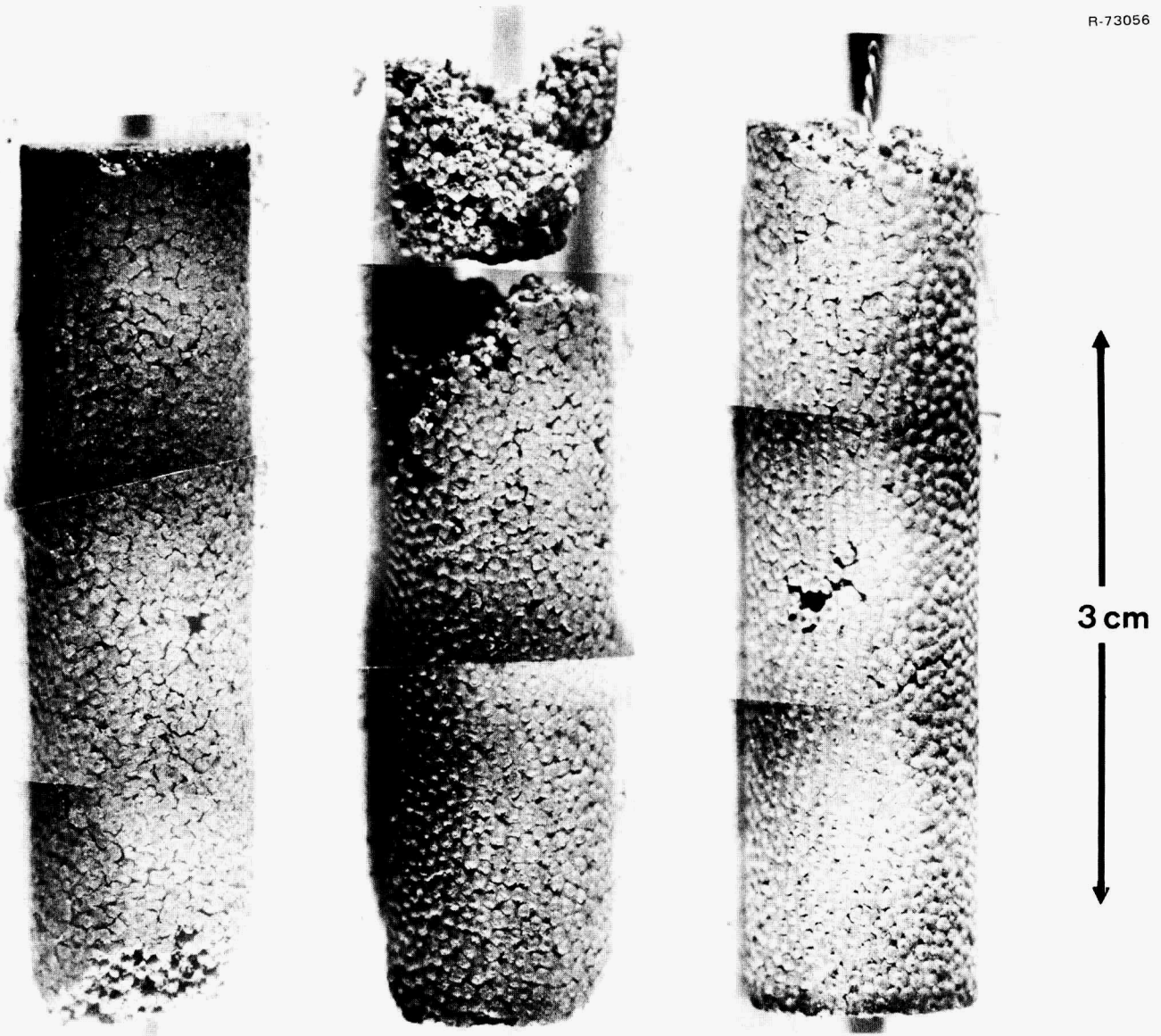


Fig. 40. Fuel rods 5-2, 5-3 and 5-4 (left to right) after irradiation. Rods carbonized in packed Al_2O_3 .

Table 10. Summary of OF-1 postirradiation observations

Rod ^a	Rod type	Carbonization technique	Fissile particle coater	Filler type ^b		Thermo-couple	General condition of rod	Stereoscopic examination
				GLC-1089 ^c	6353 ^d			
1-1	1	Packed bed	12.7 cm (5 in.)		x		Rod in 2 pieces, but no extensive debonding.	No broken particles observed.
1-2	1	Packed bed	12.7 cm (5 in.)		x		Rod in 2 pieces, but no extensive debonding.	No broken particles observed.
1-3	1	Packed bed	12.7 cm (5 in.)		x		Rod in 2 pieces, but no extensive debonding.	No broken particles observed.
1-4	1	Packed bed	12.7 cm (5 in.)		x		Rod in 2 pieces, but no extensive debonding.	A number of broken inert particles observed on surface, but no broken fissile particles.
2-1	2	In-block	12.7 cm (5 in.)		x		Rod intact with slight debonding at top.	No broken particles observed.
2-2	2	In-block	12.7 cm (5 in.)		x		Rod in 2 pieces, but no extensive debonding. One-half of rod is bonded to 2-3.	No broken particles observed.
2-3	2	In-block	12.7 cm (5 in.)		x		Rod in 2 pieces, but no extensive debonding. One-half of rod is bonded to 2-3.	No broken particles observed.
2-4	2	In-block	12.7 cm (5 in.)		x		Rod intact with no debonding. Bonded to half of 2-3.	No broken particles observed.
3-1	4	Packed bed	2.5 cm (1 in.)		x		Rod in 2 pieces, but no extensive debonding.	No broken particles observed.
3-2	4	Packed bed	2.5 cm (1 in.)		x		Rod essentially intact, with some debonding at top.	No broken particles observed.
3-3	6	Packed bed	12.7 cm (5 in.)		x	x	Rod intact, with slight debonding at top.	No broken particles observed.
3-4	5	Packed bed	12.7 cm (5 in.)		x	x	Rod intact with slight debonding at top.	No broken particles observed.
3-5	6	Packed bed	12.7 cm (5 in.)		x	x	Rod intact with slight debonding at top.	No broken particles observed.
4-1	3	In-block	12.7 cm (5 in.)	x			Rod essentially intact, with some debonding at both ends.	No broken particles observed.
4-2	3	In-block	12.7 cm (5 in.)	x			Completely debonded.	A few broken particles (3) were observed; but was unable to identify what type.
4-3	3	In-block	12.7 cm (5 in.)	x			Rod intact with some debonding at the top. Bonded to 4-4.	No broken particles observed.

Table 10 (continued)

Rod ^a	Rod type	Carbonization technique	Fissile particle coater	Filler type ^b		Thermo-couple	General condition of rod	Stereoscopic examination
				GLC-1089 ^c	6353 ^d			
4-4	3	In-block	12.7 cm (5 in.)	x			Rod intact and bonded to 4-3.	No broken particles observed.
5-1	8	Packed bed	2.5 cm (1 in.)		x	x	Completely debonded.	A large number of broken particles (>20) observed with cracked and missing coatings. Unable to identify the type of particles.
5-2	7	Packed bed	2.5 cm (1 in.)		x	x	Rod intact with some debonding on bottom.	No broken particles observed.
5-3	8	Packed bed	2.5 cm (1 in.)		x	x	Rod essentially intact with debonding at top.	A large number of broken particles (13) observed with cracked and missing coatings. Unable to identify the type of particles.
5-4	7	Packed bed	2.5 cm (1 in.)		x	x	Rod intact with slight debonding on top.	No broken particles observed.

^aThe first number is the hole number and the second is the relative rod position from top to bottom.

^bA-240 pitch binder.

^cAbout 34 wt % filler.

^dAbout 29 wt % filler.

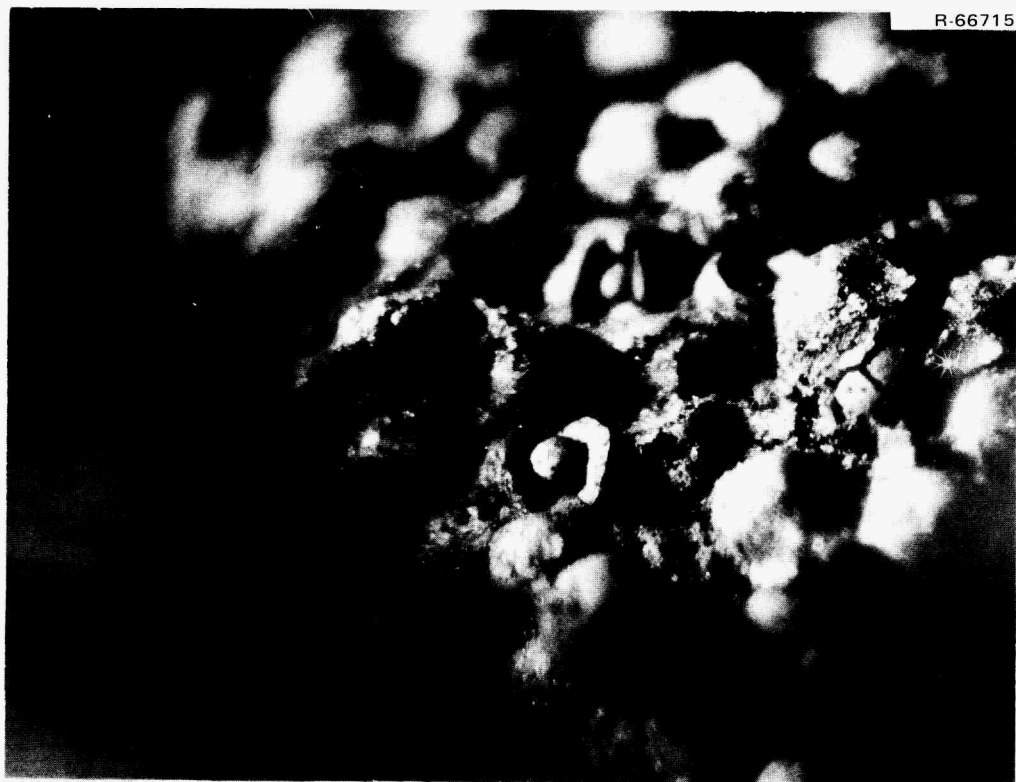


Fig. 41. Broken particles visible on surface of rod 5-1. (20X)

capsule irradiated in the removable beryllium facility of the High Flux Isotope Reactor (HFIR) with similar experience.¹⁸ Failures in these rods will be discussed further in the Metallography section.

Because rods could not be inspected after in-block carbonization, only those rods carbonized in packed Al_2O_3 could be analyzed for dimensional changes (Table 11). As expected from previous irradiation tests, the slug-injected rods at the higher temperature and fast flux positions experienced the greater shrinkages.^{18,19} From the limited number of rods where length measurements could be taken, the shrinkage appears to be relatively isotropic. A plot of the fuel rod diametrical change as a function of fast fluence (>0.18 MeV) is shown in Fig. 42. The fuel rods exhibited shrinkage up to a fast fluence of about 8×10^{21} neutrons/cm² at which point a turnaround was encountered and the rods began to swell. The turnaround was encountered at a higher than usual fast fluence.¹⁸⁻²² The various pitch-coke yields (13–21%) and matrix densities (0.47–0.57 gm/cm³) seemed to have little effect on the shrinkage. One odd data point was from fuel rod 5-3 (fuel type 8), which had numerous particle failures that may have affected its dimensional behavior.

The diametrical change of the OF-1 graphite magazine as a function of the fast fluence (>0.18 MeV) is shown in Fig. 43. The magazine, made of H-451 graphite, exhibited shrinkage up to a fast fluence of about 1×10^{22} neutrons/cm² at which point the graphite exhibited a turnaround and swelling began.

Between the OF-1 magazine and the nickel bulkhead was a Palorite²³ carbon insulation disc (Fig. 1). The disk, which was symmetrical before irradiation, underwent considerable shrinkage at the bottom during irradiation (Fig. 44). This area of greatest shrinkage was adjacent to the ORNL magazine.

The nickel bulkhead failed during irradiation (Fig. 45); the mechanism of failure in the bulkhead appeared to be fatigue of the metal.

18. F. J. Homan et al., *Irradiation Performance of HTGR Fuel Rods in HFIR Experiment HRB-6*, ORNL/TM-5011 (May 1976).

19. *Gas-Cooled Reactor Programs Annu. Prog. Rep. Dec. 31, 1972*, ORNL-4911, p. 115.

20. F. J. Homan et al., *Irradiation Performance of HTGR Fuel Rods in HFIR Experiment HRB-3 and ETR Experiment P13N*, ORNL/TM-4526 (October 1974).

21. F. J. Homan et al., *Irradiation Performance of HTGR Fuel Rods in HFIR Experiments HRB-4 and -5*, ORNL-5115 (June 1976).

22. C. B. Scott and D. P. Harmon, *Postirradiation Examination of Capsules HRB-4, HRB-5, and HRB-6*, General Atomic Company, GA-A13267 (November 1975).

23. Manufactured by Union-Carbide Corporation, Nuclear Division.

Table 11. Summary of dimensional changes for fuel rods in capsule OF-1

Rod	Fuel type	Average fast fluence (> 0.18 MeV) (neutrons/cm ² $\times 10^{21}$)	Postirradiation dimensional change			
			Diameters		Lengths	
			ΔD cm (in.)	Change (%)	ΔL cm (in.)	Change (%)
1-1	1	10.8	0.0343 (0.0135)	-2.74		
1-2	1	9.58	0.0348 (0.0137)	-2.78		
1-3	1	8.00	0.0297 (0.0117)	-2.38		
1-4	1	5.72	0.0246 (0.0097)	-1.97		
3-1	4	9.85	0.0373 (0.0147)	-2.98		
3-2	4	8.61	0.0338 (0.0133)	-2.70		
3-3	6	7.40	0.0325 (0.0128)	-2.61	0.0650 (0.0256)	-2.78
3-4	5	5.92	0.0272 (0.0107)	-2.17		
3-5	6	4.37	0.0234 (0.0092)	-1.87	0.0465 (0.0183)	-1.99
5-2	7	9.18	0.0391 (0.0154)	-3.14	0.1430 (0.0563)	-3.07
5-3	8	7.48	0.0203 (0.0080)	-1.62		
5-4	7	5.25	0.0262 (0.0103)	-2.09	0.1323 (0.0521)	-2.89

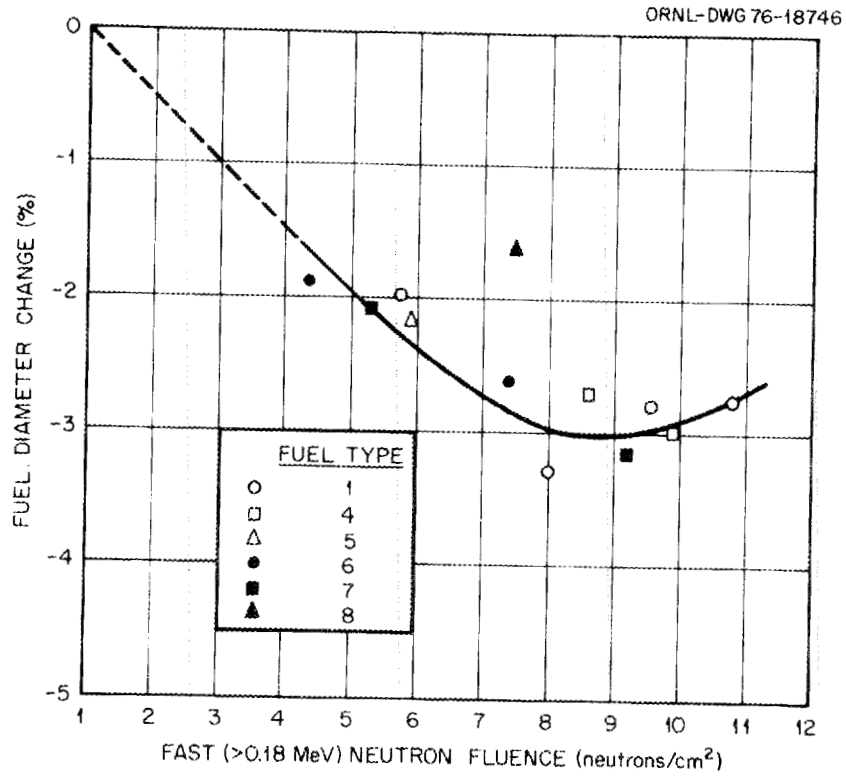


Fig. 42. OF-1 Fuel rod diameter change as a function of fast fluence exposure.

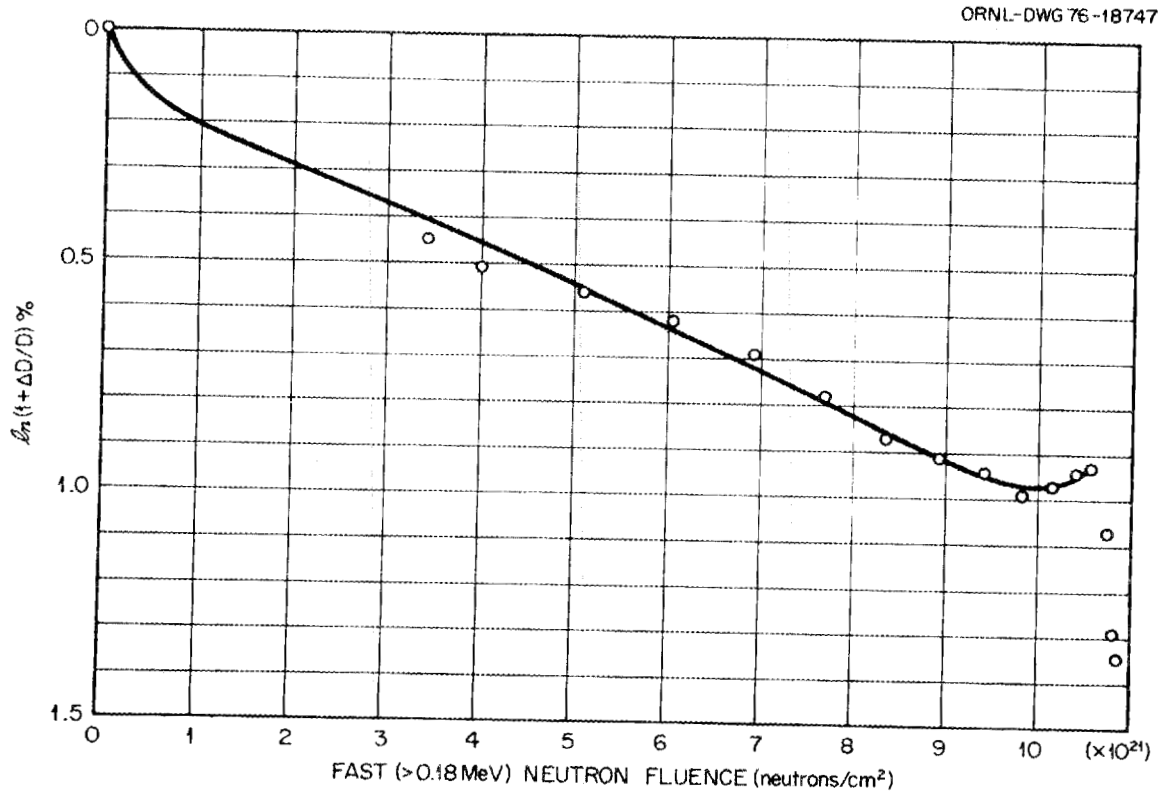


Fig. 43. Natural strain versus fluence for H-451 magazine of OF-1 (no preirradiation dimensions and assuming $D_0=2.4214$ in.).

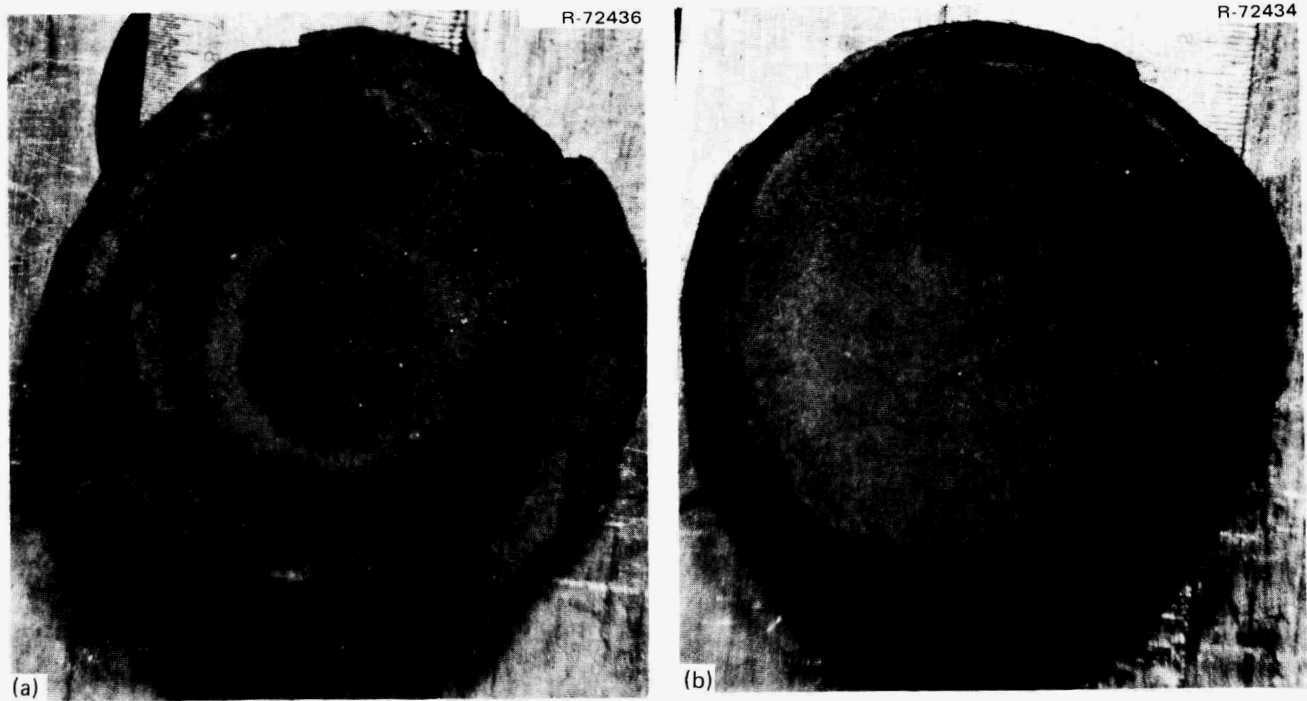


Fig. 44. Appearance of Palorite insulation disc from ORNL portion of OF-1 Capsule. (a) Top view, (b) bottom view, and (c) side view. (1.6X)

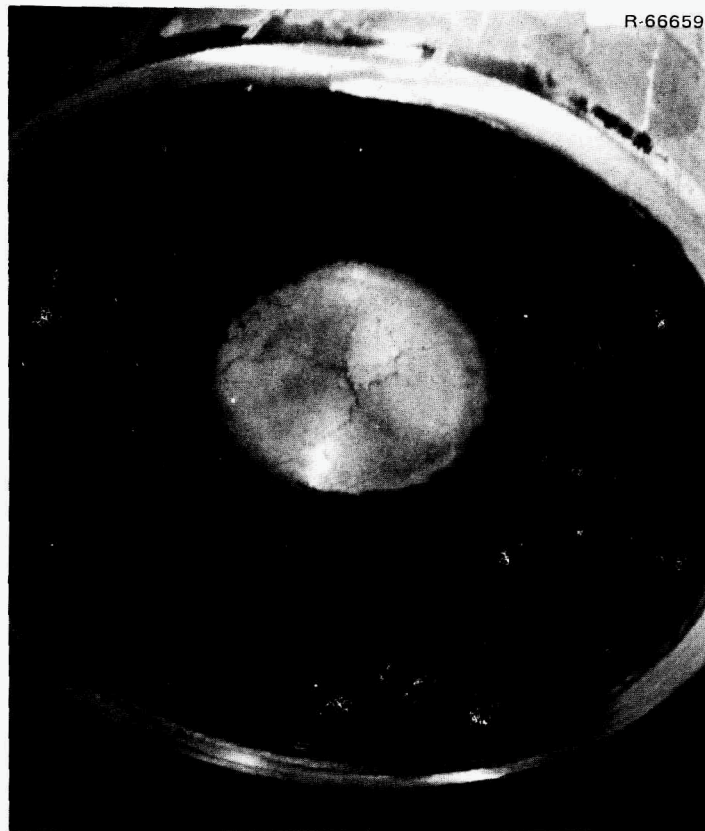


Fig. 45. Appearance of nickel bulkhead separating GAC and ORNL experiments. View is from lower (ORNL) side. (2x)

METALLOGRAPHY

Performance Evaluation of Fuel Types

Transverse sections made through fuel rods 1-1, 2-2, 3-2, 3-4, 4-1, 5-1, 5-2, and 5-3 were examined metallographically (Fig. 2). Because type 5 was representative of type 6, a type 6 rod was not scheduled for metallography. A postirradiation radial section through rod 1-1 (Fig. 46) shows fissile, fertile, inert and shim particles.

Radial sections for the different fuel types were examined before and after irradiation (Figs. 47-53). Summaries of the metallographic examination after irradiation and a comparison with the preirradiation examination are given below. The most common problem associated with the fissile particles was migration of the kernel up the temperature gradient (amoeba effect).

Fuel Type 1 (Fig. 47). No failed particles observed on postirradiation examination (PIE). Amoeba ($<5 \mu\text{m}$) observed in some of the (4.2 Th,U)O₂ particles (batch J-263) in the peripheral region of the fuel rod. The matrix densified and pulled away from the coated and shim particles with no matrix-particle interaction. (Observations made on fuel rod 1-1).

Fuel Type 2 (Fig. 48). No failed particles on PIE. Amoeba ($<5 \mu\text{m}$) observed in some of the (4.2 Th,U)O₂ particles (batch J-263). The matrix densified and pulled away from the coated and shim particles. Two relatively minor cases of matrix-particle interaction were found (Fig. 54). (Observations made on fuel rod 2-2).

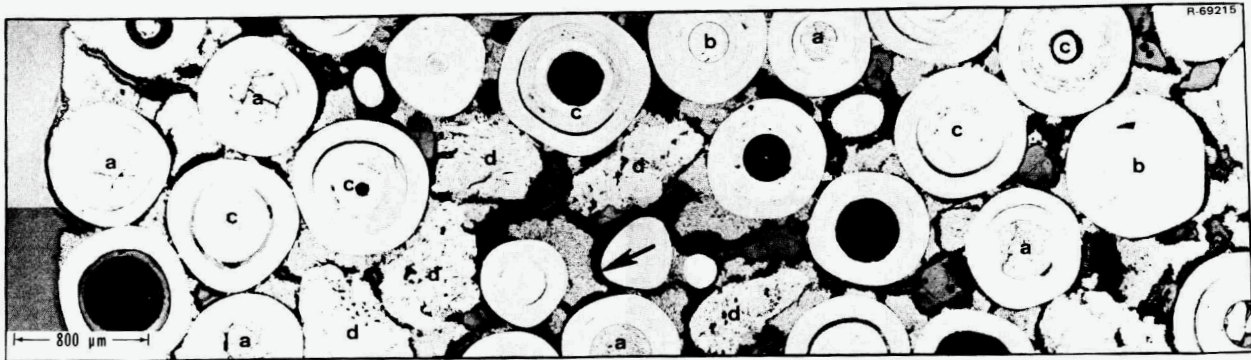


Fig. 46. A pre-irradiation radial section of rod 1-1 showing the post-irradiation appearance of (a) fissile, (b) fertile, (c) inert and (d) shim particles. Arrow indicates where the matrix has pulled away from the particles.

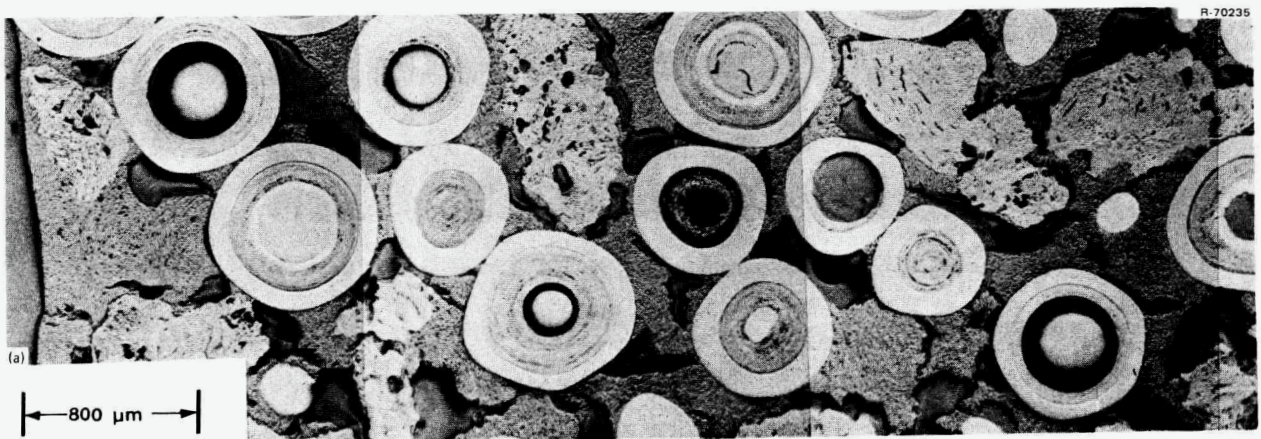


Fig. 47. Pre-irradiation (a) and post-irradiation (b) radial sections of fuel type 1 irradiated in OF-1. Post-irradiation photomicrograph is from Rod 1-1. Biso-coated $(4.2 \text{ Th,U})\text{O}_2$ and ThO_2 fuel particles and inert particles present.

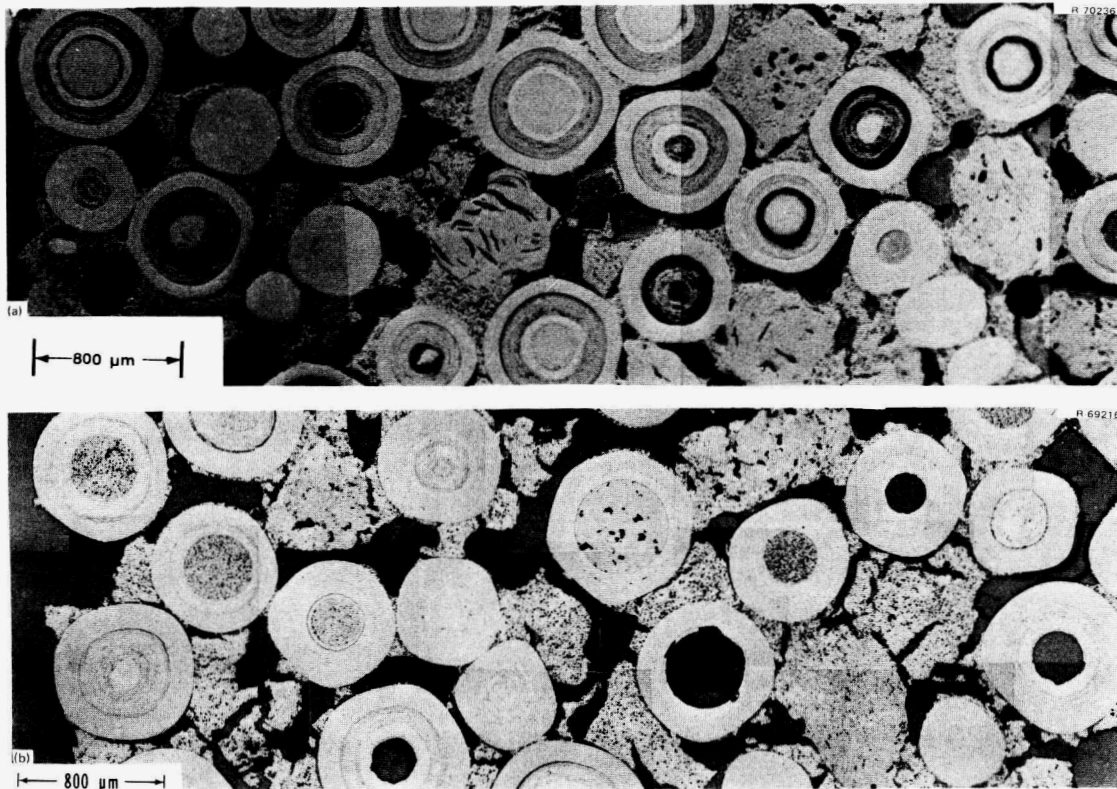


Fig. 48. Pre-irradiation (a) and post-irradiation (b) radial sections of fuel type 2 irradiated in OF-1. Post-irradiation photomicrograph is from Rod 2-2. Biso-coated $(4.2 \text{ Th,U})\text{O}_2$ and ThO_2 fuel particles and inert particles present.

Fuel Type 3 (Fig. 49). No failed particles on PIE. Amoeba ($\leq 20 \mu\text{m}$) observed in some of the $(4.2 \text{ Th,U})\text{O}_2$ particles (batch J-263). Densification of the matrix was evident and caused no matrix-particle interaction where the two had separated. (Observations made on fuel rod 4-1).

Fuel Type 4 (Fig. 50). No failed particles on PIE. Amoeba ($< 20 \mu\text{m}$) observed in the $(4.2 \text{ Th,U})\text{O}_2$ particles (batch OR-1977). The matrix densified and pulled away from the coated and shim particles with no matrix-particle interaction. (Observations made on fuel rod 3-2).

Fuel Type 5 (Fig. 51). No failed particles or amoeba observed in the $(4.2 \text{ Th,U})\text{O}_2$ particles (batch J-263) on PIE. Densification of the matrix was evident but there was no matrix-particle interaction where the two had separated. (Observations made on fuel rod 3-4).

Fuel Type 7 (Fig. 52). No failed particles or amoeba observed in the $(4.2 \text{ Th,U})\text{O}_2$ particles (batch OR-1977) on PIE. Densification of the matrix was evident but there was no matrix-particle interaction where the two had separated.

Fuel Type 8 (Fig. 53). A number of failed $(4.2 \text{ Th,U})\text{O}_2$ particles (batch Pu-291) were observed and amoeba ($< 15 \mu\text{m}$) was apparent. Failure fractions of 15 and 80% were recorded in two samples. These particles had dense buffers; optical anisotropic gradients were found in the outer pyrocarbon coatings. Also, several particles had been broken during fabrication. (Observations made on fuel rods 5-1 and 5-3).

All Fuel Types (Fig. 54). No failures or amoeba effects were associated with the fertile ThO_2 particles (batch J-262). The shim particles appear relatively unchanged.

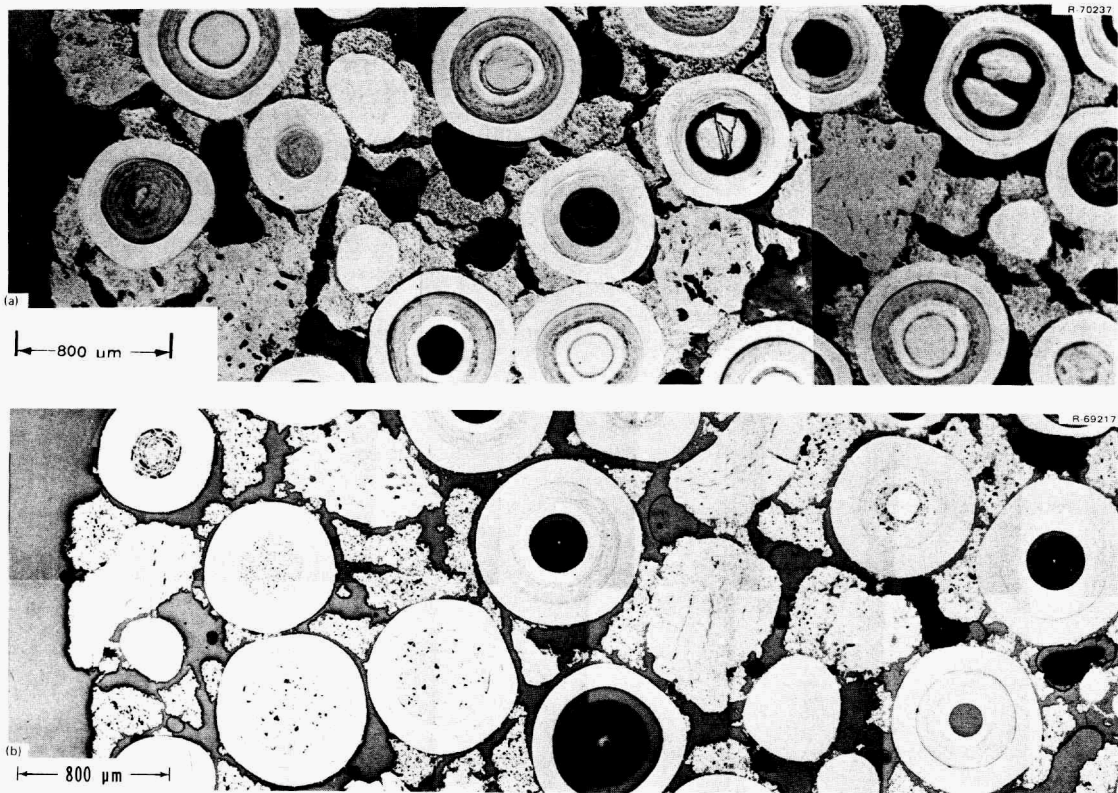


Fig. 49. Pre-irradiation (a) and post-irradiation (b) radial sections of fuel type 3 irradiated in OF-1. Post-irradiation photomicrograph is from Rod 4-1. Biso-coated $(4.2 \text{ Th,U})\text{O}_2$ and ThO_2 fuel particles and inert particles present.



Fig. 50. Pre-irradiation (a) and post-irradiation (b) radial sections of fuel type 4 irradiated in OF-1. Post-irradiation photomicrograph is from Rod 3-2. Biso-coated $(4.2 \text{ Th,U})\text{O}_2$ and ThO_2 fuel particles and inert particles present.

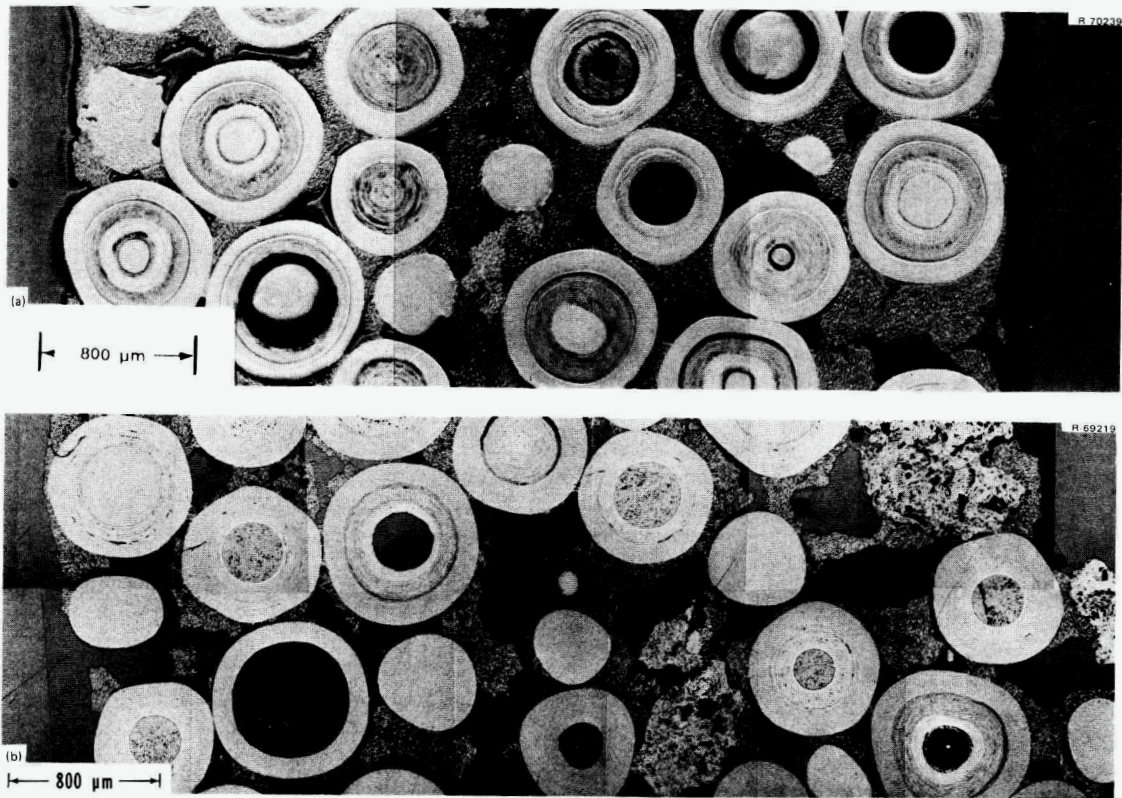


Fig. 51. Pre-irradiation (a) and post-irradiation (b) radial sections of fuel type 5 irradiated in OF-1. Post-irradiation photomicrograph is from Fuel Rod 3-4. Biso-coated $(4.2 \text{ Th,U})\text{O}_2$ and ThO_2 fuel particles and inert particles.

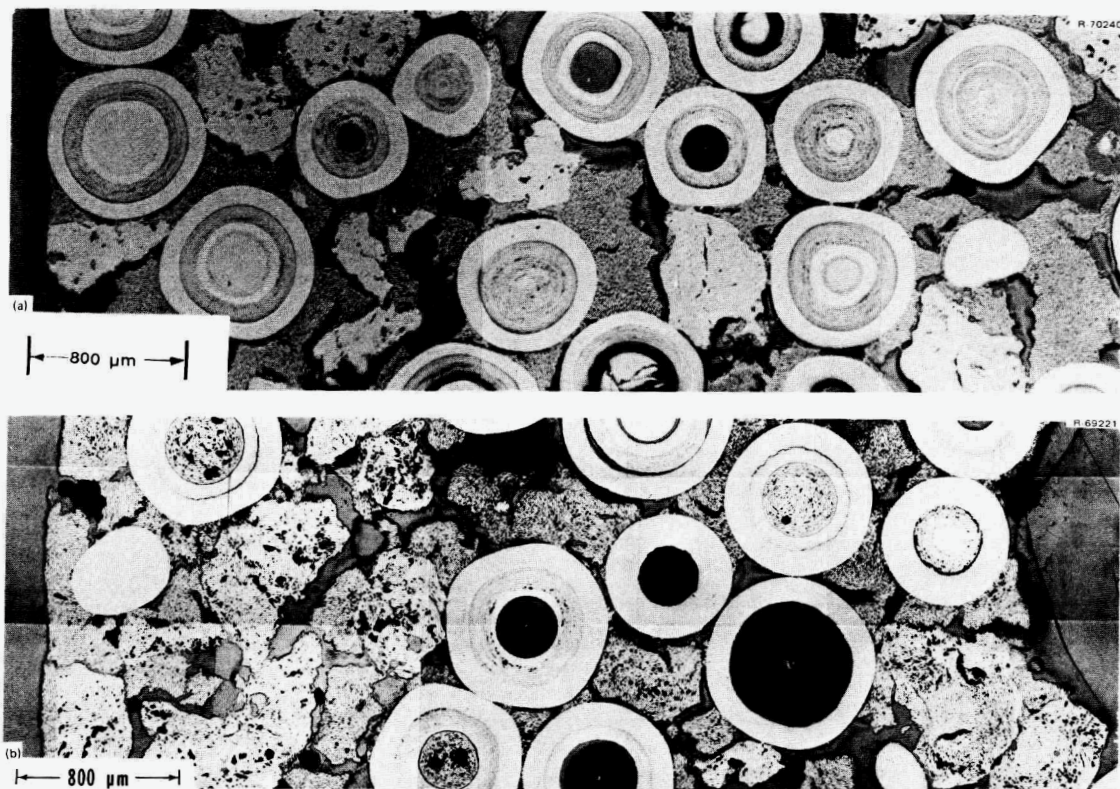


Fig. 52. Pre-irradiation (a) and post-irradiation (b) radial sections of fuel type 7 irradiated in OF-1. Post-irradiation photomicrograph is from Fuel Rod 5-2. Biso-coated $(4.2 \text{ Th,U})\text{O}_2$ and ThO_2 fuel particles and inert particles present.

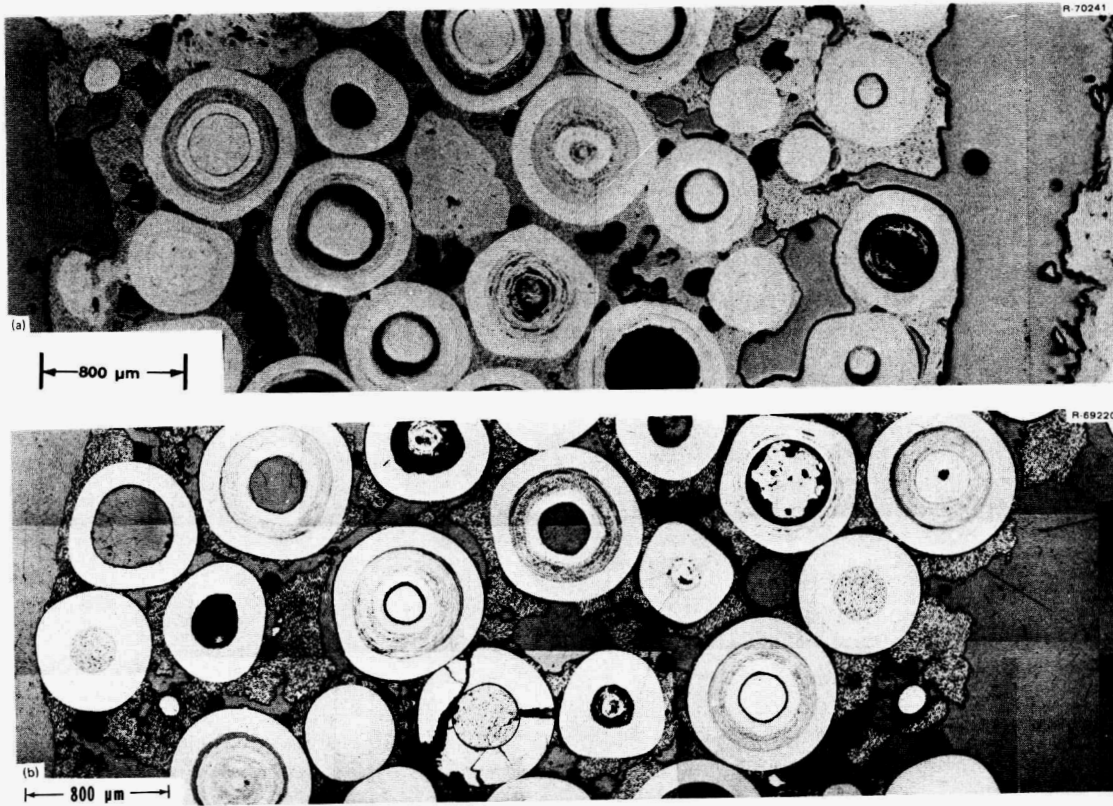


Fig. 53. Pre-irradiation (a) and post-irradiation (b) radial sections of fuel type 8 irradiated in OF-1. Post-irradiation photomicrograph is from Rod 5-3. Biso-coated $(4.2 \text{ Th,U})\text{O}_2$ and ThO_2 fuel particles and inert particles present.

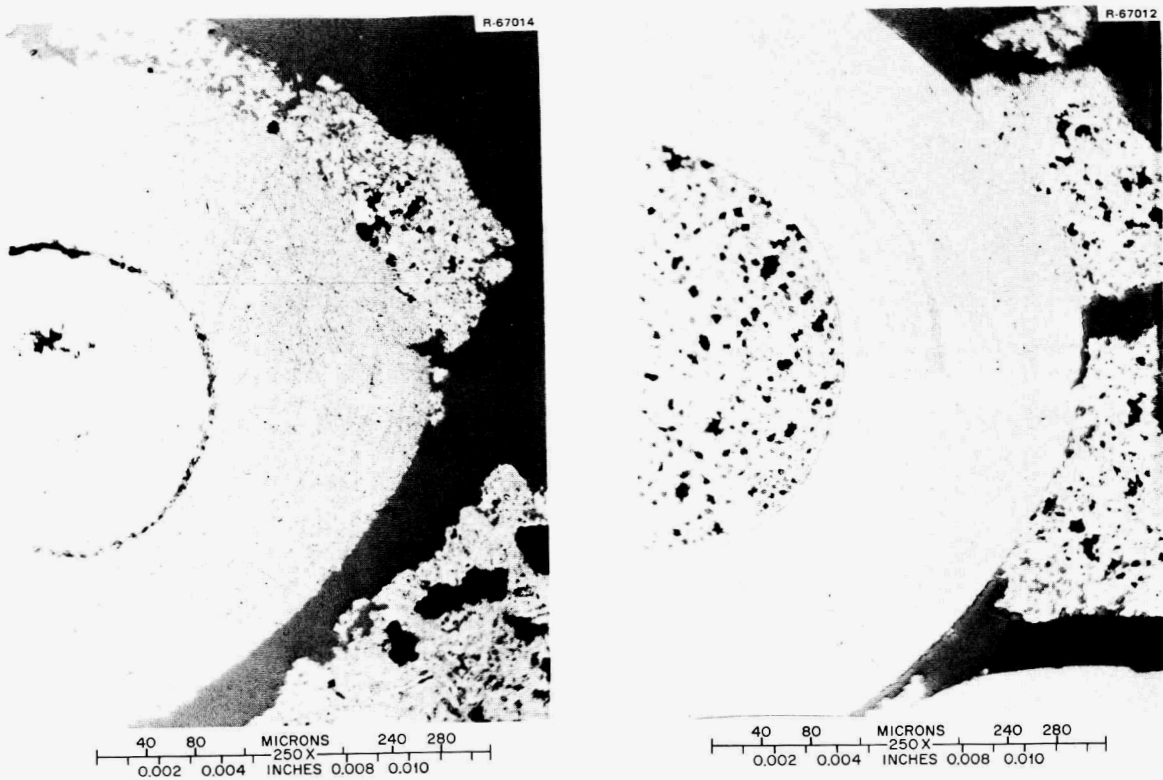


Fig. 54. Tearing of the outer coating of rod 2-2 (fuel type 2) due to matrix-particle interaction.

Comparison of Matrices

The matrices after irradiation (Figs. 55–60) may be compared with their preirradiation appearance (Figs. 10–16). Rods carbonized in packed Al_2O_3 (Figs. 55, 58, 59, and 60) had matrices whose individual filler particles (Asbury 6353) were barely discernible, although before irradiation they were clearly visible. Densification of the matrix had definitely taken place. The matrix from rod 2-2 (Fig. 56), typical of the rods carbonized in the graphite magazine, had the same “blocky” appearance as it did before irradiation, where the matrix was dense (little microporosity) and the individual filler particles (Asbury 6353) were not discernible. In all cases the matrices densified during irradiation reducing the microporosity of the matrix and increasing the macroporosity of the rod. These changes are larger in the matrices carbonized in packed Al_2O_3 , because they were much less dense and had more microporosity before irradiation. It should be noted that these observations were made metallographically, and no significant quantitative information was obtained on the porosity changes.

The matrix containing GLC-1089 filler particles (Fuel Type 3) and carbonized in the graphite magazine (Fig. 57) had the same dense appearance as the matrix containing Asbury 6353 filler particles (Fuel Type 2) and carbonized in the magazine. Comparison showed that both matrices had the same irradiation behavior and that no real differences between the two could be detected.

COMPARISON OF FISSILE PARTICLES FROM THE 2.5-cm-(1-INCH-) AND 12.7-cm-(5-INCH-) DIAMETER COATERS

Irradiated particles from batch J-263 (Fig. 61) experienced amoeba migration up to $20\ \mu\text{m}$; but no failures were observed. The PIE appearance of the kernel is typical of the mixed thorium-uranium oxides, where fission-gas bubbles and bright metallic inclusions have formed. Intermittent plastic flow of the kernel through the fission recoil zone of the buffer coating was also observed.

Particles from rod 3-2 (batch OR-1977) (Fig. 62) did as well as batch J-263. They experienced amoeba up to $20\ \mu\text{m}$ with no failures. Fission-gas bubbles, metallic inclusions, and intermittent plastic flow, as in batch J-263, were observed.

PERFORMANCE OF ^{233}U -BEARING FISSILE PARTICLES

Particles from batch Pu-291 experienced gross failures that were first observed in the visual and later confirmed with the metallographic examination (Fig. 63). Under polarized light, property gradients in the coatings (shown by optical anisotropy or activity) are visible before and after irradiation. These gradients are exaggerated during irradiation, which is why they are more clearly visible in the postirradiation photomicrograph. Cracking of the coatings resulted from differential shrinkage during irradiation. As previously mentioned, these same observations were made with the HRB-6 irradiation test, where the same batch of particles were used. It is emphasized that the failures are due to poor coating properties and not because the kernels contained ^{233}U . Appearance of the ^{233}U -bearing kernels was the same as the other fissile particle batches containing ^{235}U .

A plot of the kernel migration coefficient against reciprocal temperature for $(4\ \text{Th,U})\text{O}_2$ particles from various irradiation tests, including OF-1, (Fig. 64) shows a great deal of scatter in the data due to uncertainties with the temperatures and temperature gradients of the fuel rods during irradiation (both of which are used to compute the coefficient). A comparison of the ^{233}U -bearing particles (batch Pu-291 in rods OF-1-5-3 and HRB-6-3A) with those containing ^{235}U (all others) shows equivalent irradiation migration rates between the two types of particles.

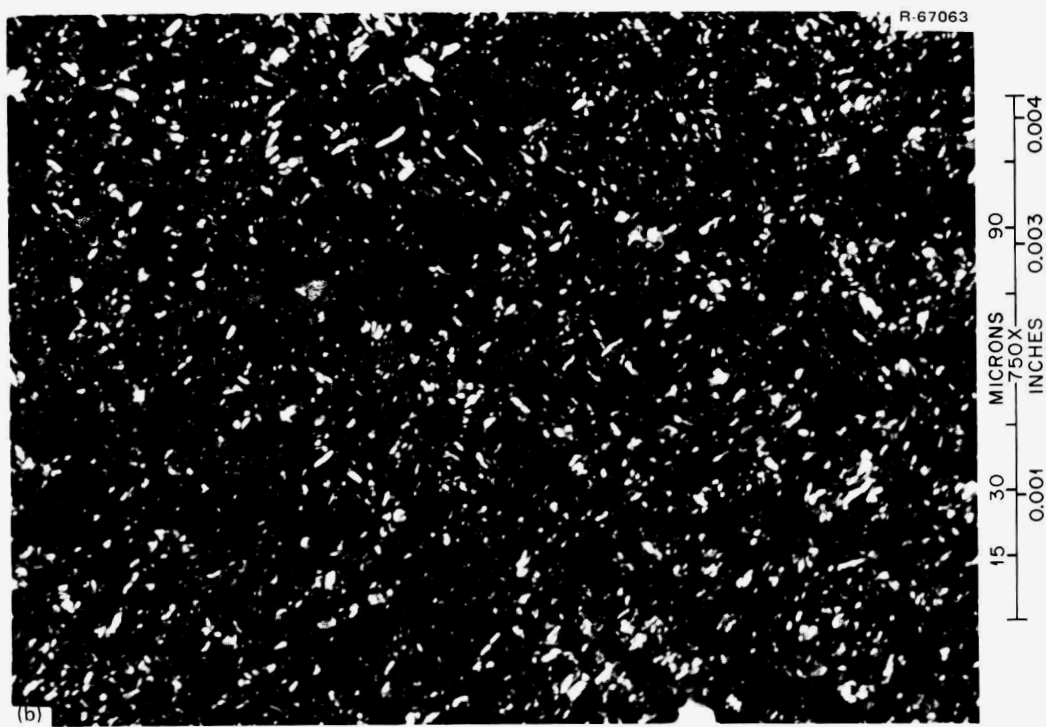
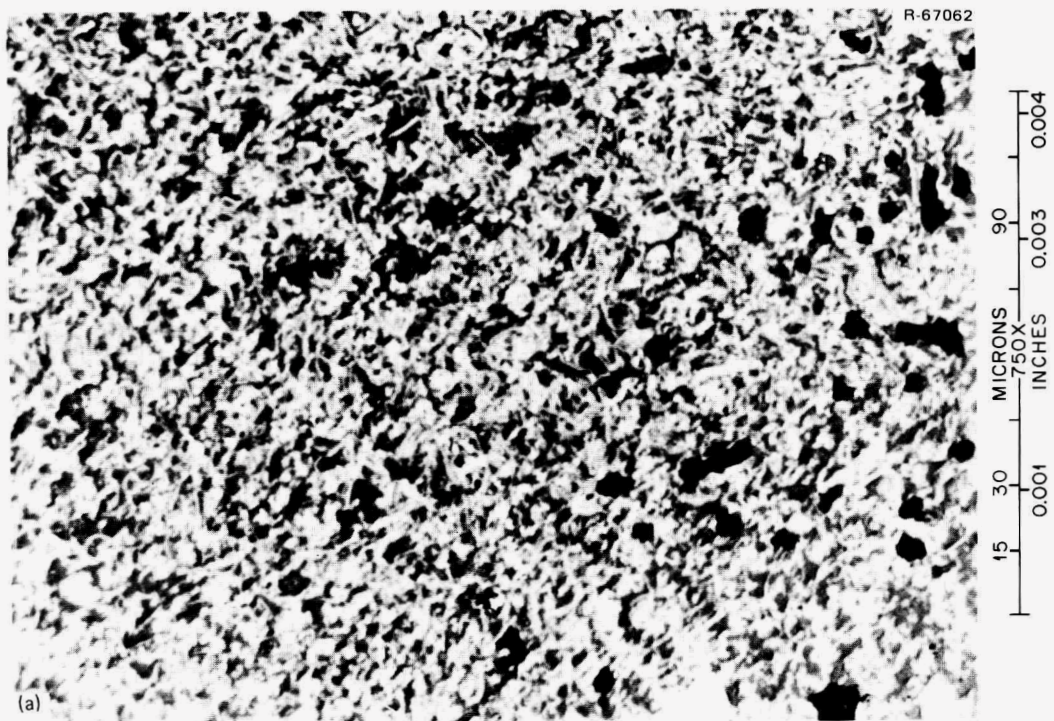


Fig. 55. Microstructure of matrix from fuel type 1 (rod 1-1) after irradiation under (a) bright field and (b) polarized light. Asbury 6353 filler particles, Ashland A240 binder, carbonized in packed Al_2O_3 .

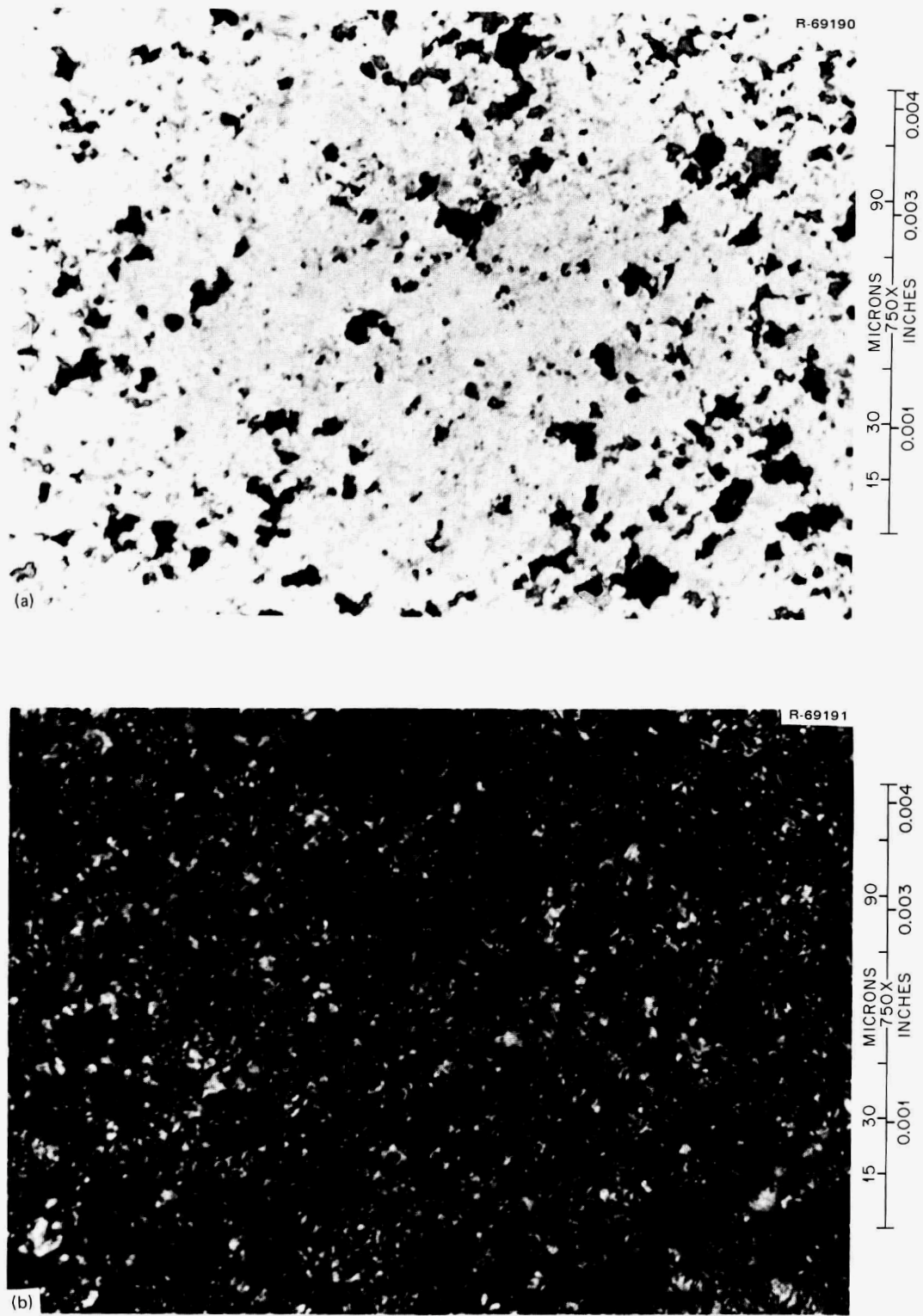


Fig. 56. Microstructure of matrix from fuel type 2 (rod 2-2) after irradiation under (a) bright field and (b) polarized light. Asbury 6353 filler particles, Ashland A240 binder, carbonized in-block.

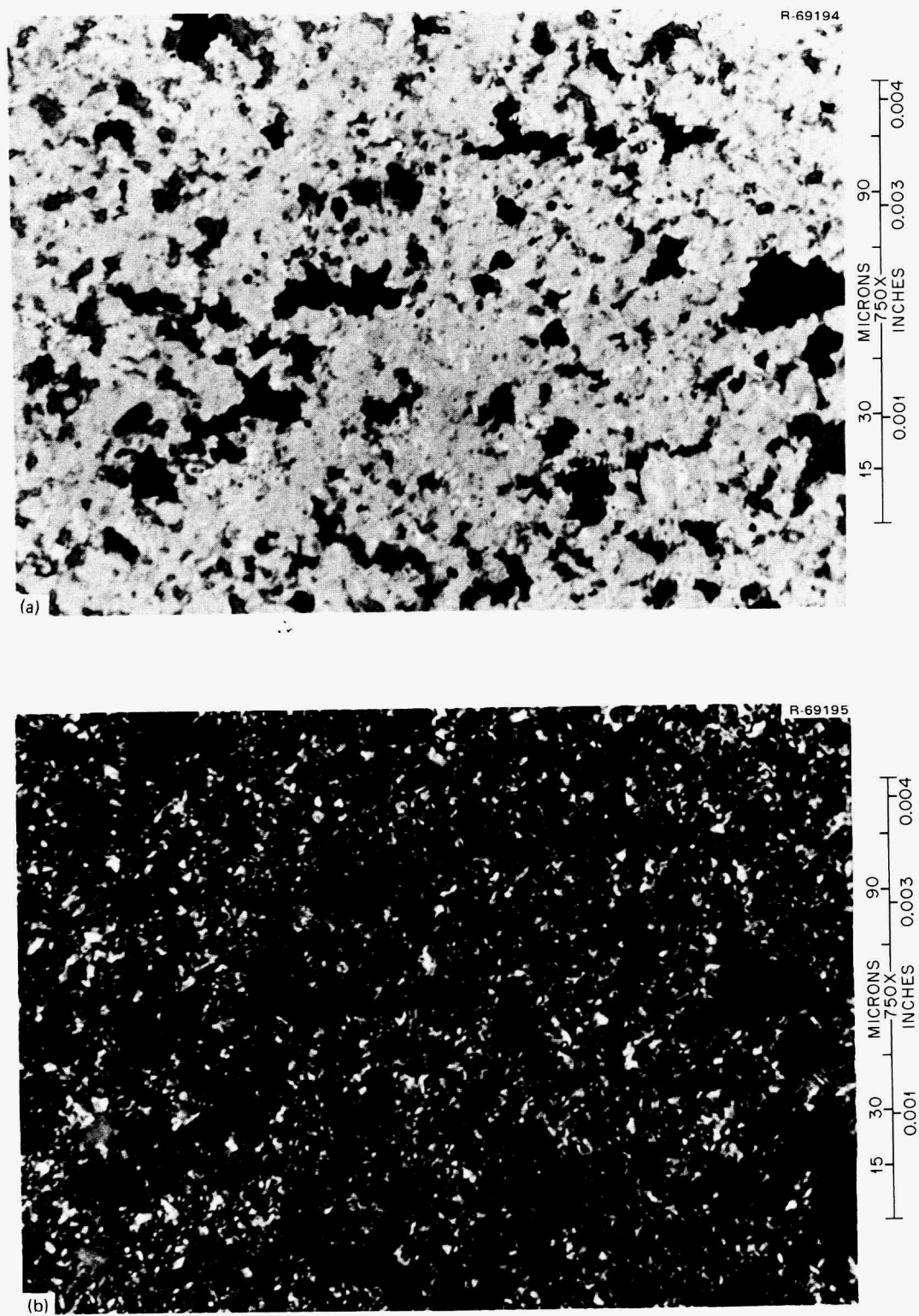


Fig. 57. Microstructure of matrix from fuel type 3 (rod 4-1) after irradiation under (a) bright field and (b) polarized light. GLC 1089 filler particles, Ashland A240 binder, carbonized in-block.

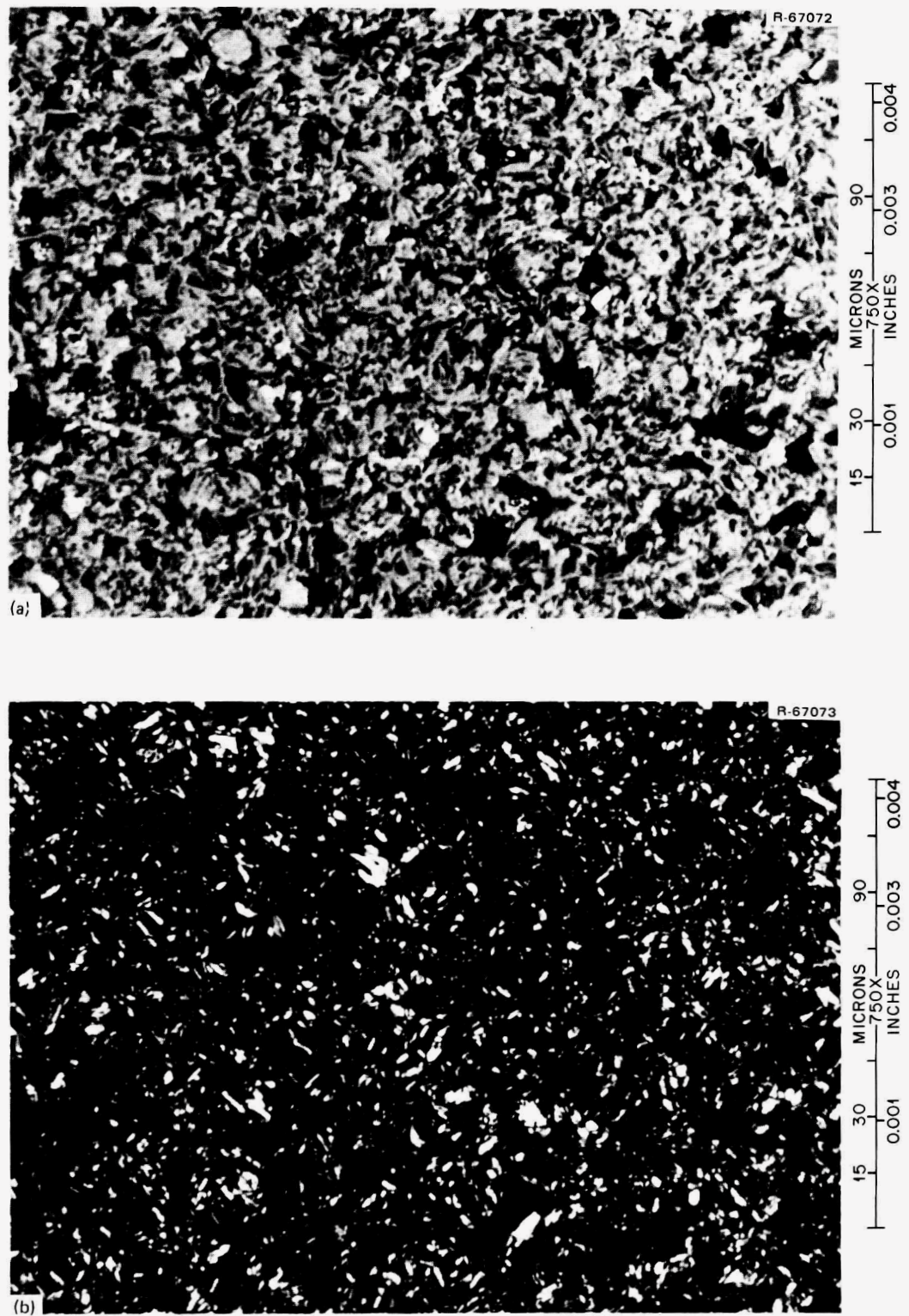


Fig. 58. Microstructure of matrix from fuel type 4 (rod 3-2) after irradiation under (a) bright field and (b) polarized light. Asbury 6353 filler particles, Ashland A240 binder, carbonized in packed Al_2O_3 . Matrix from fuel type 4 is representative of matrices from fuel types 5 and 6.

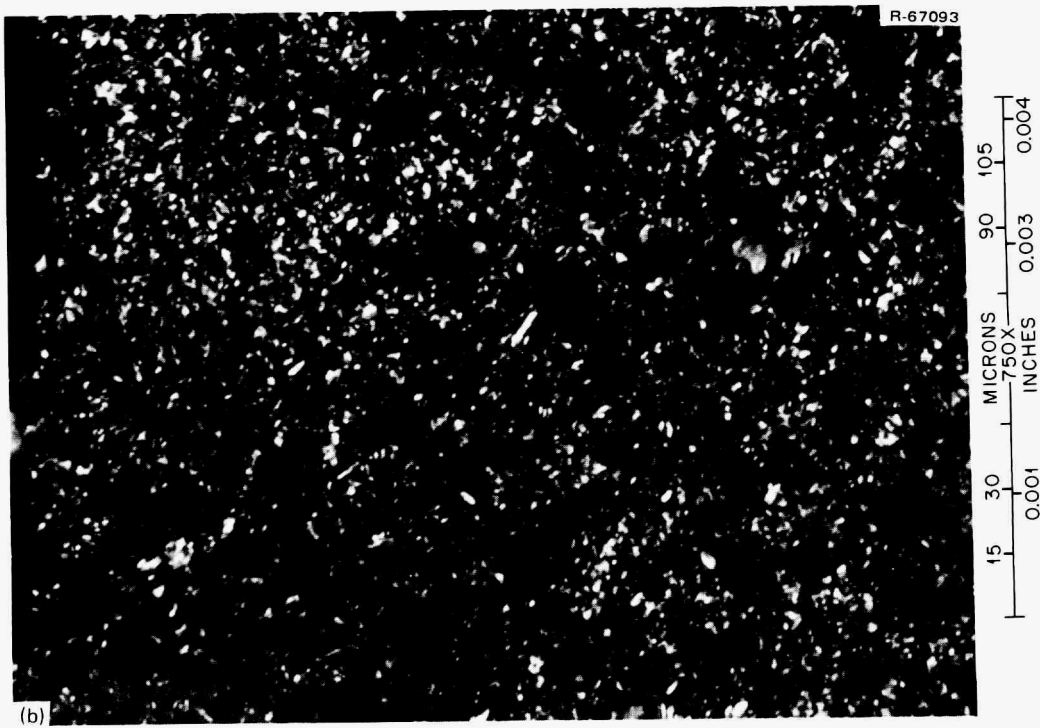
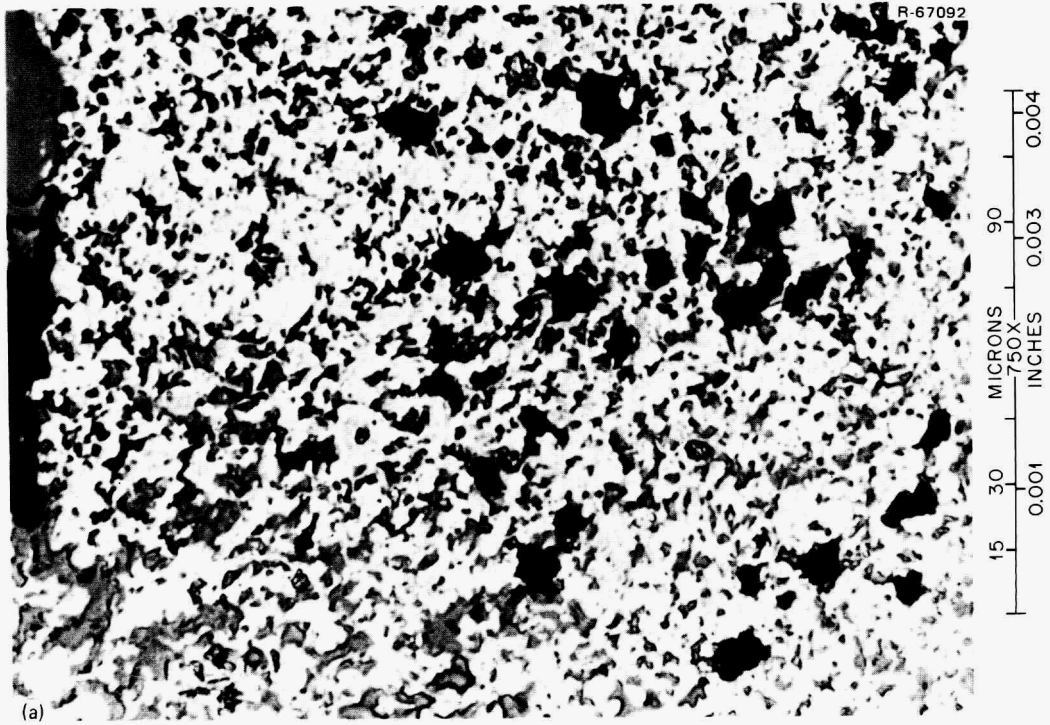


Fig. 59. Microstructure of matrix from fuel type 7 (rod 5-2) after irradiation under (a) bright field and (b) polarized light. Asbury 6353 filler particles, Ashland A240 binder, carbonized in packed Al_2O_3 .

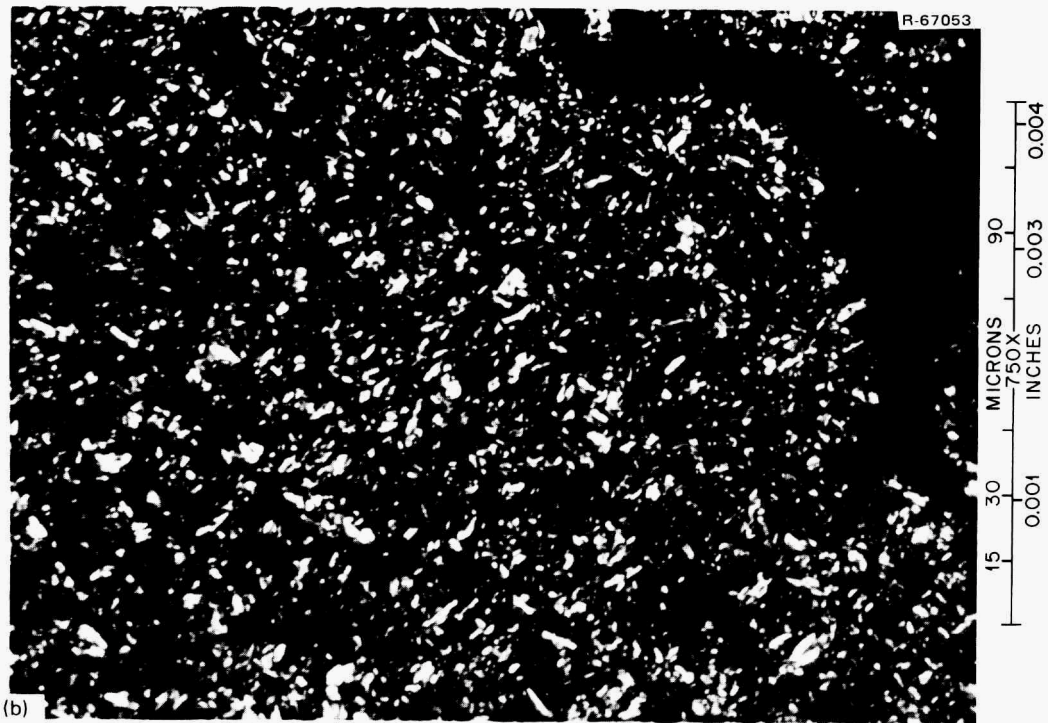
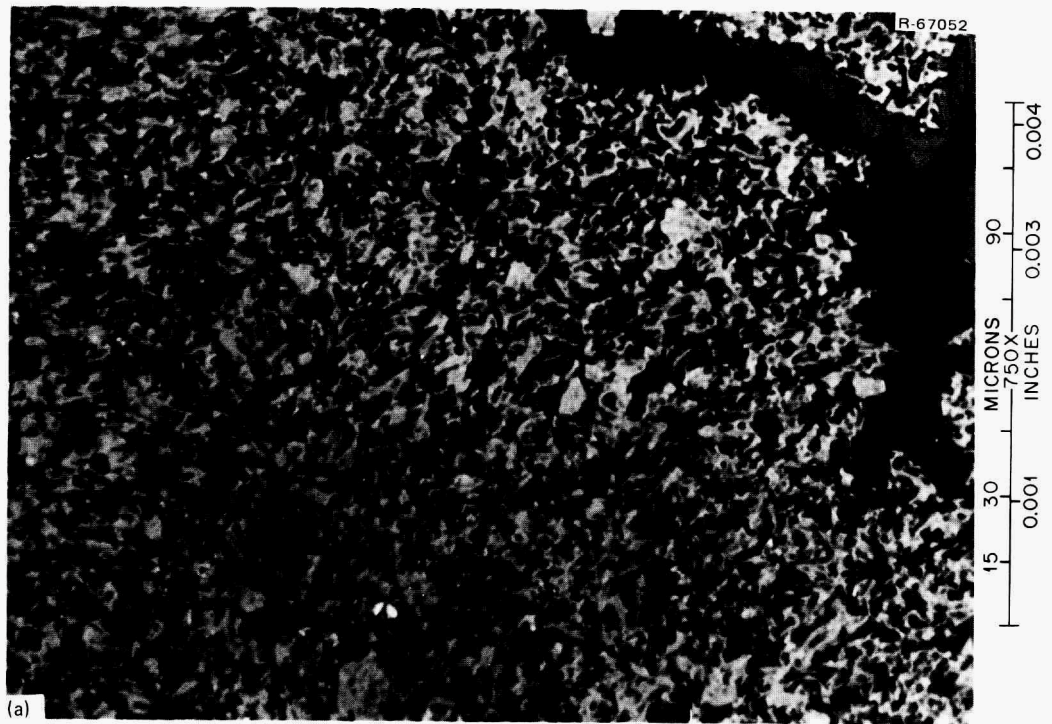


Fig. 60. Microstructure of matrix from fuel type 8 (rod 5-3) after irradiation under (a) bright field and (b) polarized light. Asbury 6353 filler particles, Ashland A240 binder, carbonized in packed Al_2O_3 .

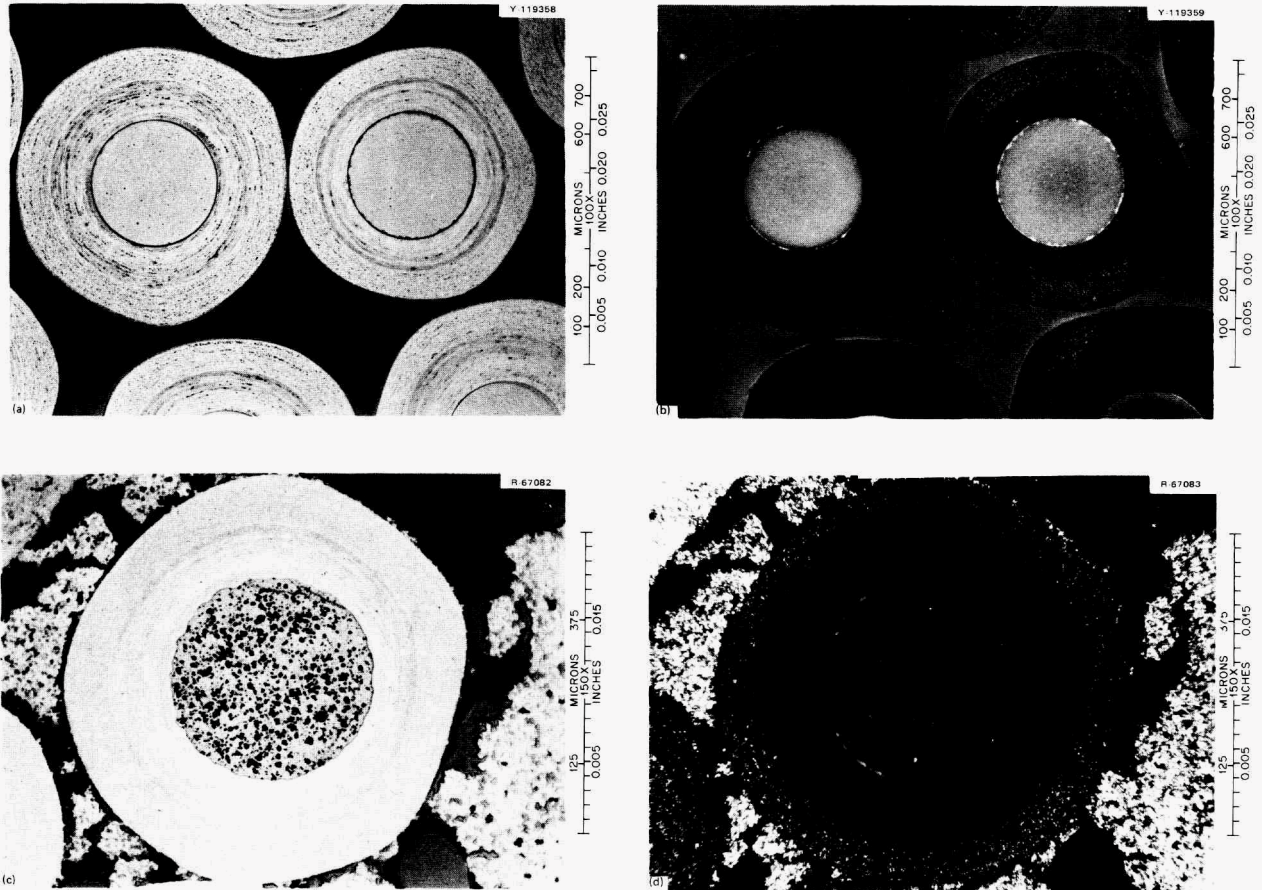


Fig. 61. Comparison of $(4.2 \text{ Th,U})\text{O}_2$ particles from batch J-263 made in a 5-in-diam. coater before irradiation, (a) and (b), and after irradiation, (c) and (d), under bright field and polarized light, respectively. The post-irradiation samples are from rod 4-1. Temperature gradient increases from left to right.

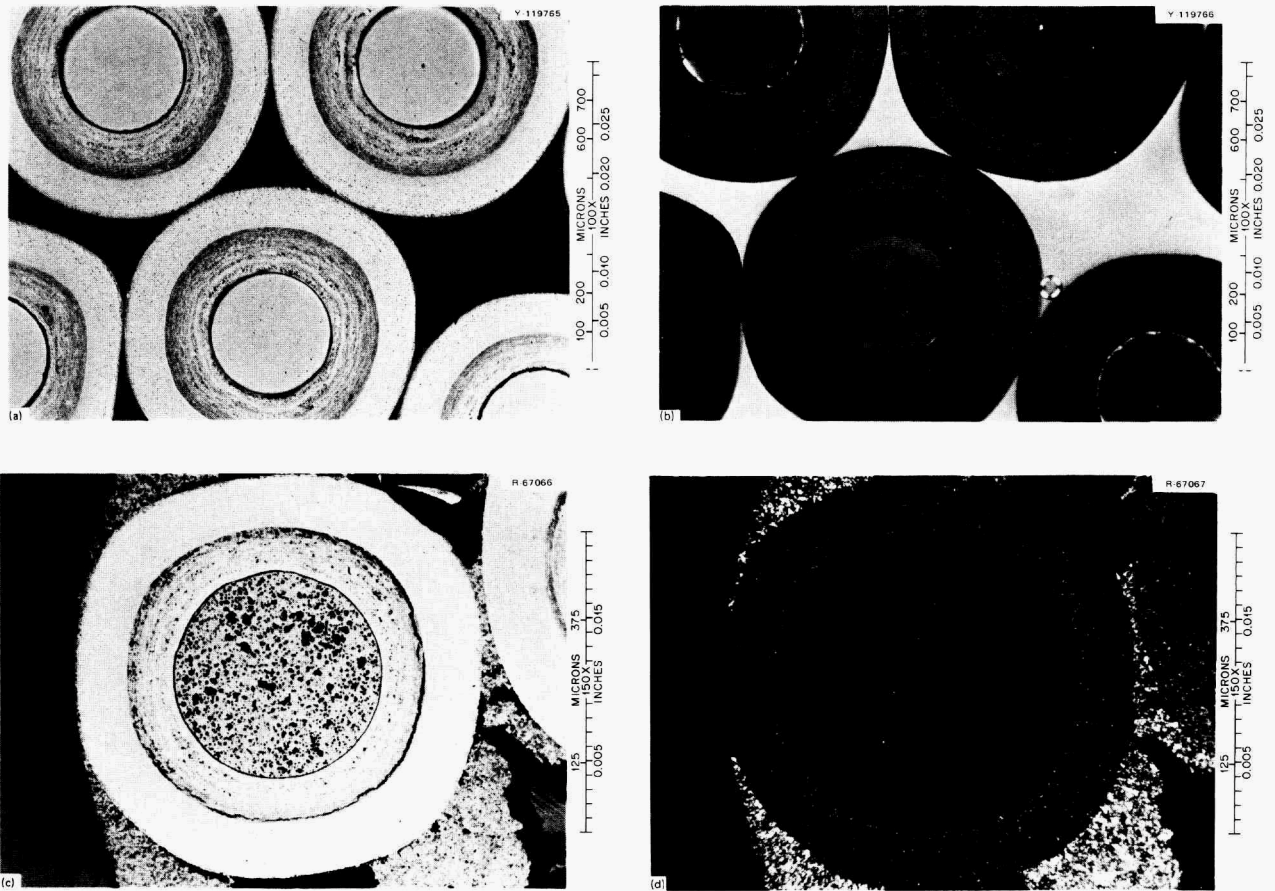


Fig. 62. Comparison of $(4.2 \text{ Th,U})\text{O}_2$ particles from batch OR1977 made in a 1-in.-diam. coater before irradiation, (a) and (b), and after irradiation, (c) and (d), under bright field and polarized light, respectively. The post-irradiation samples are from rod 3-2. Temperature gradient increases from left to right.

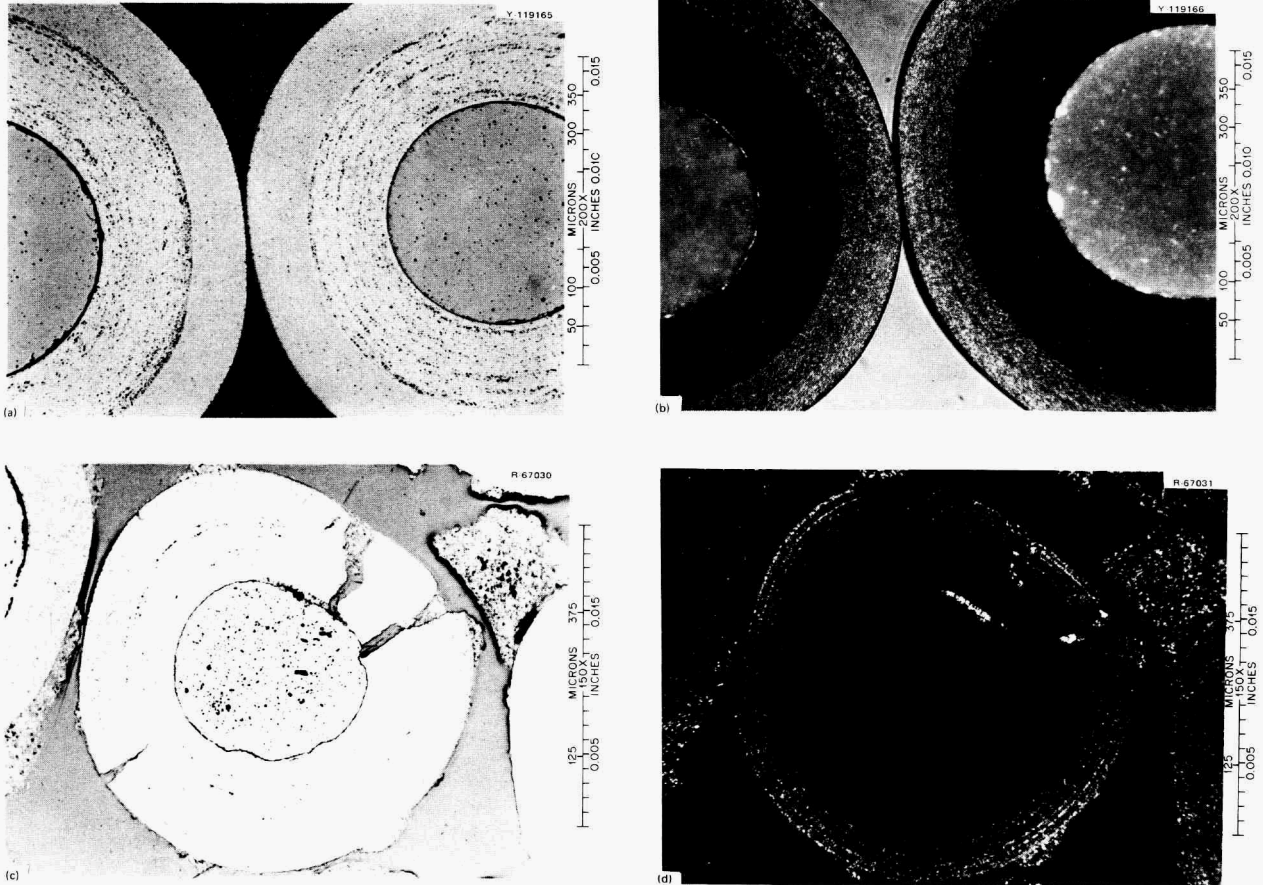


Fig. 63. Comparison of $(4.2 \text{ Th,U})\text{O}_2$ particles from batch Pu-291 using ^{233}U before irradiation, (a) and (b), and after irradiation, (c) and (d), under bright field and polarized light, respectively.

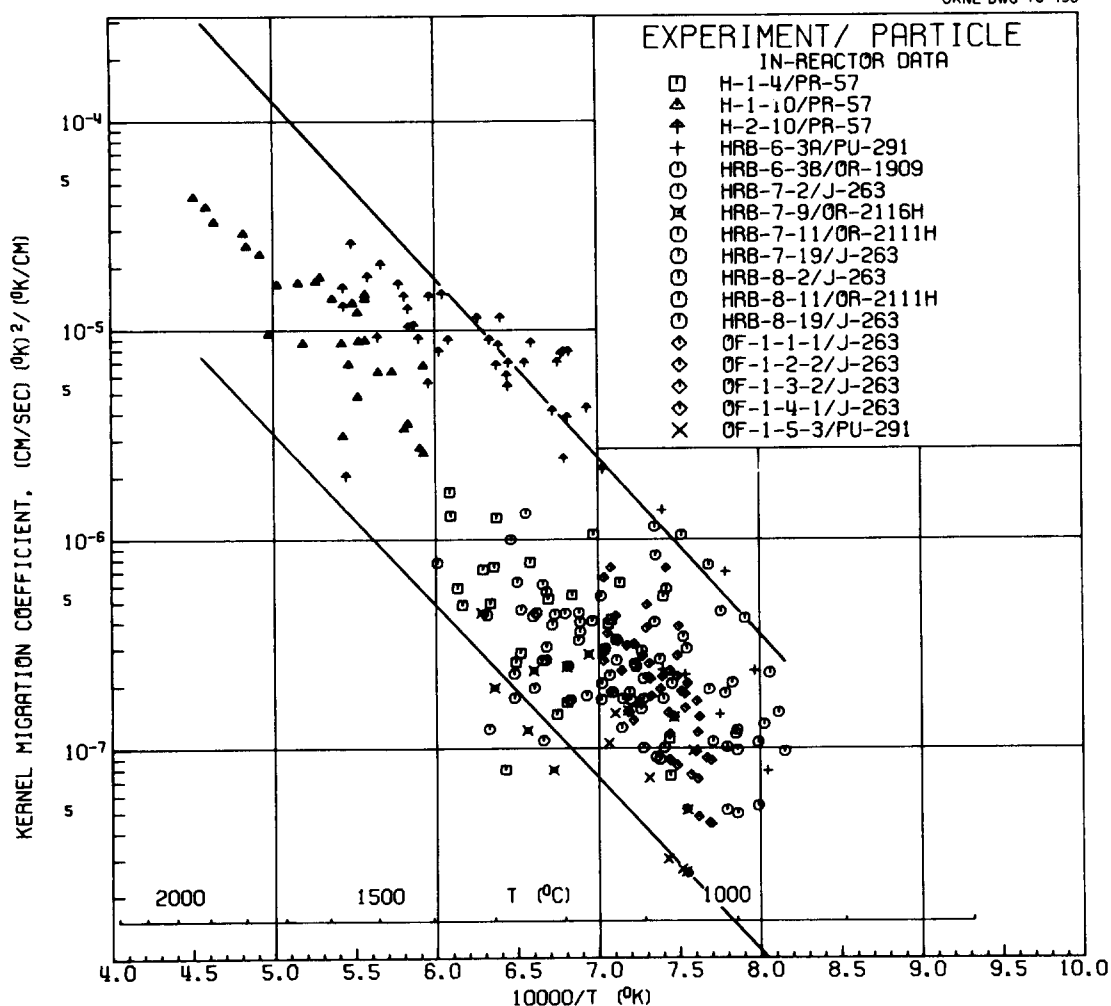


Fig. 64. Summary of kernel migration data for mixed oxide kernels with Th/U \sim 4:1.

PERFORMANCE OF FERTILE PARTICLES

As expected, fertile ThO_2 particles from batch J-262 exhibited excellent irradiation behavior (Fig. 65). No failures or amoeba effects were observed with any of the samples examined.

CONCLUSIONS

Postirradiation examination showed good irradiation performance for rods carbonized in packed Al_2O_3 and in-block. A comparison indicated that rods carbonized in-block had matrices with dense microstructures, tended to bond to the graphite magazine, and were more susceptible to matrix-particle interaction. Matrix-particle interaction, which was observed during metallographic examination of unirradiated controls for Fuel Type 3, was found only in Fuel Type 2 during postirradiation examination. Both of these fuel types were carbonized by the in-block process and had high pitch-coke yields. No matrix-particle

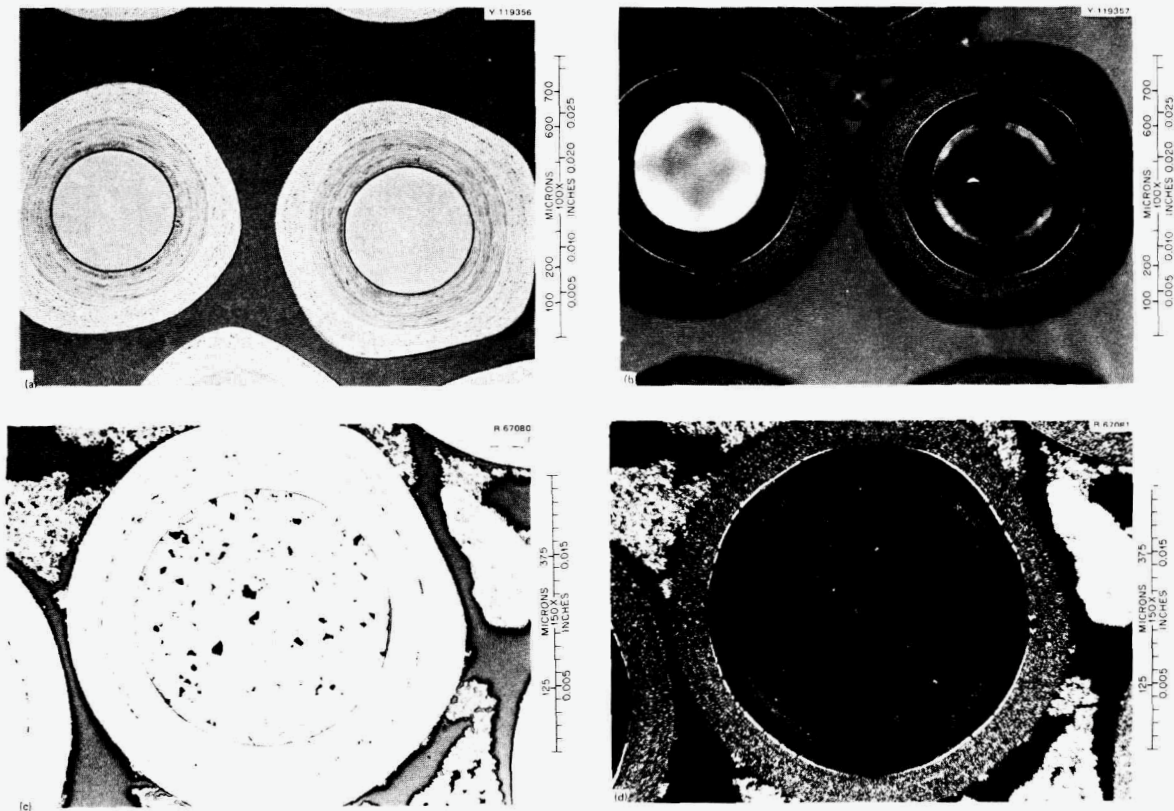


Fig. 65. Comparison of ThO_2 particles from batch J-262 before irradiation, (a) and (b), and after irradiation, (c) and (d), under bright field and polarized light, respectively.

interaction was found with any of the rods carbonized in packed Al_2O_3 in either the pre- or postirradiation metallographic examination. Evidently matrices carbonized in-block form stronger bonds with the particles than matrices carbonized in packed Al_2O_3 . Matrices using different filler particle types had similar microstructures and no difference in irradiation behavior was observed. The different carbonization techniques had no effect on the performance of the fuel particles.

The $(4\text{Th,U})\text{O}_2$ fissile particles made in the 2.5-cm-diam (1 in.) laboratory coater and those made in the 13-cm-diam (5 in.) coater had essentially identical irradiation performance. Both experienced amoeba migration with no failures.

The fissile particles containing ^{233}U experienced gross failures. Examination revealed that the failures were due to poor coating properties and not because the particles contained ^{233}U . As far as kernel performance is concerned, those kernels containing ^{233}U exhibited essentially the same irradiation behavior as kernels containing ^{235}U .

ACKNOWLEDGMENTS

The authors wish to acknowledge the efforts of many people who made significant contributions in the planning, execution, and evaluation of the irradiation capsule. We would like to thank R. B. Fitts, J. H. Coobs, and W. P. Eatherly for their help in planning and coordinating the test; W. J. Lackey, C. B. Pollock, R. A. Bradley, W. H. Miller, C. Hamby, Jr., J. D. Sease, and R. L. Hamner for fuel fabrication and characterization. The dosimetry packages were provided by H. T. Kerr. Postirradiation examination was done by the staff of the High Radiation Level Examination Laboratory, metallography by N. M. Atchley and L. G. Shrader. The authors also acknowledge the editorial work by George Griffith and the assistance of the Technical Publications Department, Information Division, in the preparation of this report.

APPENDIX A

Summary of Repair of OF-1 Sweep Gas System

The capsule was removed from the reactor during ORR cycle 119 due to a leak in the sweep gas system that served as the primary containment of the capsule.

During the routine end-of-cycle shutdown (May 19–24, 1974) following ORR cycle 118 it was discovered that the sweep gas system of capsule OF-1 could not maintain a given pressure and in fact, a constant supply flow rate of about $60 \text{ cm}^3/\text{min}$ could be maintained at a supply pressure of 633 gm/cm^2 (9 psig) while the exit lines from the capsule were closed. Several tests indicated that the leak was located in the lead pipe of the experiment so the capsule was removed from the reactor.

A helium leak detector pinpointed the axial location of the leak within the lead pipe to be about 30.5 cm (1 ft) below the level of the reactor flange. X rays were then taken of this area to determine the location of tubes and thermocouples and to find possible sources of the leak. The x rays showed a silver solder joint of 0.16 cm (0.06 in.) to 0.32 cm (0.13 in.) tubing to be located at the exact elevation predicted by the leak detection setup; and, indeed, a leak was found in the 0.16 cm (0.06 in.) tube at the base of the silver solder.

To repair the leak the 0.16 cm (0.06 in.) tube was cut just below the leak. Then the joint was heated and the faulty tube removed. Enough slack in the remaining 0.16 cm (0.06 in.) tube allowed it to be inserted into the 0.32 cm (0.13 in.) tube and silver soldered once again. After this joint was soldered, it was checked both by a pressure test and a helium leak detector. After these tests a patch was placed on the lead pipe and the experiment was installed in the reactor on June 18. During checkout the sweep system was found to be leaking once again at about the same rate as before.

The apparatus was removed from the reactor once again and this new leak was located approx. 81 cm (32 in.) further down the lead pipe. Another hole was cut into the lead pipe and two pinhole leaks were discovered in the same 0.16 cm (0.06 in.) gas line that was leaking the first time. The entire 81 cm (32 in.) of tubing from the first leak to these new leaks was removed and replaced with a new length of tubing.

A monitoring system was added to the capsule to provide a continuous helium purge of the lead pipe, as well as to provide a means for determining the integrity of the two patches on the capsule lead pipe. After the addition of this monitoring system, the capsule was again installed in the reactor; irradiation of the capsule began on July 19, 1974.

During the remainder of operation of the capsule, there was no sweep gas flow through the ORNL cell, the operating temperature was reduced significantly, and the ORNL cell suffered from time dependent gradients as the flux peak moved up the capsule.

APPENDIX B

Time temperatures histories of Chromel-P vs Alumel thermocouples
located in the graphite magazine of the OF-1 Capsule

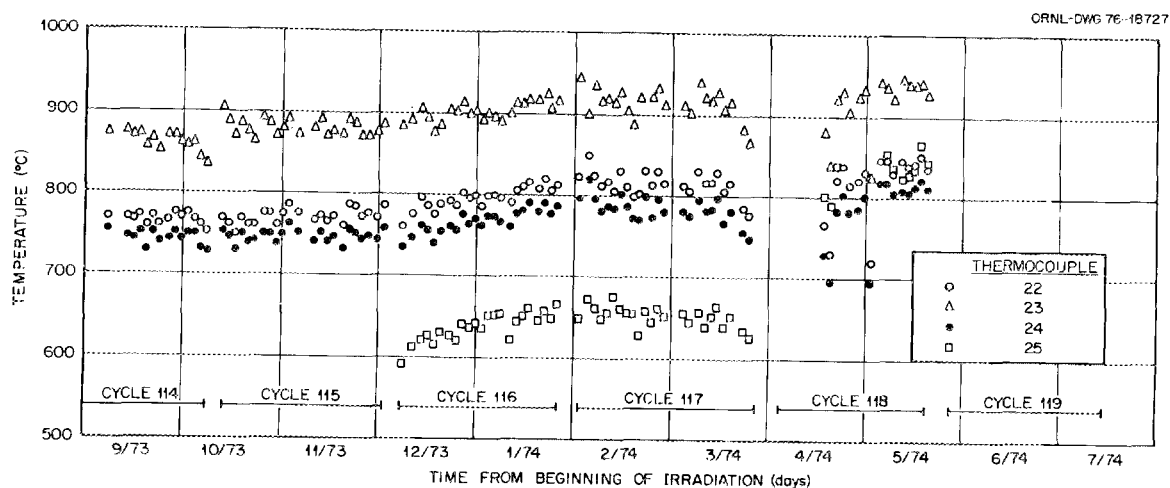


Fig. B1. Time temperature history for thermocouple nos. 22, 23, 24, and 25 in the OF-1 irradiation capsule for ORR cycles 114 through 119. All thermocouples are Chromel-P-Alumel and located in graphite magazine.

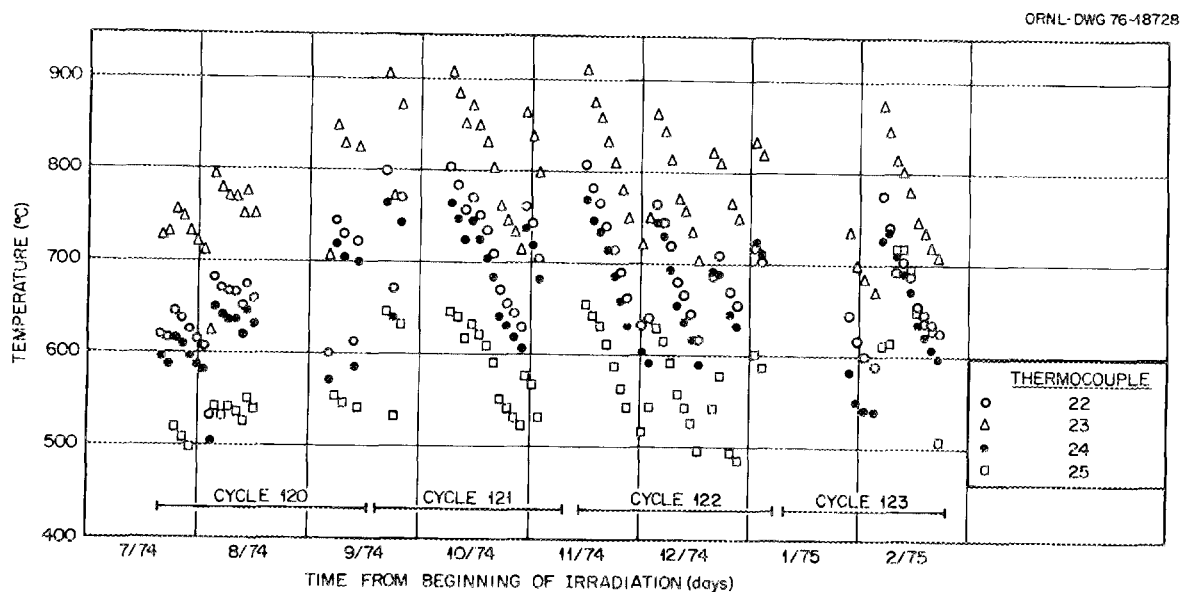


Fig. B2. Time temperature history for thermocouple nos. 22, 23, 24, and 25 in the OF-1 irradiation capsule for ORR cycles 120 through 123. All thermocouples are Chromel-P-Alumel and located in graphite.

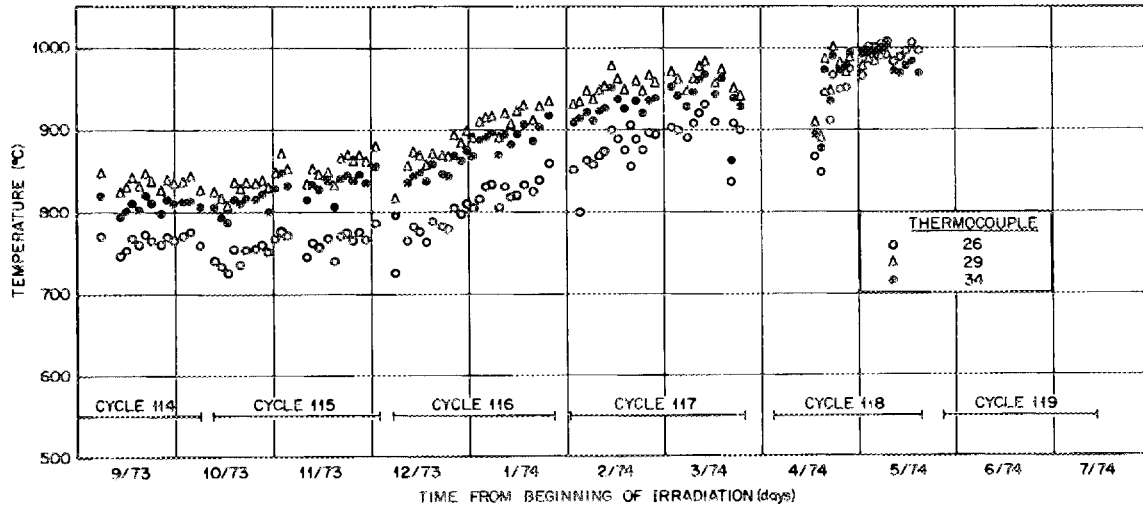


Fig. B3. Time temperature history for thermocouple nos. 26, 29, and 34 in the OF-1 irradiation capsule for ORR cycles 114 through 119. All thermocouples are Chromel-P-Alumel and located in graphite magazine.

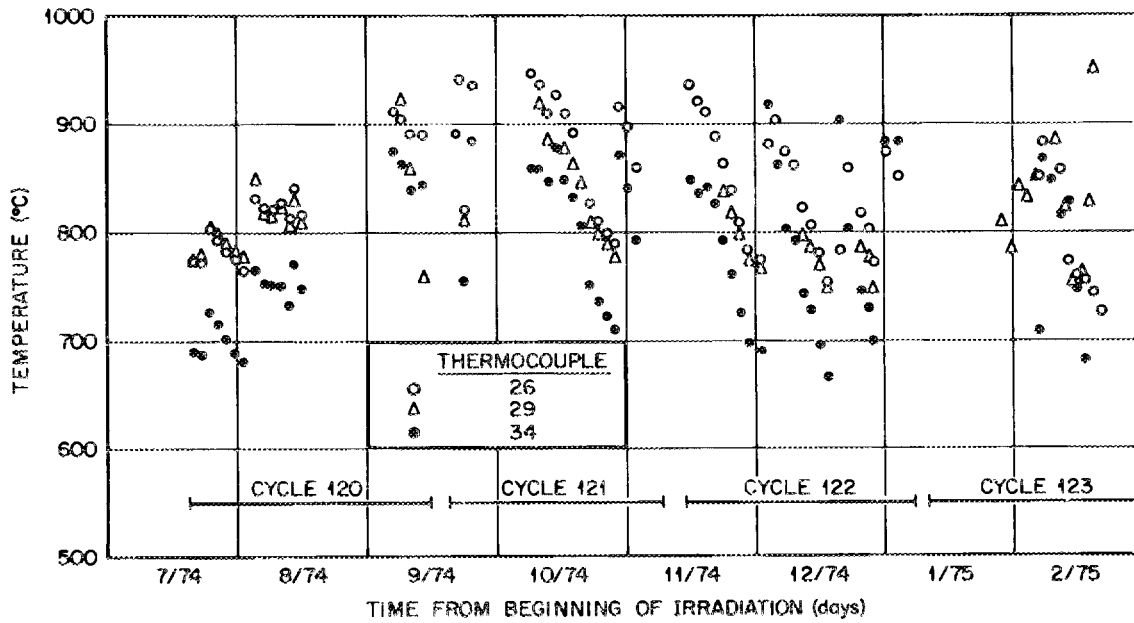


Fig. B4. Time temperature history for thermocouple nos. 26, 29, and 34 in the OF-1 irradiation capsule for ORR cycles 120 through 123. All thermocouples are Chromel-P-Alumel and located in graphite magazine.

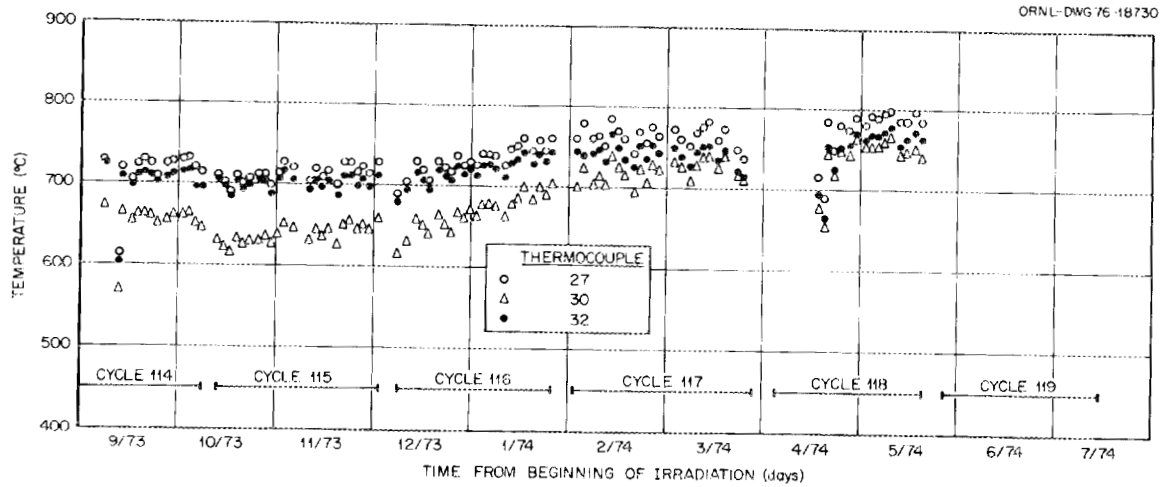


Fig. B5. Time temperature history for thermocouple nos. 27, 30, and 32 in the OF-1 irradiation capsule for ORR cycles 114 through 119. All thermocouples are Chromel-P-Alumel and located in graphite magazine.

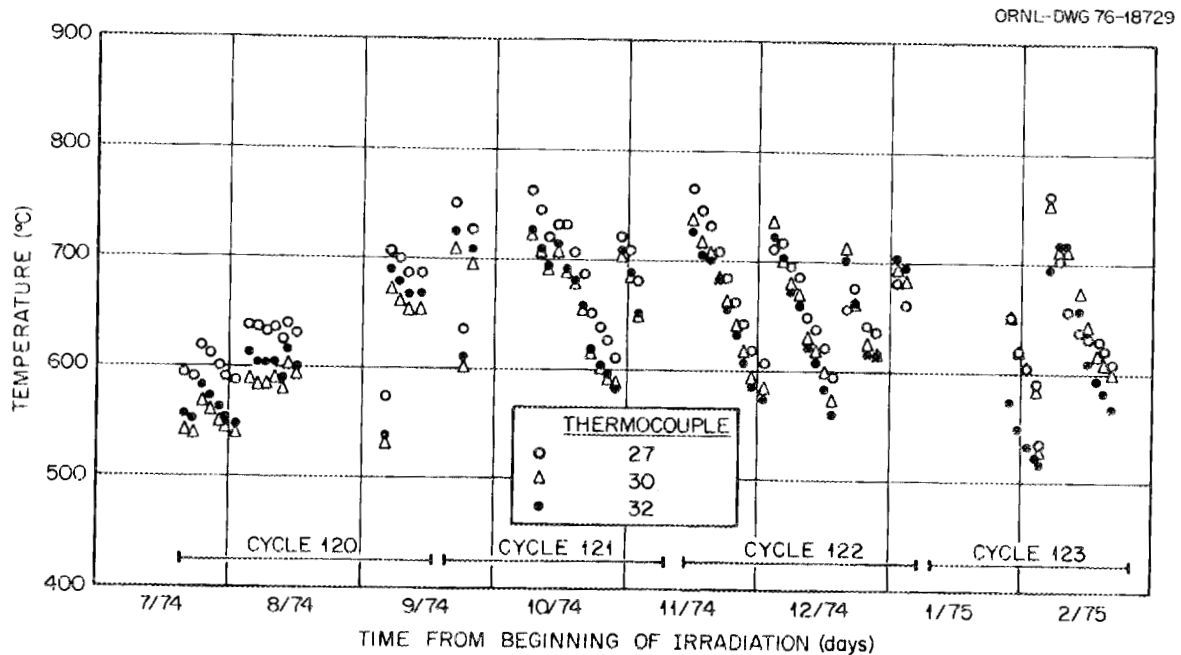


Fig. B6. Time temperature history for thermocouple nos. 27, 30, and 32 in the OF-1 irradiation capsule for ORR cycles 120 through 123. All thermocouples are Chromel-P-Alumel and located in graphite magazine.

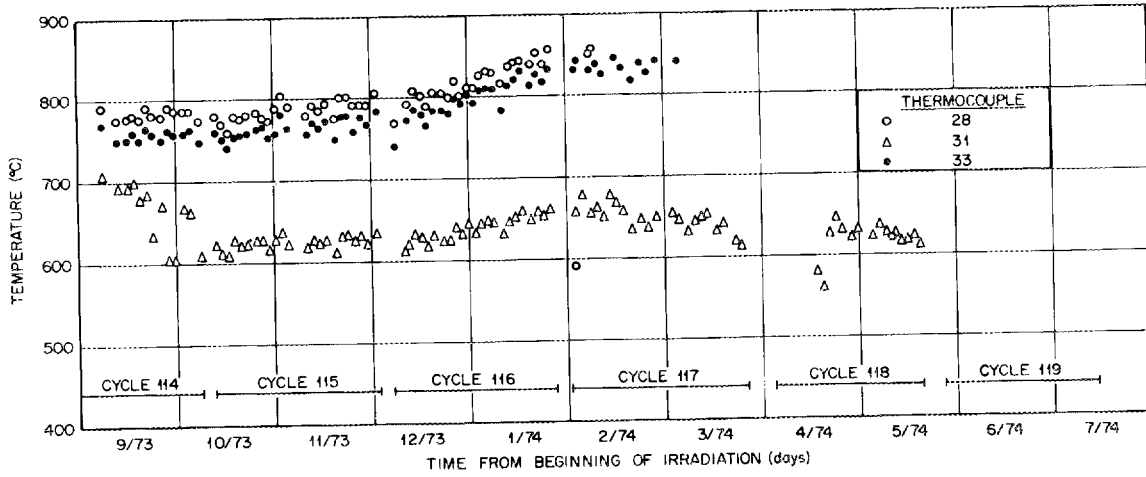


Fig. B7. Time temperature history for thermocouple nos. 28, 31, and 33 in the OF-1 irradiation capsule for ORR cycles 114 through 119. All thermocouples are Chromel-P-Alumel and located in graphite magazine.

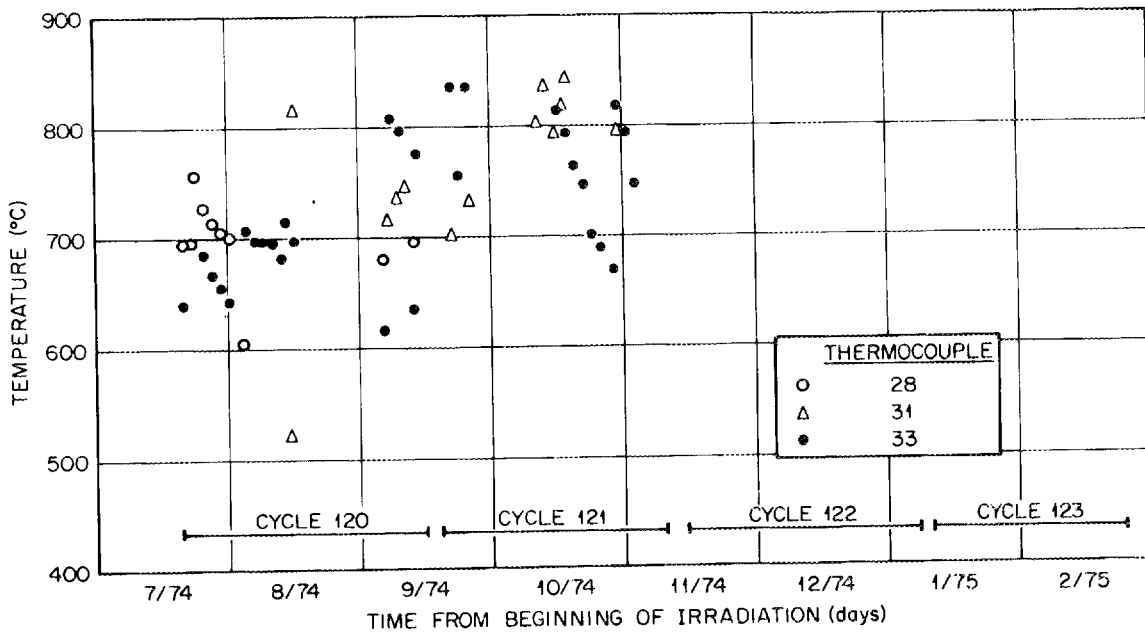


Fig. B8. Time temperature history for thermocouple nos. 28, 31, and 33 in the OF-1 irradiation capsule for ORR cycles 120 through 123. All Thermocouples are Chromel-P-Alumel and located in graphite magazine.

INTERNAL DISTRIBUTION

- | | |
|-------------------------------------|-------------------------------------|
| 1-3. Central Research Library | 45. A. L. Lotts |
| 4. Document Reference Section | 46. B. H. Montgomery |
| 5-14. Laboratory Records Department | 47. C. S. Morgan |
| 15. Laboratory Records, ORNL RC | 48. K. J. Notz |
| 16. ORNL Patent Office | 49. A. R. Olsen |
| 17. E. J. Allen | 50. A. E. Pasto |
| 18. R. L. Beatty | 51. R. L. Pearson |
| 19. R. A. Bradley | 52. H. Postma |
| 20. A. J. Caputo | 53. J. M. Robbins |
| 21. J. A. Conlin | 54. D. P. Stinton |
| 22. J. H. Coobs | 55. R. R. Suchomel |
| 23. D. Constanzo | 56. R. L. Shepard |
| 24. F. L. Culler | 57. S. M. Tiegs |
| 25. W. P. Eatherly | 58-62. T. N. Tiegs |
| 26. R. L. Hamner | 63. B. A. Thiele |
| 27. R. F. Hibbs | 64-66. K. R. Thoms |
| 28-30. M. R. Hill | 67. J. E. VanCleve, Jr. |
| 31. F. J. Homan | 68. J. R. Weir, Jr. |
| 32. D. R. Johnson | 69. R. W. Balluffi (consultant) |
| 33-37. M. J. Kania | 70. Paul M. Brister (consultant) |
| 38-39. P. R. Kasten | 71. W. R. Hibbard, Jr. (consultant) |
| 40. W. J. Lackey | 72. Hayne Palmour III (consultant) |
| 41. T. B. Lindemer | 73. N. E. Promisel (consultant) |
| 42-44. E. L. Long, Jr. | 74. D. F. Stein (consultant) |

EXTERNAL DISTRIBUTION

- 75-82. ERDA DIVISION OF NUCLEAR FUEL CYCLE AND PRODUCTION, Washington, DC 20545
 Director (2)
 R. G. Bradley (1)
 W. S. Schieb (5)
- 83-84. ERDA DIVISION OF REACTOR NUCLEAR RESEARCH AND APPLICATIONS, Washington, DC 20545
 Director
- 85-86. ERDA IDAHO OPERATIONS OFFICE, P.O. Box 2108, Idaho Falls, ID 83401
 C. E. Williams, Manager
 Barry Smith
87. ERDA OFFICE OF PROGRAM MANAGEMENT, RESEARCH AND SPACE PROGRAMS, P.O. Box 81325, San Diego, CA 92138
 J. B. Radcliffe
88. ERDA SAN FRANCISCO OPERATIONS OFFICE, 1333 Broadway, Wells Fargo Building, Oakland, CA 94612
 R. D. Thorne, Manager

- 89--91. ERDA OAK RIDGE OPERATIONS OFFICE, P.O. Box E, Oak Ridge, TN 37830
Director, Research and Technical Support Division
Director, Reactor Division
F. E. Dearing, Reactor Division
- 92--268. ERDA TECHNICAL INFORMATION CENTER, P.O. Box 62, Oak Ridge, TN 37830
For distribution as shown in TID-4500 Distribution Category,
UC-77 (Gas-Cooled Reactor Technology).
- 269--306. ERDA Exchange Agreements with Germany and Dragon Project.